Stony Brook University

Shear-Induced Platelet Sensitization and the Development of an Activation Model

A Dissertation Presented

by

Jawaad Fuad Sheriff

to

The Graduate School

in Partial Fulfillment of the

Requirements

for the Degree of

Doctor of Philosophy

in

Biomedical Engineering

Stony Brook University

December 2010

Stony Brook University

The Graduate School

Jawaad Fuad Sheriff

We, the dissertation committee for the above candidate for the

Doctor of Philosophy degree, hereby recommend

acceptance of this dissertation.

Danny Bluestein, Ph.D. - Dissertation Advisor
Professor of Biomedical Engineering

Jolyon Jesty, D. Phil. - Chairperson of Defense
Professor of Medicine

Mary D. Frame, Ph.D.
Associate Professor of Biomedical Engineering

Wadie F. Bahou, M.D.
Professor of Medicine and Vice Dean of Research, Office of Scientific Affairs

This dissertation is accepted by the Graduate School

Lawrence Martin
Dean of the Graduate School

Abstract of the Dissertation

Shear-Induced Platelet Sensitization and the Development of an Activation Model

by

Jawaad Fuad Sheriff

Doctor of Philosophy

in

Biomedical Engineering

Stony Brook University

2010

Increased shear stresses are a hallmark of flow conditions in blood recirculating devices, and patients implanted with such devices require lifelong anticoagulation to counteract the high risk of thromboembolism. Despite this limitation, manufacturers only test for hemolysis in order to optimize device design. This is primarily due to the paucity of data regarding platelet damage, a major precursor of thromboembolism. Several studies have shown that platelets exposed to constant shear stress for a specified duration become activated. However, post high-shear stress activation behavior of platelets, which is critical to understanding increased thrombotic risk associated with blood recirculating devices, is poorly understood.

Purified platelets were briefly exposed to high shear stress followed by longer periods of low shear stress. Platelet activity state (PAS) was measured using a modified prothrombinase assay. Platelets subject to an initial shear stress of 60 dyne/cm^2 and higher for 40 s showed minimal activation, but they exhibited a post-exposure activation rate that was significantly higher than for platelets that had not suffered the initial high shear insult. This *sensitization* response, although not significant, was also observed for platelets exposed to 1,000 dyne/cm^2 for

25 ms, similar to conditions found in blood recirculating devices. Shear-induced platelet sensitization was amplified when platelets were pre-treated with biochemical agonists thrombin receptor activating peptide (TRAP) and collagen, and attenuated with the addition of apyrase. This indicates physiological modulation of platelet activation after pathological shear stress exposure.

A model predicting platelet activation in response to shear stress, duration of exposure, and shear-loading rate was derived and optimized using *in vitro* sensitization results. These observations and predictive model may provide blood recirculating device manufacturers with a tool to optimize product design for minimizing platelet response and thromboembolic complications rather than hemolysis.

For Dad, Mom, Adnaan, and Nabeel

TABLE OF CONTENTS

LIST OF TABLES

LIST OF FIGURES

LIST OF ABBREVIATIONS AND SYMBOLS

ADP	Adenosine diphosphate
ATP	Adenosine triphosphate
$[Ca^{2+}]_i$	Intracellular calcium concentration
cAMP	Cylclic adenosine monophosphate
CD62P	P-selectin
ddH_2O	Double-distilled water
DMSO	Dimethylsulfoxide
EDTA	Ethylenediaminetetraacetic acid
GFP	Gel-filtered platelets
GPCR	G-protein coupled receptor
HSD	Hemodynamic Shearing Device
LDH	Lactate dehydrogenase
MCS	Mechanical circulatory support
MHV	Mechanical heart valve
PAR	Platelet Activation Rate
PAS	Platelet Activity State
PAS_0	Initial platelet activity state
PAS_{exp}	Experimental platelet activity state
PAS_{num}	Numerical platelet activity state
PGI_2	Prostaglandin I_2; prostacyclin
PF3	Platelet factor 3
PMP	Platelet-derived microparticle

PRP	Platelet-rich plasma
$\tilde{R}$	Modified Reynolds number
RBC	Red blood cell
RMS	Root-mean-square error
τ	Shear stress
τ_{av}	Average shear stress
$\dot{\tau}$	Shear-loading rate
t	Exposure time
T_{low}	Period of low shear stress exposure
TAH	Total Artificial Heart
TRAP	Thrombin-receptor activating peptide; SFLLRN-NH_2
TXA_2	Thromboxane A_2
VAD	Ventricular Assist Device
vWF	von Willebrand Factor

ACKNOWLEDGEMENTS

I would like to thank my Ph.D. advisor Dr. Danny Bluestein for his guidance and patience during the course of my graduate research. He gave me the freedom to pursue basic platelet research and approach topics that have been rediscovered only recently. Dr. Bluestein also gave me the opportunity to tackle a variety of challenges, whether it was related to class work, numerical modeling, or simply updating the lab website. Being in his Biofluids Lab has allowed me to mature both as a student and as a researcher, and has broadened my horizons.

My research would not have taken the path it did without the enthusiasm and sage advice of Dr. Jolyon Jesty. The majority of my experiments were conducted in his lab and he graciously provided the tools and equipment that our lab did not possess. He advised me through the twists and turns of platelet experiments, but always made sure I had a grasp of the big picture. I would not have survived my experimental and mathematical challenges without the sound advice and pragmatic solutions offered by Dr. Gaurav Girdhar and Dr. Michalis Xenos. I would like to thank Matteo Nobili and Dr. Alberto Redaelli of Politecnico di Milano and Dr. Umberto Morbiducci of Politecnico di Torino for their enjoyable collaboration on my first scientific publication.

My Biofluids Lab experience would not be complete without the numerous individuals who made the lab a warm and enjoyable place to work. I particularly want to thank Yared Alemu, Ted Claiborne, Dinesh Peter, Philip Chiu, Xuan Liang, and Suraj Rambhia. I would be remiss if I didn't mention the bright and diligent medical, undergraduate, and high school students that I have had the opportunity to work with and interact over the years: Lukasz Mosakowski, Danielle Macina, Jennifer Petschauer, Suraj Sookhu, Mohammed Hoque, Robert Miller, Matt Pollack, and Cassidy Werner.

I would also like to thank committee members Drs. Molly Frame and Wadie Bahou for their enthusiastic support and constructive evaluation of my dissertation. They introduced me to several platelet biology- and physiology-related concepts that I would not have considered on my own.

I would not have had the mental fortitude to embark and complete this long journey if it were not for the unconditional love, patience, and understanding of my family. Thank you Dad, Mom, Adnaan, and Nabeel.

LIST OF PUBLICATIONS

- Nobili, M., **J. Sheriff**, U. Morbiducci, A. Redaelli, D. Bluestein. "Platelet activation due to hemodynamic shear stresses: Damage accumulation model and comparison to in vitro measurements." *ASAIO Journal*, 2008. 54(1): 64-72.

- **Sheriff, J.**, D. Bluestein, G. Girdhar, J. Jesty. "High shear stress sensitizes platelets to subsequent low shear conditions." *Annals of Biomedical Engineering*, 2010. 38(4): 1442-50.

- Alemu, Y., G. Girdhar, M. Xenos, **J. Sheriff**, J. Jesty, S. Einav, D. Bluestein, "Design optimization of a mechanical heart valve for reducing valve thrombogenicity – a case study with ATS valve." *ASAIO Journal*, 2010. 56(5): 389-396.

- Claiborne, T., G. Girdhar, S. Gallocher-Lowe, **J. Sheriff**, Y. Kato, L. Pinchuk, R. Schoephoerster, J. Jesty, D. Bluestein. "Thrombogenic potential of Innovia polymer valves versus Carpentier-Edwards Perimount Magna aortic bioprosthetic valves." *ASAIO Journal*, 2010. In Press.

I. INTRODUCTION

There is an ever-increasing need for blood recirculating devices to alleviate the effects of cardiovascular diseases, such as heart failure and valvular disease, particularly among the growing elderly population. Blood recirculating devices include prosthetic heart valves, such as mechanical heart valves (MHVs), and mechanical circulatory support (MCS) implants, such as ventricular assist devices (VADs) and total artificial hearts (TAHs). Platelets are known to activate and aggregate in response to shear stress conditions in these devices. However, blood recirculating device manufacturers test and optimize for hemolysis, which occurs at shear stress levels ten-fold higher than those for platelet activation [1, 2]. Thus, blood recirculating devices are not optimized for minimal flow-induced thrombogenicity [3, 4].

The long-term goal of this dissertation was to develop a predictive platelet activation model that can be used to optimize blood recirculating devices for minimization of flow-induced thrombogenicity. Such a tool, if successfully developed and implemented, will allow manufacturers to design these devices quickly and efficiently, minimize costly *in vivo* testing trials, and shorten the bench-to-bedside time. While past studies provide a wealth of information on how platelets respond to high shear stress, they do not address platelet activation behavior post-exposure (i.e. during low shear stress circulation). This is needed to answer the question of whether platelets have the inherent ability to recover from such conditions or if natural platelet inhibitors and agonists play a role in modulating this response. In addition, the effect of the acceleration and deceleration of flow (i.e. shear stress loading rate) on platelet activation is unknown. Such information is critical to the development of an accurate predictive platelet

activation model. The short-term goal of this study was to observe the platelet activation rate response after exposure to several shear stresses and durations, as well as to examine the impact of various platelet agonists and inhibitors on the observed response. Thus, the specific aim of this dissertation was to establish a shear-induced platelet sensitization threshold and develop an improved platelet activation model that can be used to optimize the design of blood recirculating devices.

The specific aim was addressed using a variety of experimental and mathematical tools, and are broken down as follows:

Specific Aim 1. Establish a shear stress- and duration-dependent threshold beyond which platelets are sensitized, or show irreversible and increasing platelet activation.

Specific Aim 2. Demonstrate that the shear-induced platelet sensitization response is increased by the presence of platelet agonists such as thrombin, arachidonic acid, and collagen, and reduced by the presence of platelet inhibitors prostacylin (PGI_2) and apyrase.

Specific Aim 3. Develop a platelet activation model that accounts for the sensitization response and stress loading rates while significantly improving shear-induced platelet activation state prediction.

II. BACKGROUND

2.1 Platelets and Thromboembolism

Platelets are anuclear cells or subcellular fragments which are released from megakaryocytes and circulate in blood for 7 to 10 days [5, 6]. Their primary function is to maintain vascular integrity by encountering blood vessel damage, morphing into an active form, and covering the damaged area. Platelets appear in discoid form when at rest, with an average diameter of 3 μm and thickness of 0.5 μm [5]. The physiological concentration of platelets in whole blood is accepted as between 150,000 and 450,000/μl [7].

The platelet is composed of a plasma membrane, sol-gel fibrous matrix with embedded organelles, and internal membrane systems that communicate with the surface [6]. The plasma membrane is an incompressible bilayer of phospholipids with tiny folds on the exposed exterior surface, the glycocalyx. The latter is a dynamic structure that serves not only as a protective barrier, but also senses external contact and changes, relaying this information to internal components. This transfer of information is conducted via transmembrane glycoprotein receptors, past membrane-bound glycolipids, to submembranous proteins that regulate platelet response to external signals. These receptors include the GPIIb-IIIa and GPIb-IX-V complexes, GPIa-IIa, the seven transmembrane receptor family, and GPVI [8]. The seven transmembrane receptor family are G protein-coupled receptors (GPCRs) and include thrombin, adenosine diphosphate (ADP), and prostaglandin receptors [9]. Many of these proteins are associated with protein constituents, such as calmodulin, myosin, and actin filaments, that comprise the membrane contractile cytoskeleton [6]. Submembranous organelles include secretory α-

granules, dense bodies, lysosomes, and small quantities of mitochondria and other membrane-enclosed structures [6]. The α-granules are the largest and most abundant secretory granules in platelets, and they contain molecules such as β-thromboglobulin, platelet factor IV (PF4), factor V (FV), von Willebrand factor (vWF), P-selectin (CD62P), and fibrinogen, among others [10]. The dense bodies contain high concentrations of ADP, adenosine triphosphate (ATP), serotonin, Mg^{2+}, and Ca^{2+} [10].

Thrombosis is the body's hemostatic response to vessel damage, endothelial dysfunction, foreign materials, plaque rupture, and flow conditions [11, 12]. These factors are summarized in Virchow's triad of blood, surface, and flow [13]

Activation, aggregation, and adhesion are the three primary modes by which platelets participate in hemostasis and thrombosis. Activation can be triggered by chemical or mechanical agonists. Primary chemical agonists include ADP, collagen, thrombin, and thromboxane (TXA_2) [14]. Blood flow-induced shear stresses are the primary mechanical agonist [15, 16]. When platelets are activated, negatively charged phospholipids such as phosphatidylserine, which are preferentially located on the inner layer of the plasma membrane, translocate to the outer surface. Agonists acting through GPCRS increase cytosolic Ca^{2+} concentration, activate protein kinase C, trigger the reorganization of the actin cytoskeleton (causing platelet shape change), and decrease cyclic adenosine monophosphate (cAMP) sythesis, thus relieving the block on platelet signaling that otherwise limits platelet activation [17]. Cytoskeletal rearrangement begins in a few seconds and completes within one minute of exposure to agonists [5]. Platelets in suspension change from a discoid to a spherical shape and rapidly extend filopodia, while platelets attached to a surface undergo circumferential spreading [5]. The activation response is extended by recruitment of additional circulating platelets via secretion or release of mediators such as ADP,

ATP, and TXA_2 from activated platelets, as well as thrombin that is formed on the activated platelet surface [9]. These agonists act as positive-feedback mediators through GPCRs and recruit additional platelets into a growing thrombus.

Anionic (or negatively-charged) phospholipids, such as phosphatidylserine, translocate to the outer membrane of activated platelets. In the presence of Ca^{2+}, activated platelet factors V (FVa) and X (FXa) form a prothrombinase complex on this anionic activated platelet surface, allowing for the conversion of prothrombin (FIIa) to thrombin. Thrombin in turn catalyzes the conversion of fibrinogen into fibrin, which allows for stable attachment between platelets and adhesion with the endothelium, as well as traps red blood cells into a growing thrombus. It also activates additional FV to FVa and factor VIII into factor VIIIa to ensure continued prothrombinase complex and FXa generation. Approximately 80% of the FVa used in the prothrombinase complex assembly is of platelet α-granule origin [18].

Aggregation occurs when activated platelets bind to each other. Subsequent to activation, integrin $\alpha_{IIb}\beta_3$ (GPIIb-IIIa complex) undergoes Ca^{2+}-dependent conformational change and cross-links two platelets via fibrinogen or vWF, leading to platelet plug formation [19]. Fibrinogen acts primarily at shear stresses lower than 10 dyne/cm^2, found in most blood vessels, while vWF acts at higher shear stresses [12, 20]. At shear stresses greater than 60 to 80 dyne/cm^2, vWF engages with the GPIb-IX-V complex, transducing signals in platelets with subsequent activation of GPIIb-IIIa and binding with vWF [21, 22]. In addition, CD62P released from α-granules and found on the surface of activated platelets plays a role in shear-induced aggregation via a yet unknown ligand [23].

Adhesion occurs when activated platelets bind to the endothelium. Under low shear stresses, the GPIa-IIa complex on activated platelets binds to the endothelium via exposed

collagen. However, under higher shear stresses, this translocation and tethering is mediated via the A1 domain of vWF binding with the GPIbα constituent of the GPIb-IX-V complex [8, 21, 22].

Blood flow dynamics support thrombosis by allowing transport of blood cells and biological molecules to the growing thrombus [24-26]. Pathological blood flow-induced shear stresses also trigger thrombosis formation [27]. Activated platelets with long residence times in such perturbed flow regions aggregate, leading to free emboli formation [28]. These thromboemboli preferentially lodge in small blood vessel, particularly in the brain, leading to stroke and other complications.

2.2 Blood Recirculating Devices and Thromboembolism

An estimated 500,000-550,000 patients in the United States are currently in the terminal stage of end-stage heart failure, and of these, 80,000 to 150,000 patients could benefit from heart transplantation annually [29-32]. However, the number of donors (2,200 annually) is limited [31]. The number of patients with end-stage heart failure is predicted to rise over the next 20 years, particularly due to the doubling of those over age 65, among whom heart failure is most prevalent [30]. Destination therapy, as opposed to a bridge-to-transplant, with mechanical circulatory support (MCS) devices is a promising alternative for patients who are not heart transplantation candidates [3, 4, 30]. These devices include ventricular assist devices (VAD) and total artificial hearts (TAH). However, the success of such devices is marred by complications, including thromboembolism, bleeding, infections, and technical failures [4, 33]. Thromboembolic complication rates range from 2.7% to 48.8%, depending on the device type, anticoagulation protocol, demographic factors, and surgical conditions [33]. Pulsatile VADs

with texturized interior surfaces [34] show reduced thrombotic complications but suffer from significant mechanical failure over time [35, 36]. For example, the HeartMate device has a thromboembolic incidence of 2 – 4% per year without anticoagulation [37]. Continuous flow VADs have significantly improved durability, but are plagued with thrombotic complications [38]. These devices require antithrombotic therapy, ranging from low-dose antiplatelet therapy for pulsatile VADs to combinations of multiple anticoagulants for continuous flow VADs and total artificial hearts [38]. While bridge-to-transplant is successful in 75% of patients receiving transplants, the one-year survival rate drops to 34% for the 12% of patients selected for destination therapy [39]. Thus, there is a growing interest in improving the survival rate for patients undergoing destination therapy, particularly in light of heart donor shortage.

Mechanical heart valves (MHVs) continue to remain a popular choice for heart valve replacement. In 2006, there were 98,000 valve replacement procedures in the United States and 195,300 outside the United States [40]. MHVs comprise approximately 50% of these replacements [41, 42]. While bioprosthetic valves constitute an increasingly larger share of the heart valve implants in the United States (approximately 75% [40], up from 35% in 1995 [43]) due to their excellent hemodynamic characteristics and lack of need for anticoagulant therapy, they have limited durability due to leaflet calcification and tearing, mechanically induced fatigue, and tissue failure [44, 45]. As with MCS devices, patients with MHV implants are at risk for thrombus formation due to disrupted flow conditions and require lifelong anticoagulation therapy [46]. Despite this treatment, patients develop thromboembolic complications at a linearized rate of 0.7 to 6.4% each year [47, 48]. In addition, anticoagulation therapy carries the risk of uncontrolled bleeding [46, 49], particularly for patients over the age of 60 [45].

In blood recirculating devices, thrombus formation is initiated by abnormal flow patterns, which introduce high shear forces on blood cell elements, causing hemolysis and platelet activation, and change the frequency of contact between activated platelets (through recirculation and flow stagnation) [50]. In tilting disc and bileaflet MHVs, maximum turbulent shear stress during peak systole (forward flow) is 1,500 dyne/cm^2, and lasts for 20-30 ms [41]. Mean turbulent shear stresses are 200 – 600 dyne/cm^2 during this forward flow [41]. During regurgitant, or leakage, flow, which occurs when the valves are closed, shear stresses exceed 3,000 dyne/cm^2, particularly through the hinge region of the MHV [41]. Platelets exposed to these conditions are undoubtedly activated and contribute to thrombosis.

2.3 The Significance of Studying Platelet Activation over Hemolysis

Blood recirculating device manufacturers almost exclusively use red blood cell (RBC) hemolysis as a standard measure for optimizing their devices [51]. More recent studies showed that platelet activation and initiation of thrombosis are important aspects of mechanically-induced blood damage [52]. RBCs are biconcave discs with flexible membranes and high resistance to mechanical forces. Due to their size and density, they are primarily found in the core region of blood flow (Fahraeus effect), and thus are exposed to lower shear stresses. The shear stress threshold for RBC hemolysis is between 3,000 and 6,000 dyne/cm^2 [53, 54], although earlier studies established this threshold as low as 1,500 dyne/cm^2 [1, 55]. These threshold levels are different dependent on the time and method of *in vitro* exposure of RBCs to shear stress. However, platelets are smaller and have more rigid membranes. They move along the near-wall region of blood vessels and encounter higher shear stresses. Platelet lysis is significant at shear stresses greater than 250 dyne/cm^2, while change in platelet morphology,

secretion, and aggregation are noted at shear stresses above 50 dyne/cm^2 [15, 56, 57]. Emphasis on using the thrombogenic potential, rather than hemolysis, for studying complications in blood recirculating devices comes from recent studies that showed thrombosis, rather than hemolytic anemia, is the primary clinical problem associated with such devices [58].

2.4 In Vitro Studies of Flow-Induced Thrombosis

Shear stress is the mechanical agonist most relevant to platelet-mediated thrombosis formation initiated by the presence of blood recirculating devices. Approximate physiologic wall shear stresses range from 1 dyne/cm^2 in veins to approximately 30 dyne/cm^2 in large arteries to 60 dyne/cm^2 in arterioles, approaching 380 dyne/cm^2 in stenotic vessels [12, 59, 60]. Shear stresses as low as 2 – 3 dyne/cm^2 do not significantly activate platelets, but when the magnitude and duration of the shear stress increases, platelet activation levels are detectable [12].

Several researchers have attempted to examine platelet activation behavior in response to physiological or pathological shear stresses. Earlier studies exposed whole blood or platelet-rich plasma (PRP) to extremely high shear stress conditions found in artificial devices such as heart valves or MCS devices. More contemporary studies have examined platelet behavior at physiological levels found in major arteries and veins. However, few studies have attempted to link experimental platelet activation behavior to a mathematical model that may be used to predict such behavior in order to optimize blood recirculating devices for flow-induced thrombogenicity.

One of the first studies to examine shear-induced platelet activation involved exposure of PRP to a large range of shear stresses in a cone-plate viscometer. The authors determined that at shear stresses greater than 50 dyne/cm^2, platelets undergo a change in morphology, with minimal

lysis at shear stresses below 250 dyne/cm^2, indicating platelet activation [57]. Ramstack et al. exposed PRP, obtained from dogs, to shear stresses ranging from 300 dyne/cm^2 to 1,000 dyne/cm^2 in a concentric cylindrical viscometer [2]. The authors used the percentage of available platelet factor 3 (PF3, or prothrombinase activity), based on clotting time and the rate of shape change of the platelets to represent the level of activation. Reversibility in the shape change of the platelets was observed after letting the samples stand for up to 60 min post-shear exposure, implying deactivation. However, any such reversibility in PF3 availability was insignificant [2]. Wurzinger et al. exposed PRP to shear stresses ranging from 570 dyne/cm^2 to 2,550 dyne/cm^2 for short durations (7 to 700 ms) in a Couette viscometer and measured PF3 availability [61]. The authors note that platelet changes are more dependent on the magnitude rather than duration of the shear stress. Exposure to shear stresses greater than 570 dyne/cm^2 for 7 ms caused a significant increase in PF3 availability, compared to unsheared controls. From transmission electron micrographs, no discoid, or unactivated, platelets can be identified visually after 700 ms exposure to 570 dyne/cm^2, although about one-third have their granules centralized, indicating little or no activation. However platelets exposed to 1,700 dyne/cm^2 for 113 ms exhibit clear signs of activation, marked by a transition from “smooth discs” to “spiny spheres” [61, 62]. Based on these studies, Hellums et al. [15, 16] summarized the effects of shear stress magnitude and exposure time on platelet activation under conditions found in normal circulation and in MHVs (Fig. 2.1). However, most of these studies focused largely on platelet aggregation rather than activation, and therefore required a combination of extremely high shear and low durations or physiological shear for long durations.

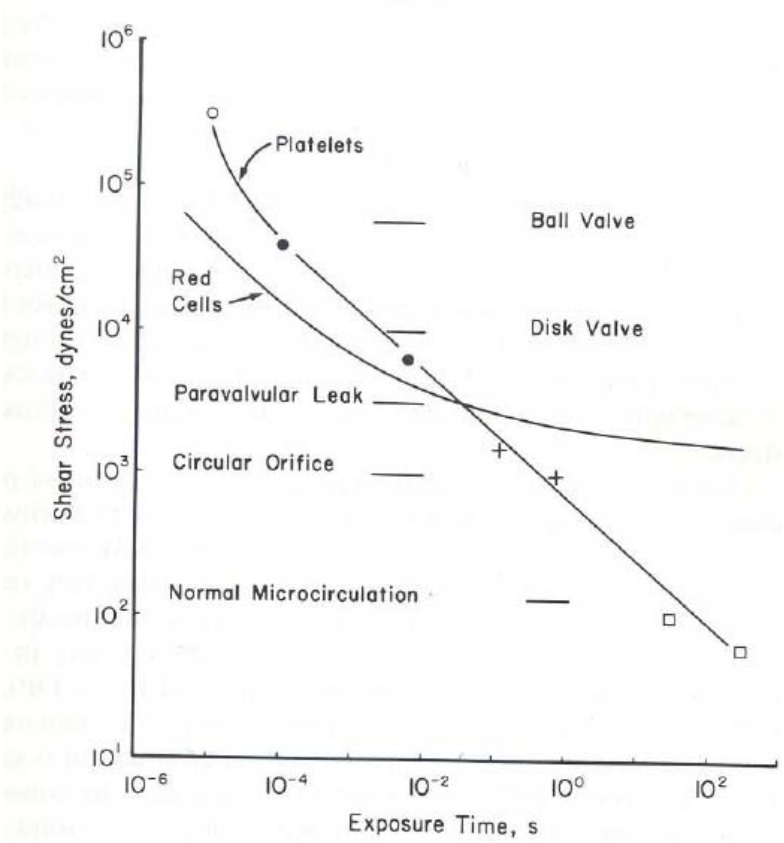

Figure 2.1. Shear stress- and duration-dependent threshold of platelet activation and RBC hemolysis. These results were compiled from the efforts of several researchers [15, 16].

Development of flow cytometric and assay techniques has allowed researchers to focus on direct measurement of platelet activation markers at lower shear stresses and shorter durations. Zhang et al. exposed PRP to constant shear stresses of 20, 50, and 100 dyne/cm^2 or a stepped pulse composed of a 5 dyne/cm^2 segment for 10 s, followed by 100 dyne/cm^2 applied for a range of durations (2.5-80 s), and concluded with 5 dyne/cm^2 for 40 s [63]. Platelet activation was quantified using CD62P expression on the platelet surface and analyzed using a flow cytometer. The authors noted that CD62P expression was greater in the case where a constant high shear stress phase was followed by a brief low shear stress segment when compared with constant low shear stress exposure. However, comparison between this complex profile with and without the subsequent low shear phase showed no difference. Furthermore, the level of platelet activation was much lower than aggregation for the same applied conditions, implying a

presence of a high threshold for shear-induced platelet activation. In a follow-up study, PRP and whole blood were exposed to100 dyne/cm^2 for variable durations, with levels of activation much lower than aggregation. A marked increase in aggregation was noted after just 10 s, whereas more than 20 s was required for a significant increase in platelet activation [64].

More recently, studies combining experimental and predictive approaches have been conducted. In such a study, gel-filtered platelets were circulated in a flow loop containing a stenotic region, with a maximal stress of 41 dyne/cm^2 and 1.4 dyne/cm^2 elsewhere [65]. Platelet activation state (PAS), or the rate of thrombin generation (formerly known as PF3 activity), was measured real-time using an acetylated prothrombin-based assay [65, 66]. While showing that experiments with the loop containing the stenosis had a significantly higher rate of activation as compared with a non-stenosed control, as expected, the authors also showed that flow rate, and therefore shear stress, also played a significant role in platelet activation rate. While the increase in activation rate did not correspond with the 4-fold increase in flow rate, it was statistically significant and indicated a platelet damage history after multiple passages [65]. In addition, platelets at a count of 200,000/μl showed a significantly larger increase in platelet activation rate than platelets at 20,000/μl exposed to dynamic shear stress conditions in a capillary flow loop, demonstrating that shear-induced platelet activation is also driven by count-dependent platelet-platelet signaling [67]. Platelet activation rate was also dependent on the shape of the applied shear stress waveform, where platelets exposed to a peak shear stress of 20 dyne/cm^2 for longer durations (square peak, 2.5s) activated at a faster rate than those exposed for 0 s (triangular peak) [68]. In addition, shorter durations between peak shear stresses caused a faster increase in PAS, potentially due to transient vortices spawned by abrupt deceleration of flow. However, there is a lack of experiments that examine platelet response after exposure to the high shear stress

conditions described earlier. In addition, the role of the shear loading rate, i.e. acceleration and deceleration as found in blood flow through blood recirculating devices, has not been studied in detail.

2.5 Cone-and-Plate Based Viscometer to Study Platelet Response to Shear Stress

During the past 40 years, several *in vitro* devices have been used to examine platelet behavior under shear stress. These include platelet aggregometers (with stirring) [69, 70], concentric cylinder systems [71, 72], jet devices [73], capillary viscometers[56, 74, 75], parallel plate chambers and rotational viscometers [62, 76-78]. However, the rotational viscometer, particularly the cone-and-plate viscometer [79], has become the instrument of choice in recent years due their programmability, ability to apply both constant and dynamic shear stresses, ability for use in optical measurements, and uniformity of shear stress [12]. The cone-and-plate viscometer has the added advantages of having an open platelet suspension, allowing for rapid removal of liquid for analyses, and the ability to place a monolayer of cells on the plate to examine platelet adhesion behavior.

In recent years, the ability of cone-and-plate viscometers to accurately emulate the dynamic shear stress patterns found in the human physiological circulation and in devices has garnered more interest. Sutera et al. examined platelet aggregation using a programmable cone-and-plate viscometer that was capable of introducing rapid acceleration and deceleration [80]. Schnittler et al. modified this viscometer into a shearing device that exposed cultured cells to both steady and pulsatile flow [81].

However, secondary flow effects may affect experimental observations [82-86], and flow behavior in the cone-and-plate viscometer must be well understood. Sdougous et al. defined a

modified Reynolds number, $\tilde{R} = (r^2 \omega \alpha^2)/(12v)$, which is dependent on the cone radius *r*, angular velocity ω, cone angle α, and dynamic viscosity *v* [87]. The cone-and-plate region retains controllable laminar and uniform flow characteristics at $\tilde{R} < 0.5$ [88].

While most prior studies have examined platelet response under constant low and high shear stresses, more recent studies have examined the platelet activation behavior under dynamic physiologic and pathologic conditions [64, 68, 89, 90] found in human circulation and in devices. The computer controlled cone-and-plate viscometer thus provides a highly accurate, dynamic emulator of *in vivo* conditions. It also bypasses the need for an animal model and provides a valuable source of experimental data to be used as inputs for computational fluid dynamic simulations of cardiovascular devices and pathologies.

2.6 Mathematical Models of Platelet Activation

Several studies have focused on the formulation of platelet "stimulation" (i.e. activation) functions based on experimental observations. Ramstack et al. derived the function $s_0 = 1 - a\exp[cK_2\tau_b]$, where the stimulation term s_0 is defined as fractional PF3 activity [2]. This term is dependent on the applied constant shear stress τ_b, and constants *c, a,* and K_2, as obtained from nonlinear least squares fitting of experimental data. However, this model is highly dependent on the diameter and length of the tube (incorporated into constant *a*) and does not account for transient flow effects (i.e. acceleration and deceleration). The Platelet Stimulation Function (PSF) derived by Boreda et al. states that platelet stimulation is due to a combination of shear stress and exposure time such that $PSF = \tau t^{0.452}$, based on flow velocities in experimental models of coronary stenoses [91]. This formula is based on a model of fractional platelet lysis [92], as measured by lactate dehydrogenase (LDH) release, that is dependent on both shear stress

(τ) and exposure time (t_{exp}), in the form $(\Delta LDH / LDH)(\%) = A\tau^{\alpha} t_{exp}^{\beta}$. This model in turn is based on a previous model of RBC hemolysis [93]. The constants A, α, and β are based on the experimental observations of Wurzinger et al. [61], described earlier. Recent studies utilized these LDH-based models, as well as linear "level of activation" formulation [94-96], to predict platelet activation response to flow through mechanical heart valve (MHV) hinge regions [97, 98]. While these models generally fit experimental data well, they do not address the issue of dynamic shear stress conditions (i.e. accelerating and decelerating flow), and it is not clear if using these power-law formulations describes shear-induced platelet activation behavior.

A more recent model addresses the transient nature of the flow field and senescence, or past damage history, of the platelet [99]. This formulation is based on a red blood cell hemolysis model [100], where a phenomenological damage index, dependent only on shear stress and time, was applied to individual cells increases as the cell passes through the circulation, culminating in a critical value reflecting the destruction or removal of the cell. The rate of damage accumulation is dependent on the instantaneous shear stress and past damage history. The behavior of the damage accumulation curves was confirmed with results from previous studies [100-102]. This model accounts for the transient nature of the flow field and prior damage history, while applying an upper limit on the level of platelet activation so that it does not exceed a damage fraction of 1 ("fully activated"). However, the model assumes a "perfect memory," where platelets undergo a continuous loop through the valves, rather than circulating through the body. In addition, the model as utilized in the study relies on individual platelet paths rather than bulk platelet behavior, which may be more relevant in the clinical setting. Finally, due to the novel nature of the study, the results have not been verified experimentally to validate the use of a blood-damage model for platelet behavior.

Another recent platelet activation model [68] was based on the power law RBC hemolysis model of Grigioni et al. [102]. The latter was derived by making the earlier, simple power law RBC damage model [93] mechanical dose-dependent. This approach allowed the shear-exposed RBC to retain its previous damage history, a feature lacking from prior RBC damage models, with the exception of Yeleswarapu et al. Nobili et al. used this approach to derive a model to predict PAS (Section 2.4) in response to dynamic shear stress waveforms [68]. The model takes the form:

$$PAS = \int_{t_0}^{t} Ca \left[\int_{t_0}^{\phi} \tau(\xi)^{b/a} d\xi + \left(\frac{PAS(t_0)}{C} \right)^{1/a} \right]^{a-1} \tau(\phi)^{b/a} d\phi \tag{2.1}$$

The inner integral represents the mechanical dose applied between experimental observation points and is integrated from time $t_0 = 0$ to φ, while the outer integral represents the PAS for each observation interval. The shear stress, τ, is approximated as a constant shear stress for the given interval, while a, b, and C are constants determined by optimizing the model with experimental values measured by our group for several different shear stress waveforms [68]. $PAS(t_0)$ is the PAS measured at time $t = 0$, prior to any exposure to shear stress. While this phenomenological model accounts for the prior shear loading history of the platelet, it neglects the role of the shear loading rate, or the acceleration and deceleration phases of the peak shear stress. This shear loading rate, or even turbulent flow effects, may have a significant impact on the platelet activation behavior [94, 103].

III. MATERIALS AND METHODS

3.1 Platelet Preparation

Informed consent was obtained from healthy adult volunteers of either sex who had not taken aspirin or ibuprofen for 2 weeks, as approved by the Stony Brook University IRB. Whole blood, 30 ml, was drawn by antecubital venipuncture and collected into 3 ml acid-citrate dextrose (ACD-A), and centrifuged at 650 x *g* for 6 minutes. Platelet-rich plasma (PRP) was separated from red blood cells and gel-filtered at 3 ml/min through a 220-ml column of Sepharose 2B beads (60-200 μm diameter, 2% agarose; Sigma-Aldrich, St. Louis, MO) equilibrated in platelet buffer, consisting of Hepes-modified Ca^{2+}-free Tyrode's buffer containing 0.1% fatty-acid-free bovine serum albumin [104]. Platelet collection was monitored using a Pharmacia UV optical density recorder. Between filtrations, beads were flushed with 0.05% w/v sodium azide (Sigma-Aldrich, St. Louis, MO). At least once a week, beads were washed in 50 mM NaOH and 0.5% sodium dodecyl sulfate, and rinsed copiously with double distilled water (ddH_2O). These processes ensured minimal platelet activation during the gel filtration.

Gel-filtered platelets (GFP) were counted using a Z1 Particle Counter (Coulter, Miami, FL) and diluted with platelet buffer to a concentration 20,000/μl, unless otherwise stated. Platelets were maintained on a gentle orbital shaker (Red Rotor PR70, Hoefer Scientific, Holliston, MA) at room temperature until use, within 6 hours. GFP were incubated with 3 mM $CaCl_2$ (final) 10 min prior to experiments.

3.2 The Platelet Activity State (PAS) Assay

Platelet activity state (PAS) was measured using the modified prothrombinase method developed by Jesty and Bluestein [66] with further modifications [65]. Thrombin generation is a powerful marker of platelet activation in response to several biochemical and mechanical agonists. However, generated thrombin has a positive feedback response on platelet activation. To observe the direct relationship between the mechanical agonist, in this case shear stress, and thrombin generation, the positive feedback is removed by using acetylated prothrombin (Ac-FIIa) instead of normal prothrombin. This substitution demonstrates a linear increase in thrombin generation over time [65]. This modification to the thrombin generation cascade is summarized in Figure 3.1.

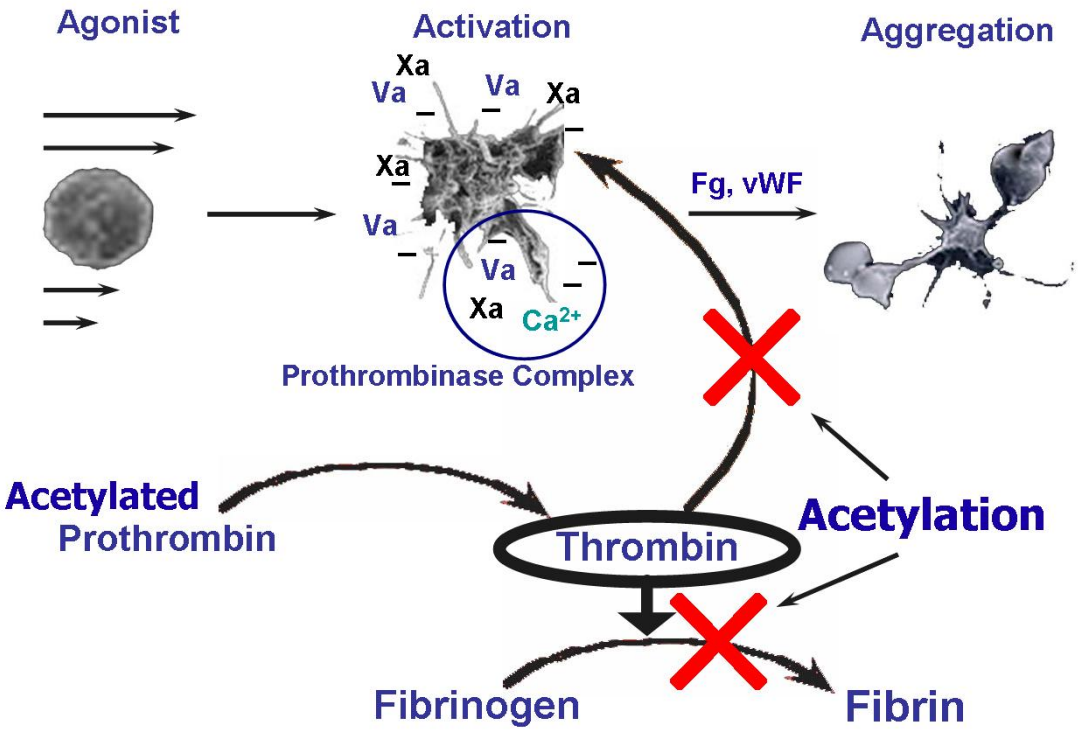

Figure 3.1. The Platelet Activity State (PAS) assay. Prothrombin acetylation prevents fibrin formation and positive thrombin feedback to further activate platelets. This allows for a direct correlation between the agonist, in this case shear stress, and PAS, measured by thrombin generation. Adapted from [26].

Ac-FIIa was prepared by treating 10 μM prothrombin in 100 mM $NaHCO_3$ + 5 mM $CaCl_2$ with 3 mM sulfo-N-succinimidyl acetate for 20 minutes at room temperature [65].

Experimental platelet samples were withdrawn at different time points from the experimental setup and assayed using the PAS assay. For an initial platelet concentration of 20,000/μl, PAS was measured as follows: A 100 μl tube containing (final concentrations) 5,000 platelets/μl, 200 nM Ac-FIIa, 5 mM Ca^{2+}, and 100 pM Factor Xa (FXa) was incubated at 37°C for 10 min. For larger platelet concentrations, such as 100,000/μl and 150,000/μl, larger tube volumes were used to ensure adequate platelet sample volume. However, the final concentrations remained as described above. A 10 μl sample from the incubated tube was assayed for thrombin generation using 0.3 mM Chromozym TH (CH-TH, Tosyl-Gly-Pro-Arg-4-nitranilide acetate, Roche Diagnostics, Indianapolis, IN) in a 96-well microplate reader (Vmax, Molecular Devices, Sunnyvale, CA) at 25°C. Thrombin generation was analyzed over 7 minutes at an absorbance wavelength of 405 nM. The resultant values at each time point, expressed as change in absorbance/min, were normalized against the thrombin generation rate of fully activated platelets, obtained by sonication (10 W for 10 s, Branson Sonifier 150 with microprobe, Branson, MO). Thus, all PAS values are expressed as a fraction of the thrombin generation for fully activated platelets.

3.3 Materials for the PAS Assay

The tubes in which platelets were incubated with Ac-FIIa, Ca^{2+}, and FXa in the concentrations noted earlier were buffered with Hepes-buffered saline with 0.1% bovine serum albumin, fatty-free acid (HBS:BSA) at a physiological pH of 7.4. For the microplate wells, CH-TH was dissolved in 0.15 M NaCl, adjusted to a concentration of 1 mM, and buffered with HBS:BSA + 5 mM ethylenediaminetetraacetic acid (EDTA) at a pH of 7.4.

Platelet buffer used for experiments was a Hepes-modified Ca^{2+}-free Tyrode's buffer, consisting of (final concentrations) 135 mM NaCl, 5 mM D(+)-glucose, 2.7 mM KCl, 0.5 mM Na_2HPO_4, 1 mM $MgCl_2$, 1 mM $Na_3C_6H_5$ (Trisodium Citrate), 0.1% BSA, and 10 mM Hepes. NaOH was used to adjust the pH to 7.4.

3.4 Flow Cytometry

Flow cytometry is an alternative and widely-accepted method to examine expression of platelet activation antigens. PAS measurements were compared to flow cytometry results quantifying expression of P-selectin, an activation-dependent platelet surface marker derived from platelet α granules, and obtained using a FACScan instrument (Calibur, Becton Dickinson, Franklin Lakes, NJ). Platelets (20,000/µl in 80 µl platelet buffer) were withdrawn at different time points in a manner similar to that for the PAS assay, but were fixed with 1% paraformaldehyde (in distilled H_2O). Fixed platelets were treated with a phycoerythrein (PE)-labeled antibody against P-selectin (20 µl, anti-CD62P, BD Biosciences, Franklin Lakes, NJ) at room temperature and shielded from light for 30 minutes. The negative control was an equal concentration of Mouse IgG_1 platelet PE control (BD Biosciences, Franklin Lakes, NJ). These samples were then diluted in platelet buffer prior to cytometry. The analysis gating included all

platelets and particles larger than 1 μm. The P-selectin expression was measured as the percentage of CD62P-positive events out of 10,000 total events falling within this gate. These values were normalized against results obtained for platelets treated with 100 μM Thrombin Receptor Activating Peptide (TRAP)-6 (Sigma-Aldrich, St. Louis, MO), a powerful thrombin analog, for 2 minutes at 37°C. TRAP treatment ensures that approximately 95% of platelets will register a positive result for P-selectin expression.

It is important to note that the PAS assay quantifies thrombin generation, while CD62P is a marker of P-selectin expression, and the correlation between the two allows for comparison between results of the experiments in this dissertation with other studies that use CD62P as a marker of platelet activation. Thrombin generation is the end result of the prothrombinase complex formation on the activated platelet membrane surface, while CD62P is released from the α-granules and expressed on the surface.

3.5 The Hemodynamic Shearing Device (HSD)

Platelets were exposed to controlled dynamic shear stress waveforms in the HSD, a modification and improvement of the system developed by Blackman et al. [105]. It combined cone-and-plate and Couette features (Fig. 3.2) and was designed so that the shear stresses in the Couette region and under the cone are equivalent according to

$$\tau_{Cone-Plate} = \tau_{Couette} \rightarrow$$
$$\mu\frac{\omega}{\alpha} = 2\mu\frac{R_o^{\,2}R_i^{\,2}}{R_o^{\,2}-R_i^{\,2}}\left(\frac{1}{r^2}\right)\Bigg|_{r=R_i} \Rightarrow \alpha = \frac{1}{2}\left[1-\left(\frac{R_i}{R_o}\right)^2\right] \qquad (3.1)$$
$$(\text{small } \alpha, (R_i/R_o) \rightarrow 1)$$

The viscosity, μ, is 1 cP, as measured for GFP in platelet buffer at 37°C; α is the cone angle, 2°; ω is the angular velocity of the cone; and R_o and R_i are the inner radius of the ring and the outer

radius of the cone, respectively. The resultant design yielded a Couette gap of 720 μm and a cone that was lowered to a position 10 μm above a stationary plate using a micrometer mounted on the cone [68]. Prior studies indicate that periodical acceleration and deceleration destroy the uniformity of the shear stress somewhat, but this may be kept to a minimum by ensuring the modified Reynolds number, $\tilde{R} = (r^2\omega\alpha^2)/(12\nu)$, is below 0.5, the limit of secondary flow effects [85, 86, 88].

Platelet-contacting surfaces were manufactured from ultra-high molecular weight polyethylene (UHMWPE) and treated with silicone (in heptane solution, Sigmacote, Sigma-Aldrich, St. Louis, MO) 10 min prior to experiments. The HSD was placed in an incubator at 37°C and high humidity. For experiments, 2 ml GFP was added to the HSD. This volume was low enough so that no spilling occurs at high cone velocities, but high enough so sufficient volume remained when multiple platelet samples are withdrawn. Platelets were withdrawn from the Couette region using fine pipette tips at defined time points for the PAS assay. After each experiment, all platelet-contacting surfaces were washed with 50 mM NaOH + 0.5% sodium dodecyl sulfate (SDS, Sigma-Aldrich, St. Louis, MO).

Dynamic shear stress waveforms were simulated by a computer-controlled microstepper motor (VS23B, Compumotor Division, Parker Hannifin Corporation, Rohnert Park, CA), programmed in BASIC with the supplied Motion Architect software, and transferred via a ZETA6104 microstepping drive. Example codes for the shear stress waveforms may be found in Appendix A.

The advantage of the HSD was that it exposed the entire platelet population to a uniform shear stress, eliminating possible "dilution" effects and variable shear stresses that are present in capillary flow loops. Furthermore, this setup allowed for exposure of platelets to highly-

controlled dynamic shear stress patterns present in trajectories of individual platelets through prosthetic devices and cardiovascular pathologies.

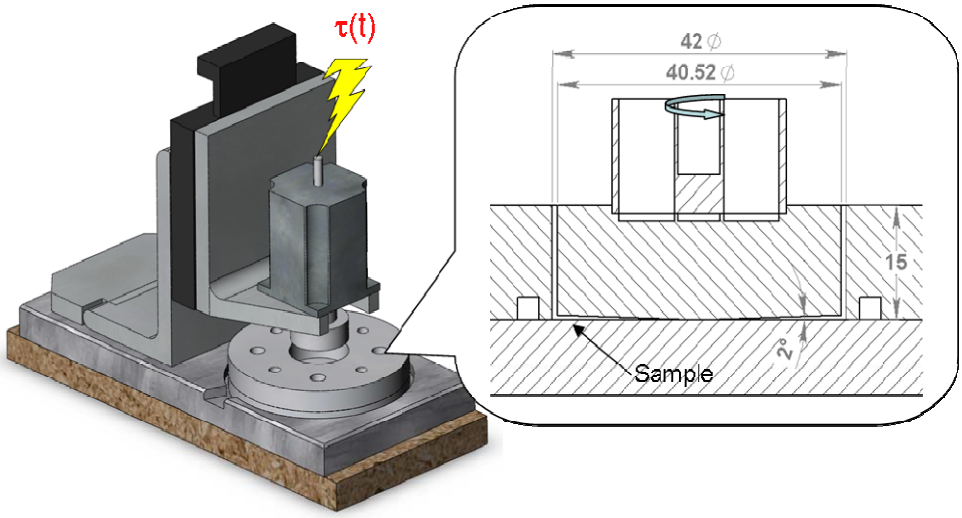

Figure 3.2. The Hemodynamic Shearing Device (HSD), a computer-controlled cone-plate and Couette viscometer that is capable of emulating dynamic shear stress conditions.

3.6 Effect of Shear Stress and Duration on Platelet Activation Rate (PAR)

3.6.1 Role of Low Shear Stress Exposure Time and Platelet Count in Shear-Induced Platelet Activation

In prior experiments with exposure of platelets to repeated square and triangular shear stress waveforms [68], it was observed that extending the low shear stress period between peaks resulted in a lower PAS at progressive time points when compared to the most dynamic condition (i.e. shortest low shear stress period). It was hypothesized that platelet activation is dependent on duration of the low shear stress period between high shear stress peaks, and that this behavior is more pronounced at higher platelet counts. The latter was anticipated as a result of an earlier study that showed that platelets at a count of 200,000/µl had a significantly higher

platelet activation rate than those at 20,000/μl when exposed to a constant shear stress of 9 dyne/cm^2 through a capillary flow loop over a 42-min period [67].

Platelets were prepared from fresh whole blood as described earlier (Section 3.1) and diluted to a count of 20,000/μl or 100,000/μl in platelet buffer prior to experiments. Triangular waveforms (Fig. 3.3) were programmed and applied in the HSD (Fig. 3.2). For each waveform, the baseline and peak shear stresses were 1.5 and 100 dyne/cm^2, while the total acceleration and deceleration time was 1 s. The low shear stress exposure time (T_{low}) was either 10 s or 60 s. Since the HSD can only achieve peak shear stresses of 70 dyne/cm^2 at a platelet mixture viscosity of 1 cP, dextran (90-95% purity, MW ≈ 5 million Da, Sigma-Aldrich, St. Louis, MO) was introduced to increase the viscosity to 3 cP, shifting the shear stress ceiling to 210 dyne/cm^2. This resultant viscosity was close to the accepted whole blood viscosity of 3.5 cP. Samples for the PAS assay (Section 3.2) were removed every 3 minutes. The total experimental duration was 30 min. PAS values were normalized against sonication for each experiment, as described in Section 3.2, and plotted to obtain a best-fit line. Platelet activation rate (PAR) was determined from the linear slope for each experiment. Four comparisons were performed: (1) Variable counts at T_{low} = 10 s, (2) variable counts at T_{low} = 60 s, (3) variable T_{low} at 100,000/μl and (4) variable T_{low} at 20,000/μl.

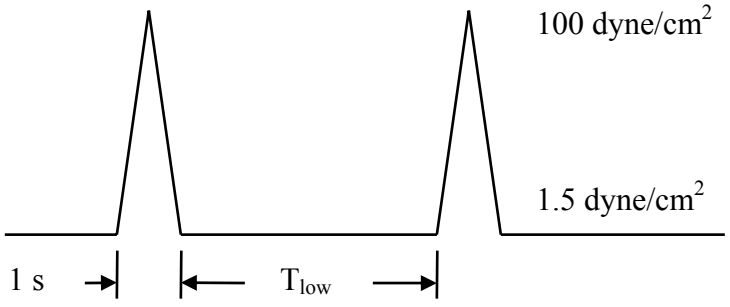

Figure 3.3. Triangular shear stress waveform to mimic flow conditions in generic devices. Low shear stress periods were either 10 or 60 s in length.

3.6.2 Platelet Activation Behavior after Single Exposure to High Shear Stress

To determine platelet activation behavior after exposure to a single dose of high shear stress, platelets at a count of 20,000/μl were exposed in the HSD to a shear stress waveform consisting of a high shear stress phase, 70 dyne/cm^2 for 40 s, and subsequent low shear stress, 1 dyne/cm^2, for 59 min [106]. PAS was quantified at 0 min, immediately after high shear stress exposure, every 3 min until 15 min, and then every 15 min thereafter, for a total experimental duration of 60 min. A 1 dyne/cm^2 shear stress exposure for 60 min was used as the negative control. Normalized PAS values immediately after the high shear stress period through 60 min were fitted to a straight line to determine the PAR.

3.6.3 Dependence of Post-High Shear Platelet Activation on Shear Stress Magnitude and Duration

Prior studies have shown the existence of a shear-induced platelet activation threshold (Section 2.4). However, such a threshold has not been indicated for the platelet activation rate (PAR). The elucidation of such is important, particularly for platelet activation models that depend on the shear stress history of platelets.

Platelets were prepared and diluted to 20,000/μl as previously described and exposed to a single dose of high shear stress [106]. The shear stress waveform started at 1 dyne/cm^2 for 15 s to allow for initial platelet sampling, followed by a high shear phase of a given duration, after which platelets were exposed to 1 dyne/cm^2, for a total experimental duration of 15 min (Fig. 3.4). The acceleration/deceleration rate was fixed at 89.96 dyne/cm^2·s for all cases. The

maximum time required for acceleration/deceleration for this high shear stress phase was 0.767 s.

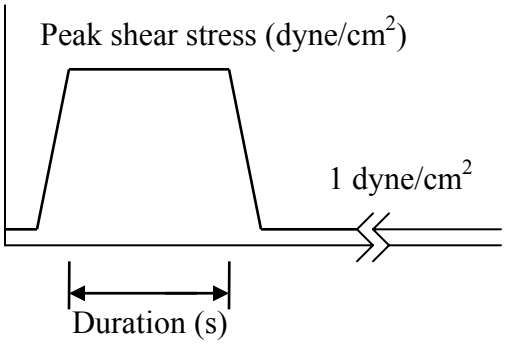

Figure 3.4. Schematic of waveform to study platelet activation after high shear stress exposure. Platelets were pre-exposed to a single dose of high shear stress of pre-defined duration, followed by 1 dyne/cm^2.

First, the role of shear stress magnitude was examined. Platelets were exposed for 40 s to a high shear stress magnitude ranging from 20 dyne/cm^2 to 70 dyne/cm^2. Second, the role of high shear stress duration was examined by exposing platelets to 70 dyne/cm^2 for periods ranging from 5 s to 40 s. For comparison, the accepted pathological shear stress level is 50 dyne/cm^2 [12]. For both sets of experiments, the negative control was 15 min-exposure to 1 dyne/cm^2. For each day of experiments, each case from the set (either magnitude or duration) was tested at least once. Platelet samples for the PAS assay were withdrawn at 0 min, 40 s, 3 min, and then every 3 min thereafter. PAS values from 40 s to 15 min for each experiment were fit to a line, and PAR was determined from the slope of this line.

3.7 Effect of Very High Shear Stress on Post-Exposure Platelet Activation

While the shear stress conditions in Section 3.6 are appropriate for examining platelet activation response to integral shear stress exposure (combination of shear stress and duration), they do not describe what happens after a single exposure of a platelet through a very high shear

stress region for a duration on the order of milliseconds, as may be found for platelets passing through the hinge of an MHV (Section 2.2).

Since the HSD is not capable of achieving such high shear stresses without the addition of a viscogen, a new device was necessary. A syringe-capillary pump (Fig. 3.5) answered this need. The pump (PSD/8, Hamilton, Reno, NV) was composed of 2 stepper motors: one that drove the 5 mL glass syringe with a Luer fitting (Hamilton, Reno, NV) via a connected plunger and the other which controlled the opening and closing of the input/output valves. The valve response time was on the order of milliseconds. With the exception of the syringe, all blood-contacting surfaces were composed of PVC or PTFE, which do not interact with and activate platelets. Platelets were exposed for very brief durations to the ceramic valve ports, which have minimal activation effects on platelets. The glass syringe was coated with Sigmacote (Sigma-Aldrich, St. Louis, MO) daily. Platelets were drawn from and collected in polyethylene conical tubes. Connection tubing was 18G PTFE (1.2 mm) in diameter, except for the tubing in which platelets were subject to high shear stress, and obtained from Small Parts or Fisher Scientific (Pittsburgh, PA). The high-shear test tubing was 28G (0.4 mm) in diameter. Downstream of the exit valve port (Port 5), a pressure transducer (range: 0 – 100 psi, Omega Engineering Inc., Stamford, CT) was mounted to measure the pressure drop across the length of the test tubing. This was to ensure that the pressure did not exceed 100 psi, the limit for the valve ports. The commands for the pump were programmed in LabView 9 (National Instruments, Austin, TX) and transferred via an RS-232 port. Pressure measurements were collected into LabView via a USB data acquisition (DAQ) device (National Instruments, Austin, TX).

Wall shear stress, τ_w, was pre-selected, and the volumetric flow rate (Q) was determined using:

$$\tau_w = 4\mu Q / \pi r^3 \tag{3.2}$$

where μ is the viscosity, 1 cP, and r is the radius of the tubing, 0.1835 mm. The length, l, of the tubing was determined using:

$$l = Qt_{\exp} / \pi r^2 \tag{3.3}$$

where t_{exp} is the duration of high shear stress exposure, also pre-defined. Reynolds' number, Re, was calculated using:

$$\mathrm{Re} = 2\rho V r / \mu \tag{3.4}$$

where ρ is the density, 1,000 kg/m^3, and V is the mean velocity as calculated by dividing Q by the diameter, $d = 2r$. To verify that the flow was fully developed, the capillary entrance length, l_e, was calculated, assuming laminar flow and large Re:

$$l_e = 0.06\,\mathrm{Re}\,d \tag{3.5}$$

Since τ_w is only appropriate when the platelets flow along the wall, an average shear stress, τ_{avg}, was calculated for this study, where platelets are assumed to be uniformly distributed across the cross-section of the capillary. This was because of the absence of red blood cells driving the core flow and marginalization of platelets, as in the Fahraeus effect. Knowing that the shear stress decreases linearly from a maximum at the wall (τ_w) to 0 at the center, the average shear stress was calculated as:

$$\tau_{avg} = 0.5\tau_w \tag{3.6}$$

Prior to every experiment, the syringe and test tubing were washed once with platelet buffer. This ensured that all surfaces were wetted and that no air gaps, which may perturb and activate platelets, were present. After shear stress exposure, all platelet-contacting surfaces were

washed once with 0.5% SDS + 50 mM NaOH, then at least twice with ddH_2O, and finally with air to remove any ddH_2O remaining.

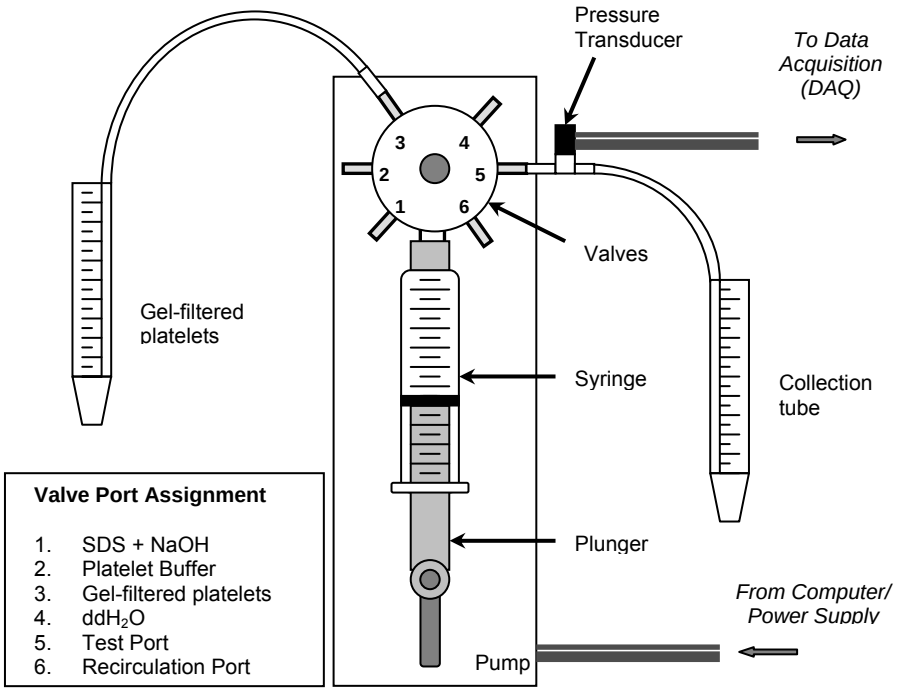

Figure 3.5. Syringe-capillary pump for very high shear stress exposure.

All experiments were done at 37°C. A platelet count of 20,000/μl was used. Platelets were drawn (through Port 3) into the syringe at a low flow rate, to ensure no shear-induced activation occurred. The volume drawn was equivalent to the desired collection volume (2.5 ml) plus the dead volume in the test tubing. Platelets were ejected through Port 5 into a collection tube at a flow rate that produced the desired average shear stress and exposure time for a given platelet in the tubing. The exposure time was defined as the dead volume in the tubing divided by the flow rate. For repeated passage experiments, collected platelets were drawn into the syringe (through Port 6) at $\tau_{av} = 50$ dyne/cm^2 and an exposure time of 161 ms, and the ejection and re-entry cycle was repeated until the desired number of passages was attained. Collected platelets were then exposed to 0.5 dyne/cm^2 for 10 min in the HSD. Samples for the PAS assay

were taken prior to shear exposure in the syringe-capillary viscometer, immediately after ("0 min") and then every 2 min. As in Section 3.6.2, PAS values were normalized against sonication values and the PAR was determined from the slope of a best-fit line. The control for all experiments was exposure of platelets to 0.5 dyne/cm^2 for 10 min without initial very high shear stress exposure.

3.7.1 Single Very High Shear Stress Exposure

Three average shear stress conditions were selected for the single passage exposure: (1) 1,000 dyne/cm^2 for 25 ms, (2) 500 dyne/cm^2 for 50 ms, and (3) 250 dyne/cm^2 for 100 ms. Condition (1) was selected as the upper limit since pressures exceeding approximately 80 psi caused the tubing joints to fail. It is important to note that the integral shear stress, or product of shear stress and exposure time, in all three cases is 25 dyne s/cm^2. These values are in the approximate range of shear stresses and exposure times that platelets experience when passing through the hinge region of an MHV (Section 2.2). The length of the 28G tubing that provided the selected combination of average shear stresses and exposure times was 22.95 cm.

3.7.2 Repeated Very High Shear Stress Exposure

The effect of repeated passages through high shear stress regions was examined using the 500 dyne/cm^2, 50 ms condition in the manner described in Section 3.10. Platelets were exposed from 10 to 80 repeats, followed by 10 min exposure to 0.5 dyne/cm^2. The total duration of the very high shear stress repeats ranged from 1 min to 8 min. As before, the length of the 28G test tubing that provided the high shear stress condition was 22.95 cm, while tubing through which platelets were returned to the syringe had a 18G diameter and length of 25.05 cm. The latter was

placed with its opening near the bottom of the collection tube so that no air gaps were present during the re-entry phase.

3.7.3 Repeated Low Shear Stress Exposure

Platelets were exposed repeatedly to an average shear stress of 15 dyne/cm^2 for 80 s, punctuated by 161 ms exposure to 50 dyne/cm^2, to recreate integral shear stresses on the order of magnitude of that found for experiments conducted in the HSD (Sections 3.6.2-3). This was done to examine if there was a difference in PAS and PAR values due to the device used. Two to 10 repeats were done for this condition, followed by 10 min exposure to 0.5 dyne/cm^2. Total duration for exposure in the syringe-capillary viscometer ranged from 7 min to 29 min. The length of the 28G diameter test tubing was 11 m.

3.8 Effect of Platelet Count and Activity Level on Post-High Shear Activation

Prior examination of the role of platelet count has shown that platelets at a physiological concentration of 200,000/µl exhibit a quadratic increase in PAS when exposed to constant shear stress in a capillary flow loop, whereas platelets at a lower count of 20,000/µl show a linear and significantly lower rate of increase in PAS [67]. This indicates a potential for platelet-platelet "crosstalk". However, it is not known if the same behavior holds for platelets exposed to subsequent low shear stress. In the present study, platelets were diluted to either 20,000/µl or 150,000/µl, exposed to 70 dyne/cm^2 for 40 s, followed by 1 dyne/cm^2 for a total duration of 15 min [106]. Platelets were sampled for the PAS assay at a final concentration of 5,000/µl as described in Section 3.1. PAR was determined post-high shear exposure in the manner elaborated earlier (Section 3.6.2).

In a variation of the platelet-platelet "crosstalk" experiment, the effect of activated platelets on quiescent (non-exposed) platelets was also studied. Platelets at 20,000/μl count were sheared at 60 dyne/cm^2 for 40 s, whereupon quiescent platelets were added to increase the overall concentration to 40,000/μl. The combined mixture was subsequently exposed to 1 dyne/cm^2 for 15 min. The positive control was the condition in which no quiescent platelets were added those exposed to the high shear stress, whereas the negative control was the condition where quiescent platelets (at a count of 40,000/μl) were exposed to 1 dyne/cm^2 for 15 min. PAS was quantified at a final platelet concentration of 5,000/μl as previously described, and PAR was determined by calculating the slope of the best-fit line from 3 min to 15 min.

3.9 Role of Lysis and Microparticles in Post-High Shear Platelet Activation

High shear stress has been shown to promote platelet lysis and cause release of intracellular components found in the α- and dense-granules which contribute to platelet activation and aggregation [61, 75]. Platelets at 20,000/μl were exposed to 70 dyne/cm^2 for 40s, followed by 1 dyne/cm^2, for a total duration of 15 min. PAS and PAR were determined post-high shear exposure as previously described. Platelet lysis was measured by the release of cytoplasmic lactate dehydrogenase (LDH), using a Cytotoxicity Detection Kit (Roche Applied Science, Indianapolis, IN, USA) in combination with a microplate reader [106]. LDH absorbance values were normalized against values for fully lysed platelets treated with the provided lysis reagent. Net lysis values were obtained by subtracting the baseline values at each time point (platelet buffer) from the lysis values for sheared platelets. The platelet lysis rate was determined by calculating the slope of a best-fit line for the LDH data in the post-high shear exposure period.

High shear stress has been shown to produce platelet-derived microparticles (PMPs), which are formed by microvesiculation and retain some procoagulant properties of platelets [107-112]. PMPs have been implicated in persistent platelet activation among patients with cardiovascular diseases [113, 114]. Therefore, it was important to examine the role these play in the post-high shear exposure platelet activation. Platelets were prepared and exposed to 70 dyne/cm^2 for 40 s as previously described. Platelets were aspirated from the HSD immediately after the high shear stress phase and centrifuged at 500 g (sample height = 1 cm) for 90 s. These settings were chosen since they yielded 85-90% platelet pelleting, as verified by counting the platelets in the supernatant (Z1 Counter, Coulter, Miami, FL). The supernatant, including any PMPs, was assayed immediately after high shear stress exposure. Then, the supernatant was exposed for an additional 14 min to 1 dyne/cm^2 and assayed again at the conclusion of the experiment. Microparticle PAS values were compared to those obtained for platelets which had been exposed to the high and subsequent low shear stress without removal [106].

3.10 Effect of Platelet Agonists and Inhibitors on Post-High Shear Activation

During physiological circulation, platelets pass through a variety of shear stress regions, with time-averaged shear stresses ranging from less than 1 dyne/cm^2 in the veins to 60 dyne/cm^2 in the arterioles [12]. While exposure to oscillatory shear stresses such as these contribute to platelet activation [65], endothelial cells restore the hemostatic balance by secreting platelet inhibitory products, such as prostacyclin (PGI_2), to compete with platelet-released agonists, such as thromboxane A2 (TXA_2) [12]. In addition, plasma membrane-bound enzymes, such as apyrase, scavenge for agonists such as adenosine diphosphate (ADP) [115]. In cases of vascular injury or exposure to pathological shear stress regions, including stenoses for patients with

coronary artery disease (CAD) and damage from MHVs, platelets are exposed to agonists such as thrombin and collagen, and the resultant thrombin generation overrides normal hemostatic responses to allow platelets to activate, aggregate, and form a hemostatic plug or clot [12]. While microparticle production in the presence of agonists [116] and platelet activation in the presence of inhibitors [67] have been studied under flow conditions, there is a scarcity of information regarding platelet activation when shear stress exposure is combined with platelet agonists and inhibitors.

3.10.1 Platelet Aggregation with Combined Shear Stress and Platelet Agonist/Inhibitor Exposure

Prior to shear stress activation experiments, platelet agonists and inhibitors were tested with platelet aggregation studies. PRP was prepared from whole blood as previously described (Section 3.1) and diluted to 150,000 platelets/μl in platelet-poor plasma. Platelet-poor plasma was obtained by centrifuging PRP at 5,600 g for 30 s and discarding the platelet pellet. For GFP studies, platelets were prepared as described earlier (Section 3.1) and diluted to 150,000/μl in platelet buffer. Aggregation studies were performed in an aggregometer (Model 560-VS, Chrono-Log Corporation, Havertown, PA) at 37°C, with either platelet-poor plasma (for PRP studies) or platelet buffer (for GFP studies) as the background control. Test solution cuvettes had a final volume of 400 μl and optical readings were performed under turbidometric conditions. For GFP aggregation studies lacking plasma, 0.5 mg/ml (final) fibrinogen was added to the GFP test cuvette. Daily controls with 30 μM ADP were conducted for all cases. In all platelet agonist cases, optical readings were performed for 1 min prior to addition of the agonist, to ensure a level baseline. After the addition of the agonist, optical readings were recorded for 5 min or when the plotted curve leveled off. For analysis, the slope for the first 60 s after the

initial shape change was measured. In addition, the overall amplitude after the initial shape change was recorded.

Platelet aggregation readings in GFP were conducted for 3 agonists: thrombin receptor activating peptide (TRAP, synonym: SFLLRN-NH_2, Sigma-Aldrich, St. Louis, MO), collagen (type I fibrils, Chrono-Log Corporation, Havertown, PA), and arachidonic acid (Sigma-Aldrich, St. Louis, MO). TRAP was prepared into 800 μM stock solution by diluting the provided powder in ddH_2O. A final concentration of 20 μM was used for the aggregation study, based on trial runs in GFP indicating that the selected concentration was the lowest value that produced a significant aggregation curve. Collagen was obtained as a 1 mg/ml suspension of fibrils in isotonic glucose solution of pH = 2.7, with a final concentration of 10 μg/ml used in experiments. Prior studies showed this concentration was sufficient to cause significant aggregation, although not microparticle formation [116, 117]. A 100 mg/ml solution of arachidonic acid in DMSO was diluted to a final concentration of 0.5 mM for experiments, as determined by trial aggregation runs. The TXA_2 mimetic, U-46619 (Sigma-Aldrich, St. Louis, MO), was initially used in place of arachidonic acid, but it showed rapid disaggregation behavior after initial aggregation in GFP and was excluded from the experiments.

PRP aggregation trials were conducted for 2 platelet inhibitors to verify their activity in unsheared platelets: apyrase (synonym: ATPase, Sigma-Aldrich, St. Louis, MO) and prostacyclin (PGI_2, Sigma-Aldrich, St. Louis, MO). The provided apyrase powder was dissolved to a concentration of 2 mg/ml in HBS: 1% BSA + 0.1 mM EDTA, with a final concentration of 1 unit (U)/ml for experiments. PGI_2 was prepared 1 mM in DMSO solution, with a 1 μM final experimental concentration. The positive control for both inhibitors was unsheared platelets treated with 30 μM ADP.

Platelet aggregation was observed with and without pre-exposure to 70 dyne/cm^2 for 40 s. Platelets were sheared in the HSD as previously described (Section 3.6.2) and 400 µl samples were added to cuvettes immediately after the high shear exposure. Platelets were incubated with 0.5 mg/ml fibrinogen for 1 min, whereupon the agonist was added, and readings were commenced as described earlier.

3.10.2 Platelet Activation after High Shear Stress and Agonist Exposure

The ability of platelet agonists to modulate the activation behavior of platelets during the low shear stress phase following initial high shear stress exposure was examined. GFP were prepared as described previously (Section 3.1) and diluted to 150,000/µl, with 3 mM $CaCl_2$ (final) added 10 min prior to experiments. The agonist (20 µM TRAP, 10 µg/ml collagen, or 0.5 mM arachidonic acid) was added to the GFP and gently mixed for approximately 10 s. The mixture was placed in the HSD and exposed to 1 dyne/cm^2 for 3 minutes to allow sufficient time for the agonist to interact with platelets. Then, the shear stress was increased to 70 dyne/cm^2 for 40 s, followed by 1 dyne/cm^2 for an additional 14 min, for a total experimental duration of 18 min. Samples for the PAS assay (Section 3.2) were taken at 0 min, 3 min, after the high shear phase, 6 min, and every 3 min thereafter. PAS values were normalized against sonication values (Section 3.2) and PAR values were determined from the post high-shear exposure PAS values as described previously (Section 3.6.3). The control for each agonist was shear stress exposure without the agonist, but with the addition of the vehicle for the agonist. For TRAP and collagen, an equal volume of platelet buffer was added, while for arachidonic acid, an equal volume of DMSO was added. The final percentage of DMSO, 2.5%, does not increase PAS values when compared to samples without DMSO.

3.10.3 Platelet Activation after High Shear Stress and Inhibitor Exposure

The ability of platelet inhibitors to modulate the activation behavior of platelets during the low shear stress phase following initial high shear stress exposure was examined. GFP were prepared as described previously (Section 3.1) and diluted to 100,000/μl in the case of the ADP scavenger apyrase, 150,000/μl for PGI_2, and 20,000/μl for the intracellular Ca^{2+} inhibitor BAPTA-AM. Apyrase (1 U/ml) and PGI_2 (1 μM) were prepared as previously described (Section 3.9.1), and added and gently mixed with GFP immediately prior the experiment [106]. Platelets for experiments involving intracellular Ca^{2+} depletion were prepared by gel-filtration in platelet buffer without bovine serum albumin, which interferes with the Ca^{2+} inhibitor treatment. GFP was obtained (Section 3.1) and then split into two samples of equal volume, where one was preloaded with 20 μM BAPTA-AM (Sigma-Aldrich, St. Louis, MO) and the other was defined as the control. Both samples were incubated at 37°C for 30 min and gel-filtered separately through two columns (to ensure identical secondary filtration), to remove solution-phase BAPTA.

Apyrase- and BAPTA-treated platelets were exposed to 70 dyne/cm^2 shear stress for 40 s, followed by 1 dyne/cm^2 for 14 min, whereas PGI_2-treated platelets were initially pre-exposed to 1 dyne/cm^2 for 3 min, followed by the high shear stress and subsequent low shear stress exposure. Samples for the PAS assay (Section 3.2) were taken at 0 min, after the high shear phase, 3 min, and every 3 min thereafter for apyrase and BAPTA-treated platelets, while samples for the PGI_2-treated platelets were taken in the manner described for the agonists (Section 3.9.2). PAS values were normalized against sonication values (Section 3.2) and PAR values were determined from the post high-shear exposure PAS values as described previously (Section

3.6.3). The control for each inhibitor was shear stress exposure without the inhibitor, but with the addition of the delivery vehicle. For apyrase, an equal volume of HBS: 1% BSA + 0.1 mM EDTA was added, while for PGI_2, an equal volume of DMSO was added. The final percentage of DMSO, 2.5%, does not increase PAS values when compared to samples without DMSO. However, a slight, but non-significant increase in PAS values was noted for samples with HBS: 1% BSA + 0.1 mM EDTA. The control for BAPTA-treated platelets was untreated platelets which had undergone a secondary filtration as previously described.

3.11 Platelet Variability Statistics

All PAS results were analyzed in terms of the platelet activation rate, or the slope of the line fit to PAS values after high shear stress exposure. The use of a straight line as opposed to a higher-order curve was justified using the Pearson's chi-square test:

$$\chi^2 = \sum_{i=1}^{n} (O_i - E_i)^2 / E_i \tag{3.7}$$

where O_i is the observed PAS value and E_i is the expected PAS value based on the linear or polynomial fit. The χ^2 value is divided by N-1 degrees of freedom, where N is the total number of observations. A lower χ^2 value yields a better fit. In most cases, the χ^2 for the polynomial fit was slightly lower than or equivalent to the value for the linear fit, and therefore the linear fit was adopted across all experiments. For all experiments, PAS values are presented with standard error (SEM) bars. Experiments whose platelet activation rates fell outside the 95% confidence interval (i.e. 2 standard deviations) were not included in the statistical analyses.

The selection of parametric tests (such as Student's t-test and one-way ANOVA) is dependent on the normal distribution of platelet activation rates. For all experiments, normal

distribution of rates for each unique condition was verified using the Shapiro-Wilk test. Independent samples Student's t-test was used when only two groups were being compared, while one-way ANOVA with Tukey's *post hoc* test was performed when more than two groups were compared. For microparticle experiments, statistical analysis was performed on the PAS values. In all cases, the significance level, α, was 0.05. For the lysis experiments, PAR was correlated with the platelet lysis rate using Pearson's correlation coefficient. All statistical analyses were performed in SPSS 18.0 (SPSS Inc., Chicago, IL).

3.12 Development of a Platelet Activation Model

As described earlier (Section 2.3), device manufacturers use hemolysis rather than platelet activation to optimize their products due to the scarcity of experimentally-based predictive models for the latter. Several groups, including our own, have attempted to address this paucity by deriving such phenomenological models, but they are limited in that they are device-dependent or do not fully account for the dynamic nature of the shear stresses applied to platelets [2, 68]. According to Grigioni, any formulation for phenomenological blood cell trauma should account for the following conditions [102]:

Condition 0 – It must not clash with the principle of causality, where decreasing shear stress does not reduce the damage due to mechanical loading [101].

Condition 1 – It reproduces what the equation $Damage = C\tau^{\alpha}t^{\beta}$ predicts when a uniform mechanical load is acting on the cells, since it is based on rigorous experimental validation.

Condition 2 – It must account for the previous load history sustained by the cells.

Based on these conditions two general models were derived using the simple phenomenological (Section 3.12.1) and Grigioni (Section 3.12.2) approaches, respectively. The

latter is so-called because it follows the steps established in an earlier publication [102]. In addition, a variation of both models, the two-step optimization approach (Section 3.12.3), was also studied.

3.12.1 Simple Phenomenological Model

In the above conditions, damage was taken to mean red blood cell damage, but it may be extrapolated to indicate platelet lysis or platelet activation as well. Thus, the equation in Condition 1 was selected as the starting equation for the model:

$$PAS(\tau,t) = C\tau^{\alpha}t^{\beta} + PAS_0 \tag{3.8}$$

where the platelet activation state, *PAS*, is dependent on the shear stress, τ, and exposure time, *t*. The constants *C*, α, and β are derived from the optimization of Eq. 3.8 to experimental data, where PAS_0 is the platelet activation state at the start of the experiments. While this satisfies Condition 1, it does not account for the potential decrease in stress (Condition 0) or the loading history of the platelets (Condition 2). Thus Eq. 3.8 was expanded (Appendix B1) and the following equation was derived:

$$PAS(\tau,t) = C\tau^{\alpha}t^{\beta} = C\underbrace{\int_{t_0}^{t_{total}} \beta t^{\beta-1}\tau^{\alpha}dt}_{\text{Constant shear stress}} + C\underbrace{\int_{t_0}^{t_{total}} \alpha\tau^{\alpha-1}t^{\beta}\,\dot{\tau}dt}_{\text{Shear loading rate}} + \underbrace{PAS_0}_{\substack{\text{Prior activation}\\ \text{history}}} \tag{3.9}$$

where t_{total} is the total duration of the experiment and $\dot{\tau}$ is the shear loading rate. In discrete form, Eq. 3.9 becomes:

$$PAS(\tau,t) = C\beta\sum_{i=1}^{n} t_i^{\beta-1}\tau_i^{\alpha}\Delta t_i + C\alpha\sum_{i=1}^{n}\tau_i^{\alpha-1}t_i^{\beta}\left|\tau_i - \tau_{i-1}\right| + PAS_0 \tag{3.10}$$

The absolute value of the difference between two shear stresses is taken for the shear loading rate to ensure that a negative loading rate does not decrease the overall PAS value. Thus, all 3 conditions listed above were satisfied. Eq. 3.10 is similar to the model derived in our lab previously, but does not assume that the constants C, α, and β are equal to 1 [89]. It is important to note here that Eq. 3.10 and all prior models are phenomenological and not based on any platelet mechanistic model. This implies that platelet activation is driven purely by shear stress, exposure time, and shear loading rate. While shear-induced platelet activation is more complex (Section 2.1), prior phenomenological models show a good fit between experimental results and predicted platelet damage or activation [68, 92].

3.12.2 Grigioni Model

While it addresses the shear loading rate that previous models [68, 102] neglect, Eq. 3.9 does not truly satisfy Condition 2 for blood damage formulations. While PAS_0 is taken into account, it does not have an impact on the effect of loading at each interval an experimental observation is made. Thus, the Grigioni approach [102], with modifications for PAS [68], was followed to derive a model that is inclusive of the shear loading rate. Differential analysis was performed on Eq. 3.8 (Appendix B2) to obtain the Grigioni model with shear loading rate:

$$PAS = C\beta\left[\int_{t_0}^{t_{total}}\left(\int_{t_0}^{t_{total}}\tau(\xi)^{\alpha/\beta}d\xi+\alpha/\beta\int_{\tau(t_0)}^{\tau(t_{total})}\xi\cdot\tau(\xi)^{\alpha/\beta-1}d\tau+D(t_0)\right)^{\beta-1}\tau^{\alpha/\beta}dt\right.$$
$$\left.+\int_{\tau(t_0)}^{\tau(t_{total})}\alpha/\beta\left(\int_{t_0}^{t_{total}}\tau(\xi)^{\alpha/\beta}d\xi+\alpha/\beta\int_{\tau(t_0)}^{\tau(t_{total})}\xi\cdot\tau(\xi)^{\alpha/\beta-1}d\tau+D(t_0)\right)^{\beta-1}t\cdot\tau^{\alpha/\beta-1}d\tau\right] \quad (3.11)$$

C, α, and β are constants, while $d\tau$ is the change in shear stress for a given time interval. The inner integral of the double integral represents mechanical dose D (Appendix B2) applied over a

time ξ, whereas the outer integral is the summation of these doses over the duration of the experiment. The latter also refers to the time points for experimental observations. The term $D(t_0)$ refers to initial dose response ($t_0 = 0$) and is given by the expression:

$$D(t_0) = \left(\frac{PAS(t_0)}{C} \right)^{1/\beta} \tag{3.12}$$

The outer integral in Eq. 3.11 consists of two parts, where the former describes the effect of constant shear stress and the latter shows the effect of shear loading. Since experimental measurements for PAS were only done during constant shear stress periods, the second part of Eq. 3.11 can be omitted:

$$PAS = C\beta \left[\int_{t_0}^{t_{total}} \left(\underbrace{\int_{t_0}^{t_{total}} \tau(\xi)^{\alpha/\beta} d\xi}_{\text{Constant shear stress}} + \alpha/\beta \underbrace{\int_{\tau(t_0)}^{\tau(t_{total})} \xi \cdot \tau(\xi)^{\alpha/\beta - 1} d\tau}_{\text{Shear loading rate}} + \underbrace{\left(\frac{PAS(t_0)}{C} \right)^{1/\beta}}_{\text{Prior activation history}} \right)^{\beta - 1} \tau^{\alpha/\beta} dt \right] \tag{3.13}$$

The above equation is the Grigioni approach to PAS, with a shear loading improvement over prior platelet activation models [68]. In discrete form, the equation becomes:

$$PAS = C\beta \sum_{i=1}^{N} \left(\sum_{j=1}^{i} \tau(t_j)^{\alpha/\beta} \Delta t_j + \alpha/\beta \sum_{j=1}^{i} t_j \cdot \tau(t_j)^{\alpha/\beta - 1} \left| \Delta \tau_j \right| + \left(\frac{PAS(t_0)}{C} \right)^{1/\beta} \right)^{\beta - 1} \tau(t_i)^{\alpha/\beta} \Delta t_i \tag{3.14}$$

The *i*-th interval refers to experimental observation time points, while the *j*-th interval refers to time points where the mechanical loading changes. For example, in the experiments used for the optimization approach, the initial high shear stress loading had three distinct components: a linear ramping of shear stress, constant high shear stress, followed by a linear decrease in shear stress. Experimental PAS values were measured at the start of the first ramping phase ($PAS(t_0)$) and at the end of the decreasing shear stress phase ($PAS(t_1)$). Thus, there are 3 mechanical dose intervals (*j*) for the single observation interval (*i*). The absolute value of the shear loading

term $\Delta\tau_j$ was taken to avoid violating the principle of causality, i.e., reduction in shear stress does not cause a decrease in PAS.

3.12.3 Optimization Approach

Constants for Eqs. 3.10 and 3.14 were calculated using a Levenberg-Marquardt optimization scheme [118, 119] in MATLAB 7.5 (MathWorks, Natick, MA), where the difference between the model prediction and experimental results was minimized:

$$\begin{aligned} &\min_{\theta} f(x) = min(PAS_{exp} - PAS_{num}) \\ &s.t.\ \theta = \{C, \alpha, \beta\} \end{aligned} \tag{3.15}$$

Eqs. 10 and 14 were substituted for PAS_{num} for the simple and Grigioni approaches, respectively. Experimental PAS values were taken from the results at each time point of the variable high shear stress and duration experiments (Sections 3.6.2-3) for each unique combination of shear stress and exposure time. Shear stress, exposure time, and shear loading rate were input into Eq. 3.10 or Eq. 3.14 fore each experimental sampling point, with each successive equation inclusive of prior equations for each unique shear stress and exposure time combination. This resulted in 66 equations (Appendix B3-4). The control cases for the variable shear stress and duration experiments, consisting of constant 1 dyne/cm^2 exposure for 15 min, were not included due to their lack of a shear loading rate.

In order to reduce the dependence of optimized constants values on the starting values, the constant C was initialized at values between 0.05 and 1, with increments of 0.05, and α and β were initialized between 0.5 and 10, with increments of 0.5 between each value, such that:

$$C = [0.05, 1];\ \alpha = \beta = [0.5, 10] \tag{3.16}$$

This produced 20 initial values for each constant, resulting in 8,000 unique sets of the three constants. For each combination of constants, iterations were performed until the cumulative root-mean-square (RMS) error between the experimental and numerical PAS values was below 1 x 10^{-5} or when 2 x 10^{4} iterations were exceeded. The combination of constants that yielded the lowest cumulative error was selected for the final model [68]. If there were several combinations of constants that yielded the lowest error, the mean values and standard errors for all such constants were selected. The resultant model was plotted with its relevant experimental values on the same set of axes for the variable peak shear stress and variable peak shear duration experiments. Since complex values are possible due to the form of Eq. 14, such results were filtered from the resulting optimized constants.

3.12.4 Two-Part Optimization Approach

In the experiments with high initial shear stress exposure followed by subsequent low shear stress exposure (Section 3.6.3), a two-part behavior was anticipated. In the first part, we hypothesized that high shear stress exposure causes a small but distinct increase in PAS. In the subsequent low shear stress exposure, we anticipated that platelets exhibit a linear increase in PAS over the remainder of the experiment, even though the control case lacking the initial high shear stress exposure was not expected to exhibit such behavior. Thus the optimization routine for both the simple and Grigioni approaches were divided into 2 parts: the first addressed only the initial high shear stress exposure (i.e. “first equations” for each unique condition) and the second optimized the constants for the remaining time points while using the constants for the first part as inputs. For the simple phenomenological approach, the optimization routine was:

$$\min_{\theta} f(x) = \min(PAS_{exp} - PAS_{num})$$

$$s.t. \begin{cases} PAS_{num_1} = C_1\beta_1 t_1^{\beta_1 - 1}\tau_1^{\alpha_1}\Delta t_1 + C_1\alpha_1\tau_1^{\alpha_1 - 1}t_1^{\beta_1}\left|\tau_1 - \tau_0\right| + PAS_0 \\ \theta_1 = \{C_1, \alpha_1, \beta_1\} \\ PAS_{num_2} = PAS_{num_1} + C_2\beta_2\sum_{i=2}^{n} t_i^{\beta_2 - 1}\tau_i^{\alpha_2}\Delta t_i + PAS_1 \\ \theta_2 = \{C_2, \alpha_2, \beta_2\} \end{cases} \tag{3.17}$$

PAS_{num1} accounts for the constant shear stress and shear-loading rate effects of the initial shear stress phase, as well as the PAS at $t = 0$. PAS_{num2} accounts for the contributions of PAS_{num1}, subsequent constant low shear stress exposure, and PAS_1. The latter is the experimental value for PAS observed at the end of the high shear stress phase. The second part of this optimization approach does not include the shear loading rate term, as this only occurs during the initial high shear stress exposure for the experiments performed. The constants were selected as before (Eq. 3.16). A similar approach was taken for the Grigioni formulation (Eq. 3.14):

$$\min_{\theta} f(x) = \min(PAS_{exp} - PAS_{num})$$

$$s.t. \begin{cases} PAS_{num_1} = C_1\beta_1\left(\tau_1^{\frac{\alpha_1}{\beta_1}}\Delta t_1 + \frac{\alpha_1}{\beta_1}t_1\tau_1^{\frac{\alpha_1}{\beta_1}-1}\left|\Delta\tau_1\right| + \left(\frac{PAS_0}{C_1}\right)^{\frac{1}{\beta_1}}\right)^{\beta_1 - 1}\tau_1^{\frac{\alpha_1}{\beta_1}}\Delta t_1 \\ \theta_1 = \{C_1, \alpha_1, \beta_1\} \\ PAS_{num_2} = PAS_{num_1} + C_2\beta_2\sum_{i=2}^{N}\left(\sum_{j=2}^{N}\tau_j^{\frac{\alpha_2}{\beta_2}}\Delta t_j + \left(\frac{PAS_1}{C_2}\right)^{\frac{1}{\beta_2}}\right)^{\beta_2 - 1}\tau_i^{\frac{\alpha_2}{\beta_2}}\Delta t_i \\ \theta_2 = \{C_2, \alpha_2, \beta_2\} \end{cases} \tag{3.18}$$

IV. RESULTS AND ANALYSIS

4.1 Validation of the PAS Assay by Flow Cytometry

The PAS assay provided a quantitative measure of the ability of platelets to generate acetylated thrombin. Two cellular processes are associated with platelet activation: flipping of the membrane bilayer to provide anionic phospholipids on the outside for prothrombinase complex formation (Section 2.1) and the release of FVa from the α-granules to the membrane. These former is required for flow cytometric analysis with Annexin V, used in previous correlations of the PAS assay with flow cytometry [65]. Another useful marker of platelet activation is P-selectin (CD62P), a cell adhesion molecule stored in α-granules and released to the platelet surface upon activation for use in subsequent aggregation [23]. Expression is measured the fluorescence of a PE-labeled marker that binds selectively to CD62P.

Platelets at a count of 20,000/μl were exposed to 70 dyne/cm^2 for 40 s followed by 1 dyne/cm^2 for an additional 59 min (Section 3.6.2). Samples were taken for the PAS assay (Section 3.1) and flow cytometry (Section 3.4) at each time point and values were computed as described earlier. Normalized PAS values from the PAS assay were compared to their related CD62P expression from flow cytometry. For the two experiments conducted, a strong linear correlation was observed between the two values, despite the methods measuring different properties of platelets. It should be noted here that the PAS assay measures the bulk platelet activity, since the generated thrombin is in suspension, while flow cytometry measures the fraction of all platelets expressing CD62P. However, CD62P activity measurement is an improvement over prior correlation with Annexin V, in that platelets incubated with the latter

could not be fixed and the delay in performing flow cytometric analysis may have yielded residual Annexin V activity due to continuing platelet activation [65]. Thus, a much stronger correlation is observed between PAS and CD62P expression.

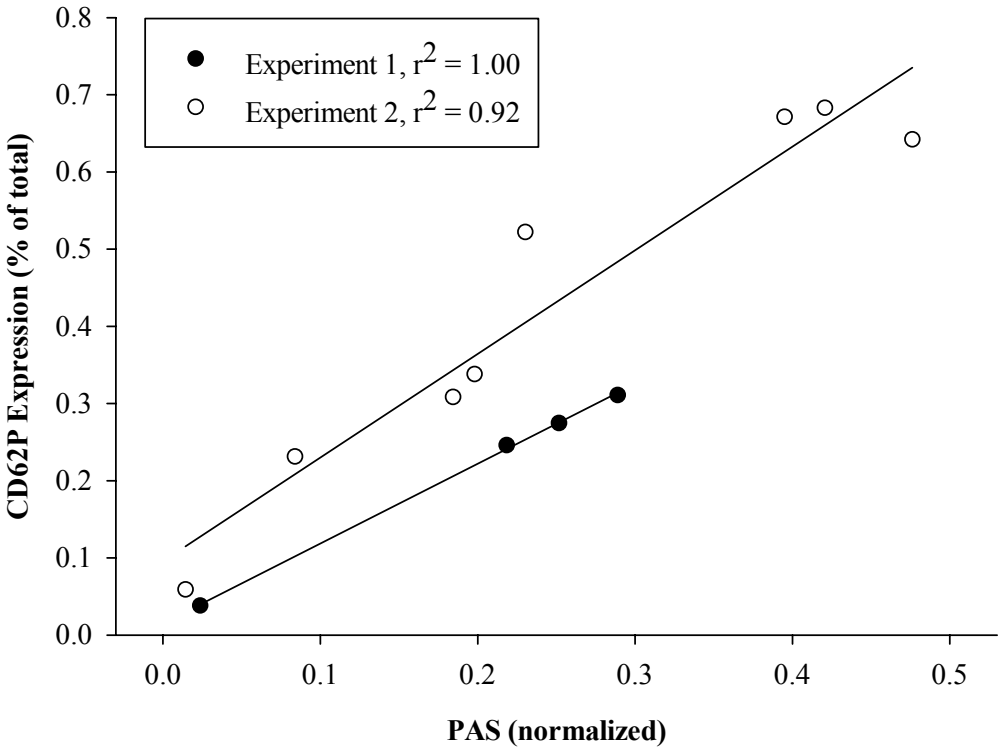

Figure 4.1. Correlation of PAS activity with flow cytometry (CD62P Expression) as measures of platelet activation. Platelets, 20,000/μl, were exposed to 70 dyne/cm^2 for 40 s, followed by 1 dyne/cm^2 for 59 min (n = 2).

4.2 Shear-Induced Platelet Activation – Role of Low Shear Stress Duration and Platelet Count

Platelets at two different counts were exposed to triangular shear stress waveforms with a peak shear stress of 100 dyne/cm^2 and baseline stress of 1.5 dyne/cm^2 and variable duration to determine if count and low shear stress exposure time play a role in the platelet activation rate (PAR). Platelets at a count of 20,000/μl or 100,000/μl were exposed to waveforms with low shear stress durations (T_{low}) of either 10 s or 60 s in the HSD, with platelet activation rates (PAR) determined from the slope of a best-fit line over the 30 min experimental duration (Section 3.6.1). For T_{low} = 10 s (Fig. 4.2a), PAR for 100,000 platelets/μl was more than 3-fold higher than

for 20,000 platelets/μl ($p < 0.05$). When the count was 100,000 platelets/μl (Fig. 4.3a), T_{low} = 10 s yielded a PAR that was 3-fold higher than that for T_{low} = 60 s ($p < 0.05$). However, significant difference was not observed between the PARs for the two counts at T_{low} = 60 s (Fig. 4.2b), nor was it observed for the two low shear stress exposure times at a count of 20,000/μl (Fig. 4.3b, $p > 0.05$).

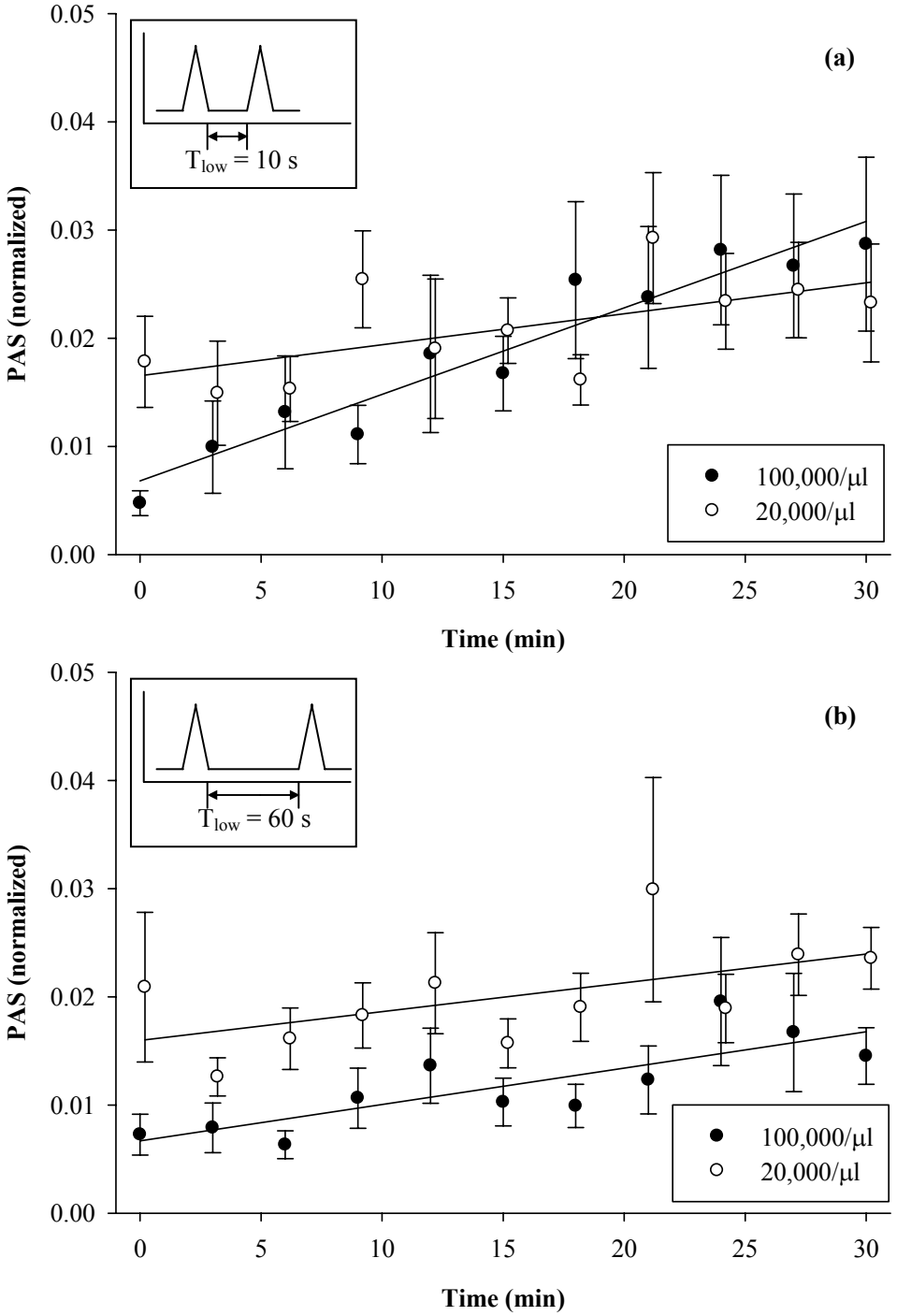

Figure 4.2. The effect of platelet count on platelet activation rate. Platelets were exposed to a triangular waveform with a peak of 100 dyne/cm^2 and low shear stress, 1.5 dyne/cm^2, with duration (T_{low}) of (a) 10 s or (b) 60 s. Statistical significance ($p < 0.05$) was observed at the 10 s low shear stress duration.

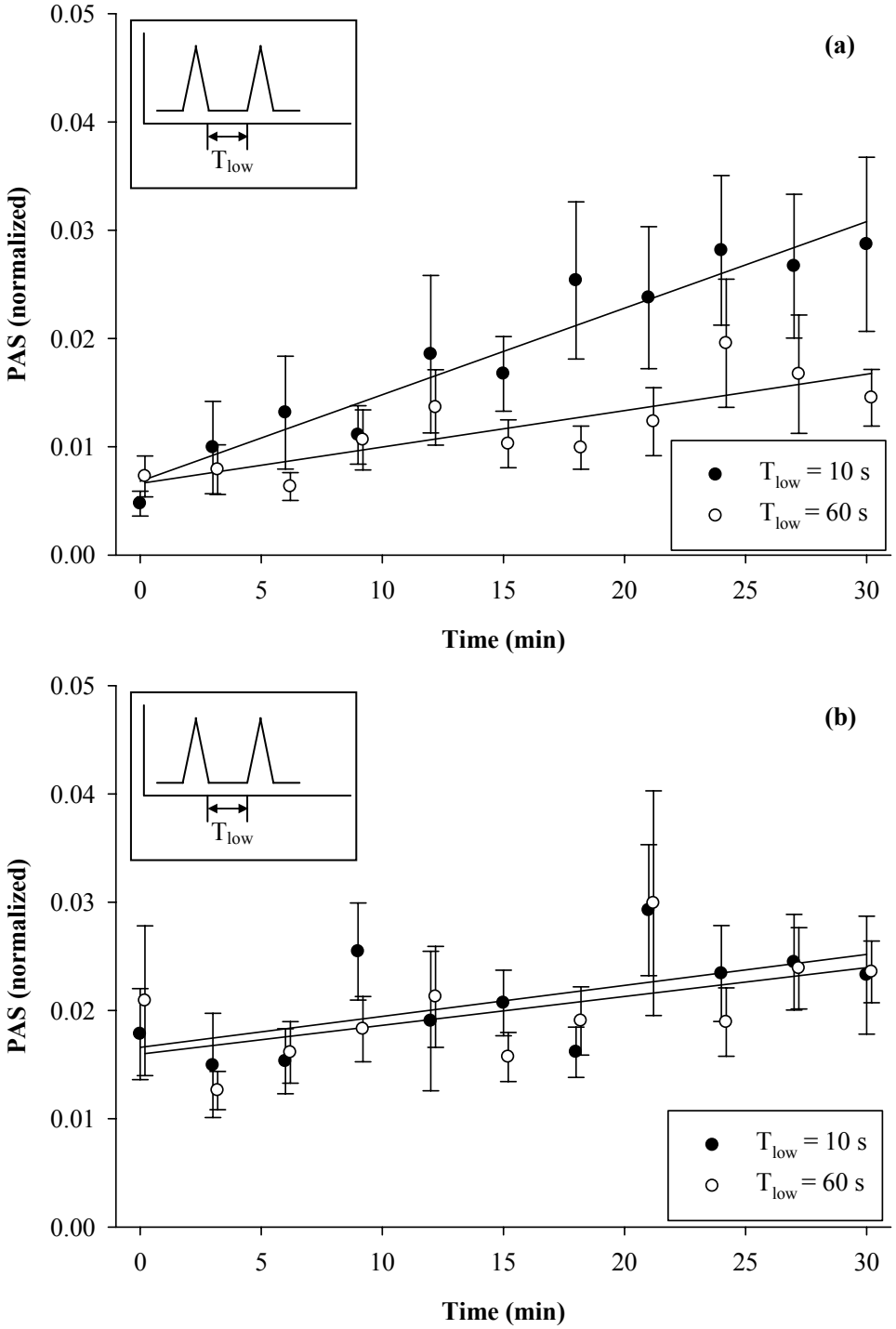

Figure 4.3. The effect of low shear stress duration (T_{low}) on platelet activation rate. Platelets at a count of (a) 100,000/µl or (b) 20,000/µl were exposed to a triangular waveform with a peak of 100 dyne/cm^2 and low shear stress, 1.5 dyne/cm^2, with T_{low} of 10 s or 60 s. Only at a count of 100,000/µl was statistical significance observed ($p < 0.05$).

4.3 Effect of Shear Stress and Exposure Time on Platelet Activation Rate

4.3.1 Platelet Activation Behavior after Single Exposure to High Shear Stress

We initially anticipated that platelet activity might stabilize or recover, i.e. thrombin generation would drop towards baseline levels, from a brief high shear stress insult when exposed to subsequent low shear stress. However, platelets exposed to 70 dyne/cm^2 for 40 s and then to 1 dyne/cm^2 for an additional 59 min showed yielded a linear increase in platelet activation during the low shear phase (Fig. 4.4). The mean PAR for 4 experiments was 50-fold greater than that for the control case, which lacked the initial high shear stress pre-exposure ($p <$ 0.05). This activation "priming", or *sensitization*, response was observed despite a low initial activation (< 5%) after exposure to high shear stress. This observation formed the basis for the rest of the studies presented.

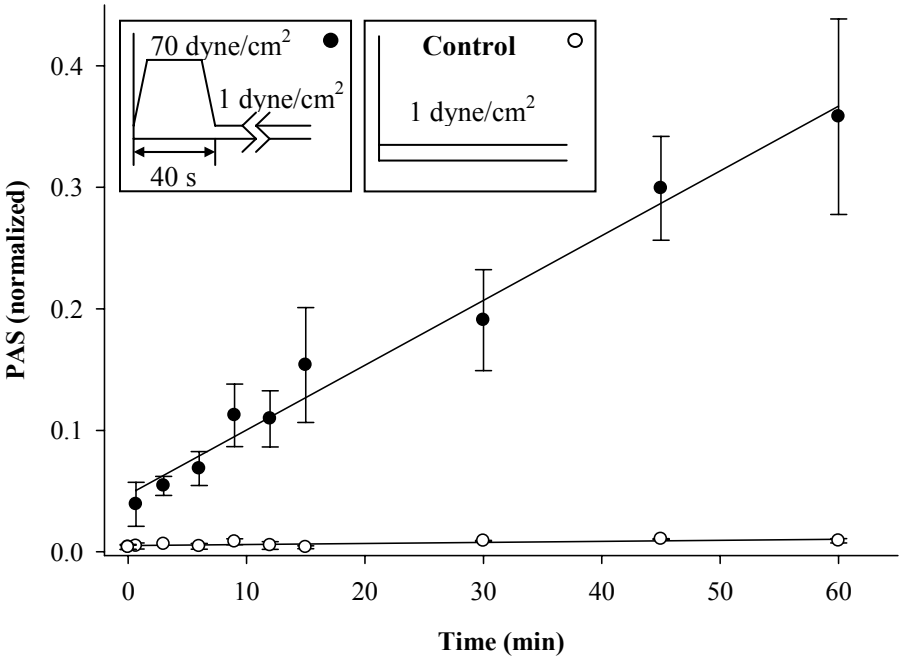

Figure 4.4. Platelet activation rate due to 40 s high shear stress pre-exposure. Platelets were exposed to shear stresses of 1 (control) and 70 dyne/cm^2, followed by 59 min exposure to 1 dyne/cm^2. PAR for the high shear stress exposure was 50-fold higher than the control case ($p <$ 0.05).

4.3.2. Shear-Induced Platelet Sensitization due to Variable Shear Stress and Exposure Time

Two variables were selected for the pre-exposure high shear stress phase: variable shear stress for a fixed duration of 40 s and variable duration at a fixed shear stress of 70 dyne/cm^2.

For the first case, seven peak shear stresses were chosen: 70, 60, 50, 40, 30, 20 and 1 (control) dyne/cm^2. Nine experiments were done for each of the conditions, with controls. Four of these conditions yielded platelet activation behavior shown in Figure 4.5. During the initial 40 s phase, the higher shear stress experiments caused a small but significant increase in PAS. After the brief exposure, the shear stress was lowered to 1 dyne/cm^2 for the remaining 14 min. A linear increase in PAS was observed during this phase. However, only with pre-exposure to 60 and 70 dyne/cm^2 were subsequent platelet activation rates significantly different from the 1 dyne/cm^2 control ($p < 0.05$). PAR values and associated p values for all conditions are summarized in Table 4.1.

For the second case, six peak shear stress exposure times at 70 dyne/cm^2 were chosen: 40, 30, 20, 10, 5 s, and again a 1 dyne/cm^2 control. Eleven experiments were done for each of the conditions, with controls. Four of these conditions yielded platelet activation behavior shown in Figure 4.6. Only with pre-exposure for 40 s was the subsequent platelet activation rate significantly different from the 1 dyne/cm^2 control ($p < 0.005$). PAR values and associated p values for all conditions are summarized in Table 4.1.

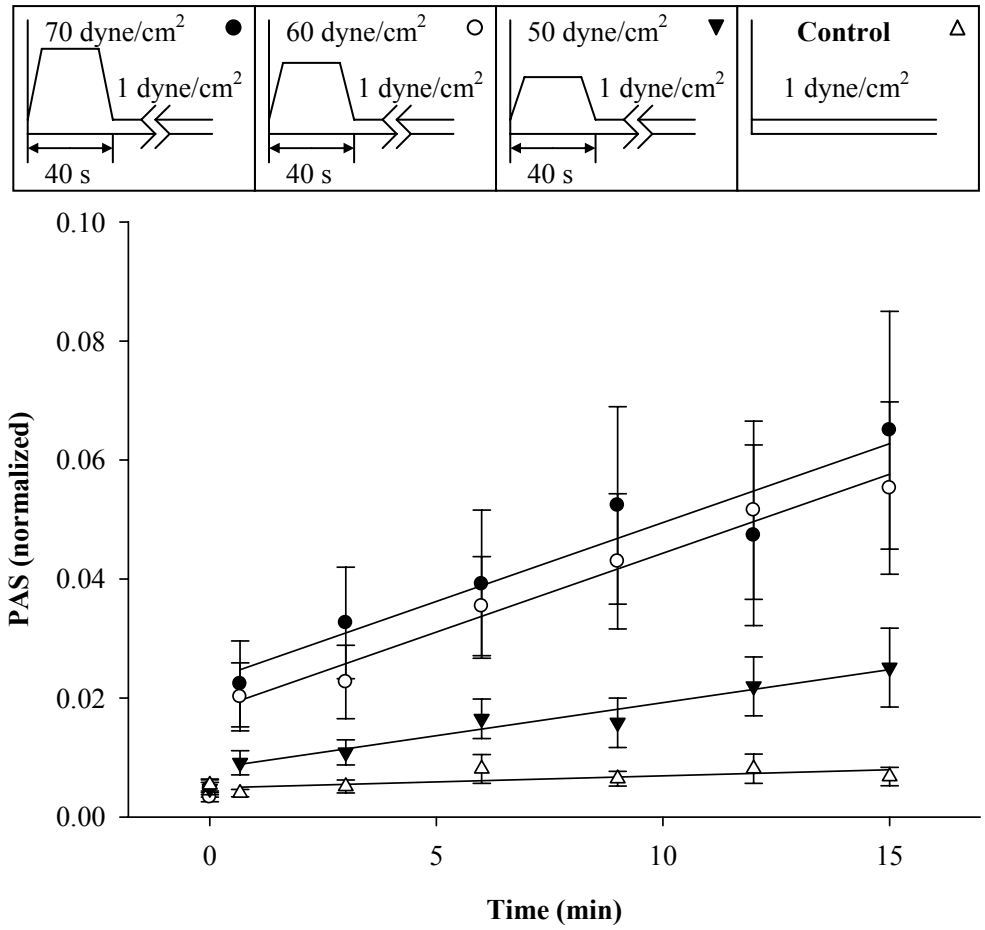

Figure 4.5. Platelet activation rate due to 40 s pre-exposure to varying shear stresses. Platelets were pre-exposed to shear stresses of 1 (control), 50, 60, and 70 dyne/cm^2, followed by 14 min exposure to 1 dyne/cm^2. PAR for the 60 and 70 dyne/cm^2 exposures were significant from the control case ($p < 0.05$).

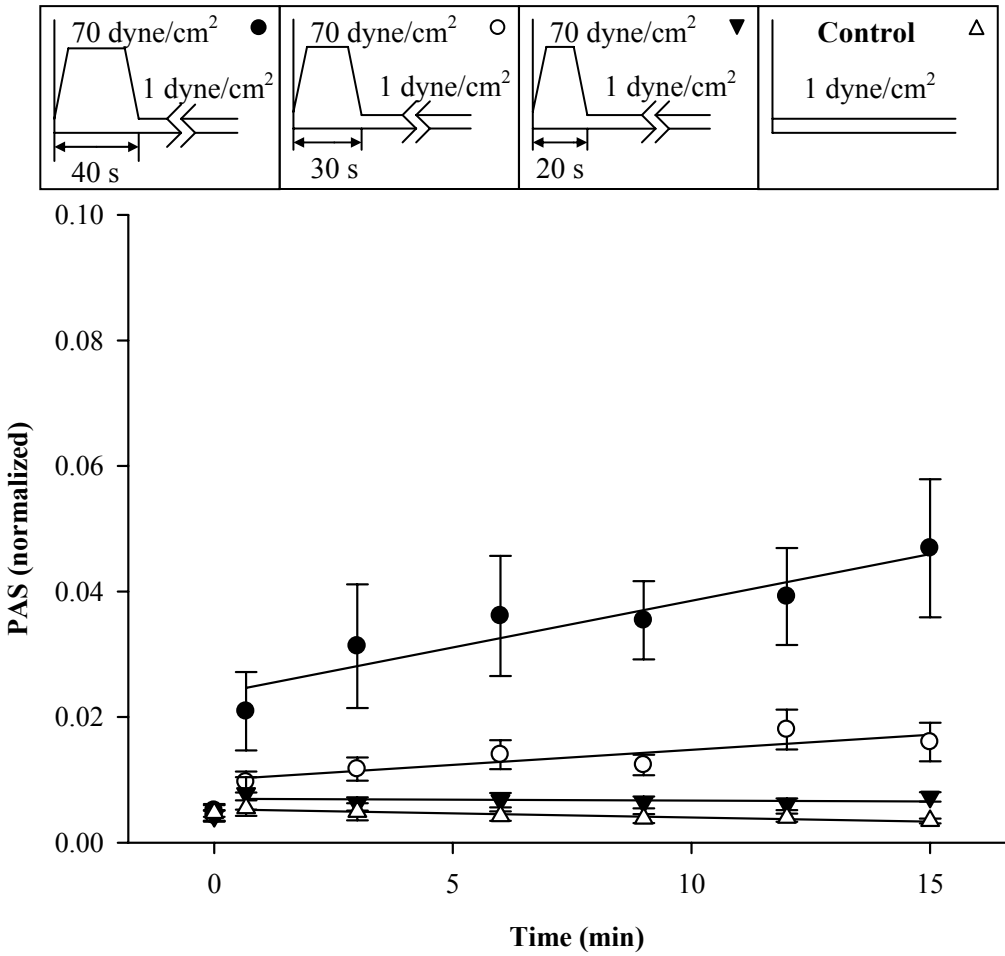

Figure 4.6. Platelet activation rate due to fixed high shear stress pre-exposure to varying durations. Platelets were pre-exposed to 70 dyne/cm^2 shear stress for 20, 30, and 40 s, followed by 14 min exposure to 1 dyne/cm^2. Only the PAR for the 40 s exposure was significant from the control case ($p < 0.005$).

Table 4.1. Platelet activation rates after pre-exposure to high shear stress

Shear Stress (dyne/cm^2)	Exposure Time (s)	Integral Shear Stress (dyne s/cm^2)	Platelet Activation Rate (ΔPAS/min) (x 10^{-4} min^{-1})	*p* vs. control
(a) Variable Peak Shear				
1 (control)	40	40	1.6 ± 0.6	-
20	40	800	-0.2 ± 1.8	> 0.5
30	40	1200	1.3 ± 1.2	> 0.5
40	40	1600	5.2 ± 3.4	> 0.5
50	40	2000	12.3 ± 3.9	> 0.5
60	40	2400	24.4 ± 8.7	< 0.05
70	40	2800	25.6 ± 9.5	< 0.05
(b) Variable Duration				
1 (control)	40	40	-1.3 ± 0.6	-
70	5	350	-0.8 ± 0.8	> 0.5
70	10	700	-0.3 ± 1.1	> 0.5
70	20	1400	2.3 ± 1.6	> 0.5
70	30	2100	4.8 ± 2.0	> 0.5
70	40	2800	14.9 ± 6.8	< 0.005

Platelet activation rates are means ± SEM of regression lines for the post-exposure, low shear phase in Figures 4.5 and 4.6, corresponding to (a) and (b), respectively. Significance (*p*) values were calculated as described in Section 3.11.

4.3.3 The Sensitization Threshold

The varying pre-exposure regimens were integrated to provide an overall measure of the initial high shear stress exposure. The product of the peak shear stress and exposure time, or integral shear stress, is expressed in dyne·s/cm^2. Subsequent PAR values were collected for each condition (n = 9 or 11) and plotted against the integral shear stress (Fig. 4.7). Only pre-exposure to 70 dyne/cm^2 for 40 s (integral = 2,800 dyne s/cm^2) and 60 dyne/cm^2 for 40 s (integral = 2,400 dyne s/cm^2) resulted in statistically significant change in PAR over the 1 dyne/cm^2 control (integral = 40 dyne s/cm^2, Table 4.1). Thus, an integral shear stress of 2,400 dyne s/cm^2 was defined as the sensitization threshold.

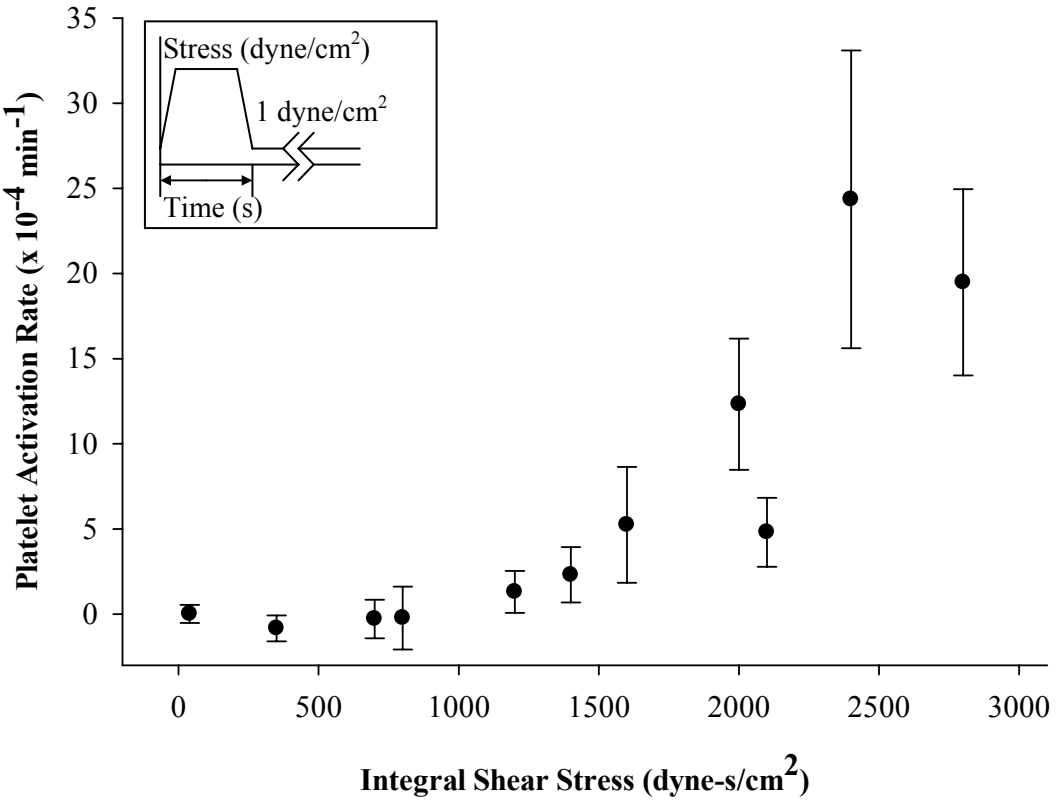

Figure 4.7. Sensitization threshold. Platelet activation rates after high shear stress exposure (Figs. 4.5 and 4.6, and Table 4.1) were plotted against the time integral of the initial high shear stress exposure. Statistical significance was observed for integral shear stresses of 2,400 and 2,800 dyne s/cm^2 ($p < 0.05$).

4.4 Shear-Induced Platelet Sensitization after Exposure to Very High Shear Stress

While a shear stress of 70 dyne/cm^2 (Section 4.3) is certainly pathological, the exposure time, 40 s, required to generate a statistically significant post- high shear stress exposure PAR exceeds the exposure time of platelets in MHVs (Section 2.2) and even arterial stenoses. Thus, the results presented earlier may be more relevant when describing platelet activation response to repeated passages through a blood recirculating device. To emulate the case of platelets passing through the very high shear stress regions of a blood recirculating device, a syringe-capillary viscometer was utilized.

4.4.1 Platelet Sensitization after a Single Exposure to Very High Shear Stress

Based on the pressure limits of the syringe-capillary viscometer during trial runs (Table 4.2), three experimental conditions were selected, all with an integral shear stress 25 dyne s/cm^2: 100 ms exposure to 250 dyne/cm^2; 50 ms exposure to 500 dyne/cm^2; and 25 ms exposure to 1,000 dyne/cm^2. Platelets were subsequently exposed to 0.5 dyne/cm^2 for 30 min in the HSD. The control was 0.5 dyne/cm^2 exposure lacking the initial very high shear stress phase. Note that all shear stresses presented are average, not wall, shear stresses in order to allow comparison with experiments performed in the HSD. Four experiments were done for each of the conditions (Fig. 4.8). While the 25 ms exposure to 1,000 dyne/cm^2 yielded a PAR more than 4-fold higher than the control, no statistical significance was obtained ($p > 0.05$). The PAR for the 1,000 dyne/cm^2 case was more than double that for the 250 and 500 dyne/cm^2 cases, despite the integral shear stress being the same (Table 4.3). This indicates that linear integral shear stress term used for comparing the different variable shear stress and exposure time conditions (Section 4.3.3) may not be appropriate for threshold determination, and that another non-linear term must be defined.

Table 4.2. Parameters for single passage through syringe-capillary pump

Shear Stress (dyne/cm^2)	**Exposure Time (ms)**	**Flow Rate (ml/min)**	**Pressure Drop (psi)**
250	100	14.58	20
500	50	29.17	51
1000	25	58.33	83

Exit flow rates were calculated from the tubing dimensions and syringe plunger velocity. The diameter of the test tubing was 0.37 mm, while its length was 22.95 cm. Pressure measurements were made at the entrance of the test tubing.

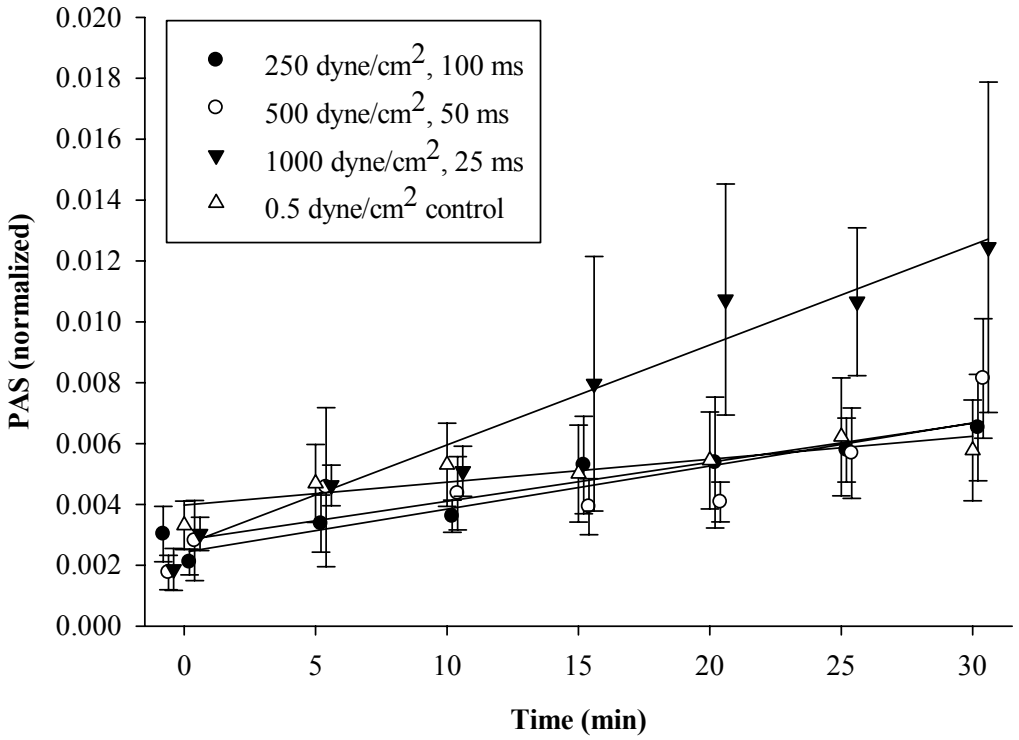

Figure 4.8. Platelet activation rate due to very high shear stress exposure. Platelets were pre-exposed to high shear stress and exposure time combinations with an integral shear stress 25 dyne s/cm^2, followed by 30 min exposure to 0.5 dyne/cm^2. No statistical significance was observed for the PAR when compared to the 0.5 dyne/cm^2 control ($p > 0.05$).

Table 4.3. Platelet activation rates after single, very high shear stress exposure

Shear Stress (dyne/cm^2)	Exposure Time (ms)	Integral Shear Stress (dyne s/cm^2)	PAR (x 10^{-4} min^{-1})	*p* vs. control
0.5 (Control)	-	-	0.76 ± 0.35	-
250	100	25	1.42 ± 0.58	> 0.2
500	50	25	1.28 ± 0.75	> 0.2
1000	25	25	3.33 ± 1.59	0.08

Platelet activation rates are means ± SEM of regression lines for the post-exposure, low shear phase in Figure 4.8. Significance (*p*) values were calculated as described in Section 3.11.

4.4.2 Platelet Sensitization after Repeated Exposure to Very High Shear Stress

Platelets were exposed multiple times to 500 dyne/cm^2 for 50 ms, with "low shear" gaps of 50 dyne/cm^2 for 161 ms, to mimic repeated passages through a blood recirculating device, such as an MHV. Pre-exposed platelets were subsequently subjected to 0.5 dyne/cm^2 for 10 min in the HSD. Four conditions were tested: 10, 20, 40, and 80 repeats, with a control case of 10

min exposure to 0.5 dyne/cm^2 without initial very high shear stress exposure. Four experiments were conducted for each of the conditions. While PAR increased with an increase in the number of repeats (Fig. 4.9), only with 20 and 80 repeats were the PAR values significant when compared to the control ($p < 0.05$). In addition, a decreasing post-exposure PAR was observed for platelets subjected to 40 repeats. Data for all the conditions are summarized in Table 4.4.

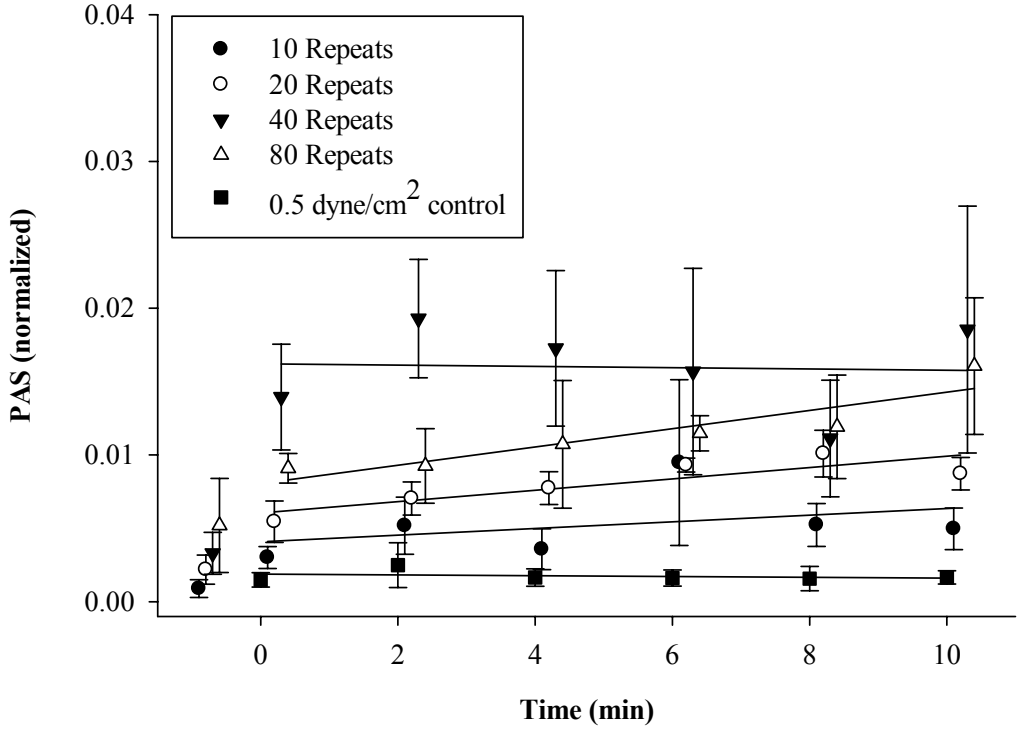

Figure 4.9. Platelet activation rate due to repeated very high shear stress exposure. Platelets were pre-exposed to repeated passages at 500 dyne/cm^2 for 50 ms, punctuated by 161 ms exposure to 50 dyne/cm^2. Pre-exposed platelets were then subjected to 0.5 dyne/cm^2 for 10 min. Statistical significance was observed for the PARs for 20 and 80 repeats when compared to the 0.5 dyne/cm^2 control ($p < 0.05$).

4.4.3 Platelet Sensitization after Repeated Exposure to Low Shear Stress

In Section 4.3, a sensitization threshold was achieved at an integral shear stress of 2,400 dyne s/cm^2. To determine whether this threshold, obtained with experimentation in the HSD, could be extrapolated to the syringe-capillary device, it was important to emulate shear stress and exposure time conditions in the HSD. Due to pressure limitations, a shear stress and exposure

time of 15 dyne/cm^2 and 80 s, respectively, were chosen, with a minimum of 2 repeats to achieve the integral shear stress similar to that at which the sensitization threshold was observed. The resulting test tubing was 11 m long and wrapped in a large coil. Platelets were exposed multiple times to 15 dyne/cm^2 for 80 s, punctuated with gaps of 50 dyne/cm^2 for 161 ms. Pre-exposed platelets were subsequently subjected to 0.5 dyne/cm^2 for 10 min in the HSD. Five conditions were tested: 2, 4, 6, 8 and 10 repeats, with a control case of 10 min exposure to 0.5 dyne/cm^2 without initial repeated low shear stress exposure. Four experiments were conducted for each of the conditions. While PAR generally increased with an increase in the number of repeats (Fig. 4.9), no statistical significance was observed when compared with the control ($p > 0.05$). In addition, a decreasing post-exposure PAR was observed for platelets subjected to 6 and 8 repeats. Data for all the conditions are summarized in Table 4.4.

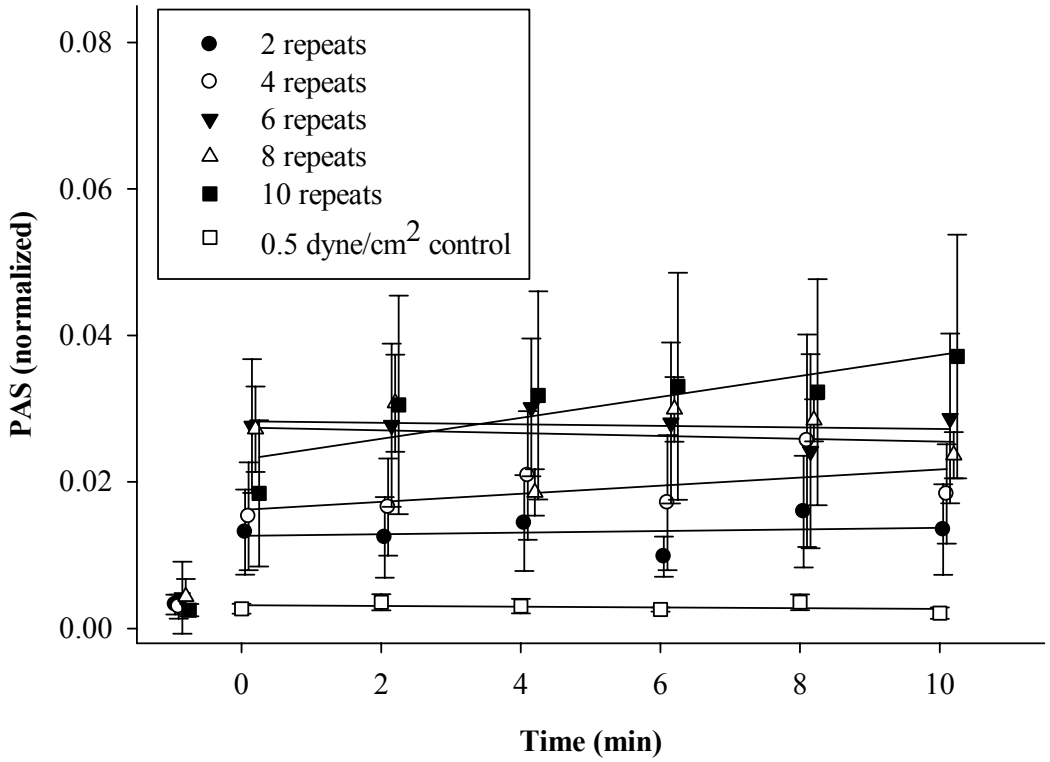

Figure 4.10. Platelet activation rate due to repeated low shear stress exposure. Platelets were pre-exposed to repeated passages at 15 dyne/cm^2 for 80 s, punctuated by 161 ms exposure to 50 dyne/cm^2. Pre-exposed platelets were then subjected to 0.5 dyne/cm^2 for 10 min. No statistical significance was observed for the PARs when compared to the 0.5 dyne/cm^2 control ($p > 0.05$).

Table 4.4. Platelet activation rates after repeated, very high and low shear stress exposure

Shear Stress (dyne/cm^2)	Duration (ms)	Repeats	Integral Shear Stress (dyne s/cm^2)	PAR (x 10^{-4} min^{-1})	*p* vs. control
(a) High Shear Stress					
0.5 (Control)	-	-	-	-0.28 ± 0.33	-
500	50	10	322.45	2.26 ± 1.44	0.09
500	50	20	652.95	3.88 ± 1.87	0.045
500	50	40	1313.95	-0.45 ± 3.39	> 0.2
500	50	80	2635.95	6.22 ± 3.09	0.05
(b) Low Shear Stress					
0.5 (Control)	-	-	-	-0.49 ± 1.47	-
15	80000	2	2408.05	1.09 ± 1.38	> 0.2
15	80000	4	4824.15	5.53 ± 2.98	0.081
15	80000	6	7240.25	-1.10 ± 4.31	> 0.2
15	80000	8	9656.35	-1.9 ± 1.94	> 0.2
15	80000	10	12072.45	14.28 ± 8.19	0.086

Platelet activation rates are means ± SEM of regression lines for the post-exposure, low shear phase in (a) Figure 4.9 and (b) Figure 4.10. Significance (*p*) values were calculated as described in Section 3.11.

4.5 Role of Platelet Crosstalk in Shear-Induced Platelet Sensitization

In prior experiments (Section 4.2), platelets at a count of 100,000/μl showed a higher PAR compared to those at 20,000/μl when exposed to a triangular shear stress waveform. In addition, platelets at 200,000/μl exhibited a parabolic increase in PAS, whereas those at 20,000/μl displayed a linear increase in PAS when exposed to an average shear stress of 9 dyne/cm^2 in a flow loop [67]. This suggested that platelet-platelet crosstalk plays a role in shear-induced platelet activation. To examine whether crosstalk behavior plays a role in shear-induced platelet sensitization, platelets at a count of 150,000/μl were pre-exposed to 70 dyne/cm^2 for 40 s, followed by 1 dyne/cm^2 for 14 min in the HSD. Exposure of platelets at a count of 20,000/μl to the same shear stress conditions served as the control. Four pairwise experiments were done

(Fig. 4.11). Subsequent low shear PAR for platelets at 20,000/μl was not significantly higher than that for platelets at 150,000/μl ($p > 0.5$, Table 4.5), negating the role of platelet-platelet crosstalk.

While platelet crosstalk was discounted for platelets exposed to the same shear stress conditions, whether these shear-sensitized platelets could cause the activation of quiescent (non-exposed) platelets was not known. For the five experiments performed (Section 3.8), quiescent platelets added to sensitized platelets pre-exposed to 60 dyne/cm^2 for 40 s increased the PAR during the subsequent 1 dyne/cm^2 exposure, though this change was not statistically significant when compared to sensitized platelets only ($p > 0.8$, Fig. 4.12). However, both PARs were higher than the PAR for quiescent platelets only ($p < 0.1$, Table 4.5). The similarity in PAR values indicates that sensitized platelets may activate quiescent platelets, since no crosstalk would yield a significantly lower activation rate for the combined platelet sample. It is important to note that the counts for the quiescent and sensitized platelet mixture, as well as the quiescent platelets only, was 40,000/μl, whereas the sensitized platelets were at a count of 20,000/μl. However, the final count in the assay was 5,000/μl for all experiments.

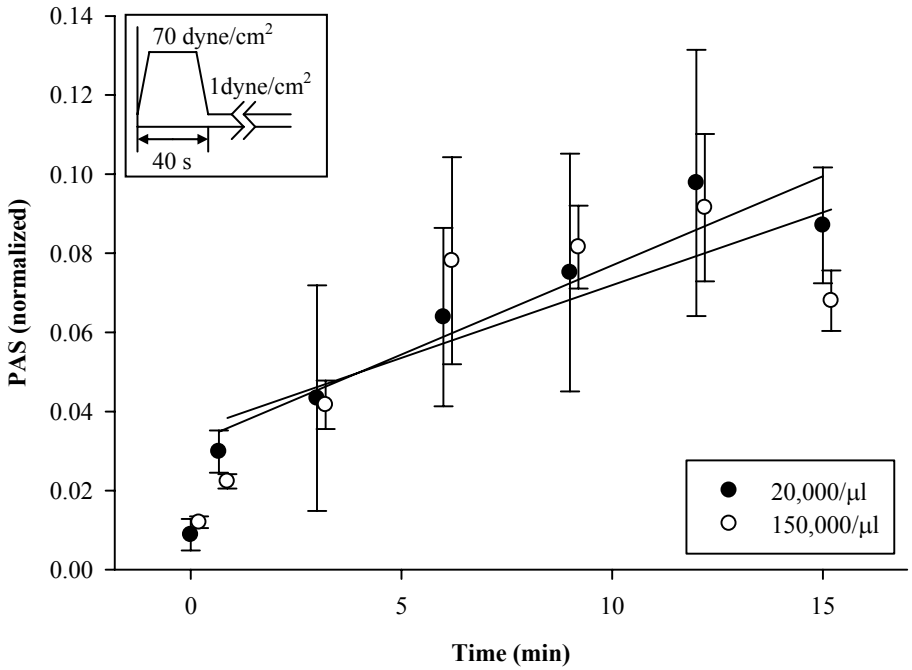

Figure 4.11. Effect of platelet count on post- high shear stress exposure activation rate. Platelets at counts of 150,000/µl and 20,000/µl were pre-exposed to 70 dyne/cm^2 shear stress for 40 s, followed by 14 min exposure to 1 dyne/cm^2. No statistical significance was observed between the PARs for two counts ($p > 0.5$).

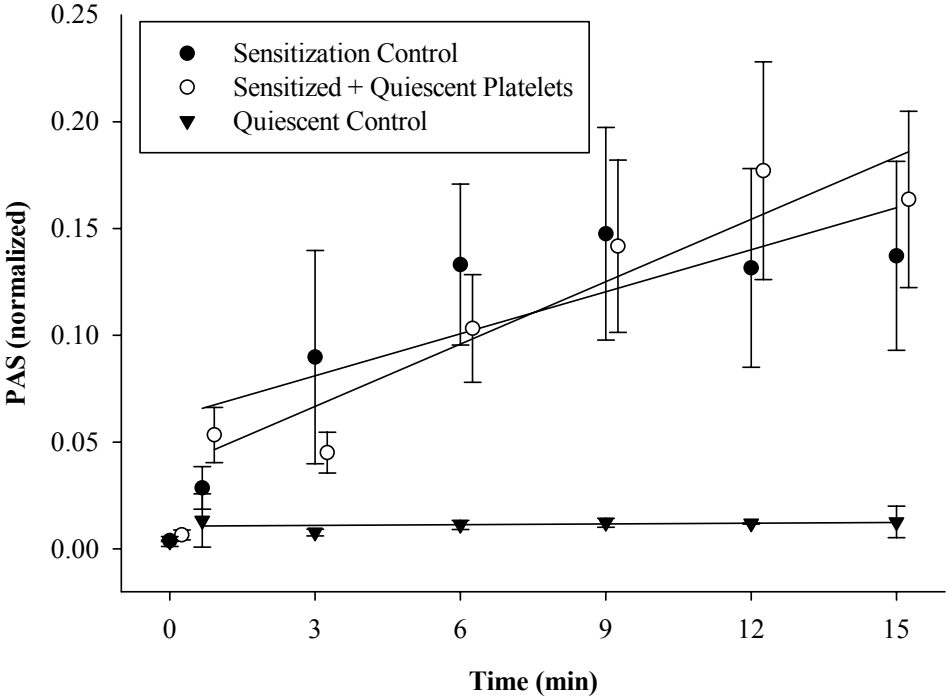

Figure 4.12. Effect of platelet activity level on post- high shear stress exposure activation rate. Platelets were pre-exposed to 70 dyne/cm^2 shear stress for 40 s, whereupon quiescent platelets were added, and the combined mixture was exposed to 1 dyne/cm^2 for 15 min. No statistical significance was observed between the PARs for the combined and sensitized platelet samples ($p > 0.8$).

Table 4.5. Role of cross-talk in platelet sensitization

Condition	Integral Shear Stress (dyne s/cm^2)	Platelet Activation Rate (ΔPAS/min) (x 10^{-4} min^{-1})	*p* value
(a) Platelet Count			
20,000/μl	2800	45.1 ± 17.2	-
150,000/μl	2800	36.8 ± 8.9	> 0.5
(b) Effect of Quiescent Platelets			
Quiescent Platelets Only	40	3.5 ± 5.3	< 0.1
Sensitized Platelets Only	2400	50.8 ± 30.1	-
Sensitized + Quiescent Platelets	2400	51.8 ± 15.0	> 0.5

Platelet activation rates are means ± SEM of regression lines for the post-exposure, low shear phase. The role of cross-talk on platelet sensitization was examined by: (a) varying the platelet count and (b) adding quiescent platelets to sensitized platelets, for a final concentration of 40,000/μl. Significance (*p*) values were calculated as described in Section 3.11.

4.6 Role of Platelet Lysis and Microparticles in Shear-Induced Platelet Sensitization

Platelet counts were taken after the initial high shear stress exposure and at the end of experiments when performing the variable shear stress and exposure time experiments (Section 4.3.2). A larger drop in count was observed over the course of the experiment with an increase in shear stress or exposure time, with a 25% decrease noted for platelets exposed to 70 dyne/cm^2 for 40 s. Cytoplasmic LDH release was measured to examine whether this platelet count drop was due to platelet lysis and correlated with the PAS at every time point (n = 5). Platelets were exposed to 70 dyne/cm^2 for 40 s, followed by 1 dyne/cm^2 for 14 min (Fig. 4.13). The initial high shear stress exposure causes a small but significant increase in both platelet activation and lysis, but the post-exposure behavior was very different. While platelet activation continued, no further LDH release was observed. While lysis might be involved in platelet activation over the initial high shear stress exposure, subsequent activation of the platelets did not involve further lysis (Pearson's coefficient $r = 0.065$, $p > 0.5$).

Platelet-derived microparticles (PMPs) provide another source of procoagulant activity, but are not detected in platelet counts, as they lie outside the range of diameters (2 – 4 μm). The thrombin generation activity of PMPs was measured by utilizing the centrifugation supernatant (Section 3.9) of platelet samples at 0 min, after 40 s exposure to 70 dyne/cm^2, and after 14 min exposure to 1 dyne/cm^2 (Fig. 4.14). A substantial proportion of the thrombin activity was due to PMP formation, both immediately after the high shear stress exposure and after the extended low shear stress phase ($p < 0.05$). PMP activity was approximately 50% of the combined platelet and PMP activity at 40 s and 15 min, suggesting that PMP formation continues throughout the low shear stress phase.

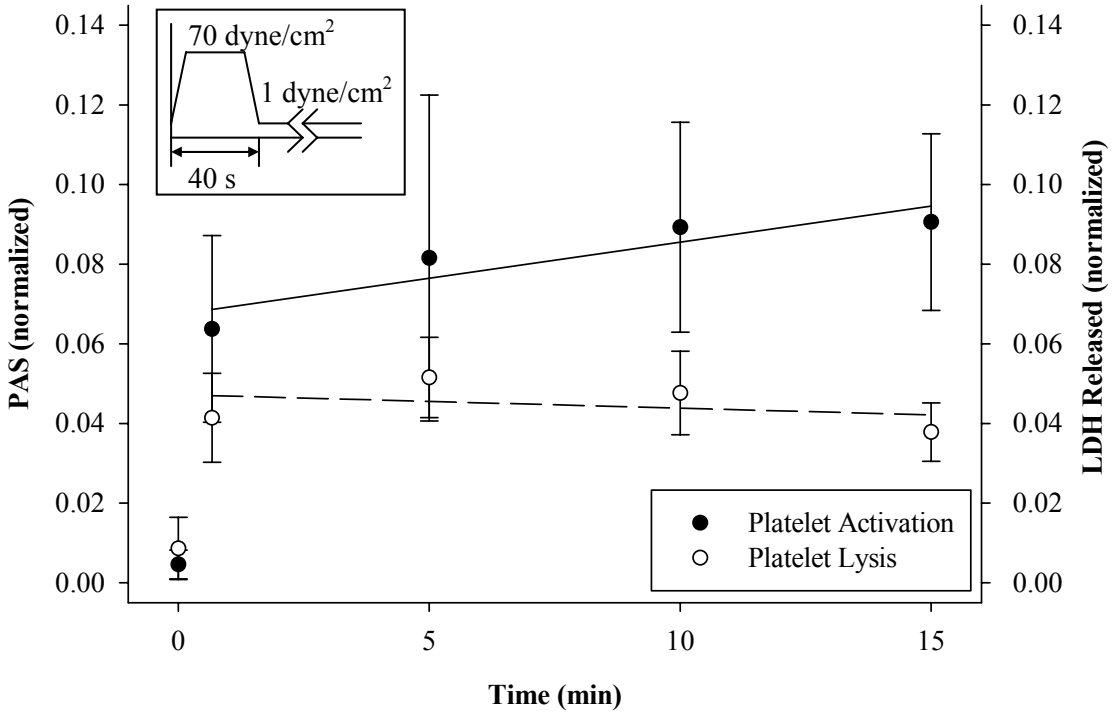

Figure 4.13. Comparison of platelet activity state and lysis. Platelets were pre-exposed to 70 dyne/cm^2 shear stress for 40 s, followed by 1 dyne/cm^2 for 14 min. No correlation was observed between the subsequent PAR and lysis rate, as assessed by LDH release ($r = 0.065$, $p > 0.5$).

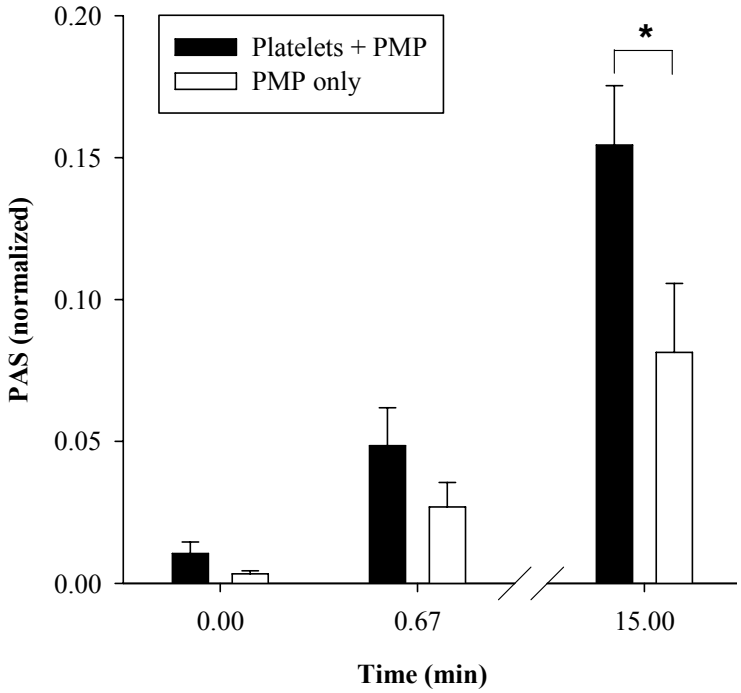

Figure 4.14. PMPs and sensitization. Platelets were pre-exposed to 70 dyne/cm^2 shear stress for 40 s, followed by 1 dyne/cm^2 for 14 min. PAS of PMPs was approximately 50% of the platelet and PMP combination immediately and 15 min after pre-exposure, but this was only statistically significant for the latter time point (* $p < 0.05$).

4.7 Modulation of Shear-Induced Platelet Sensitization with Platelet Agonists and Inhibitors

Under physiologic conditions, a variety of platelet agents play a role in amplifying or attenuating platelet responses in order to restore hemostasis. To examine whether shear-induced platelet sensitization could be modulated, platelets were treated with platelet agonists or inhibitors under pathologic shear stress conditions, and the resulting aggregation and activation responses were measured.

4.7.1 Aggregation of Shear-Exposed Platelets with the Addition of Agonists

Platelets at a count of 150,000/μl were exposed to 70 dyne/cm^2 for 40 s and immediately analyzed for their aggregation response after post-exposure treatment with 20 μM TRAP, 10 μg/ml collagen, or 0.5 mM arachidonic acid (Section 3.10.1). Controls for each case were

treatment of platelets that were not exposed to the high shear stress. Five pairs of experiments were done for each agonist, with aggregation response recorded over a 5 min period. Aggregation amplitude over the duration of the experiment was measured from the bottom of the shape change curve to the maximum of the curve, observed in most cases to occur at the end of the aggregation reading (Fig. 4.15a). The rate of aggregation was measured as the slope of the curve during the first 60 s after shape change (Fig. 4.15b). For both sets of measurements, the aggregation response of platelets treated with agonists after exposure to high shear stress was significantly lower than for platelets which had not been pre-exposed to shear stress ($p < 0.01$). This suggests some form of platelet desensitization.

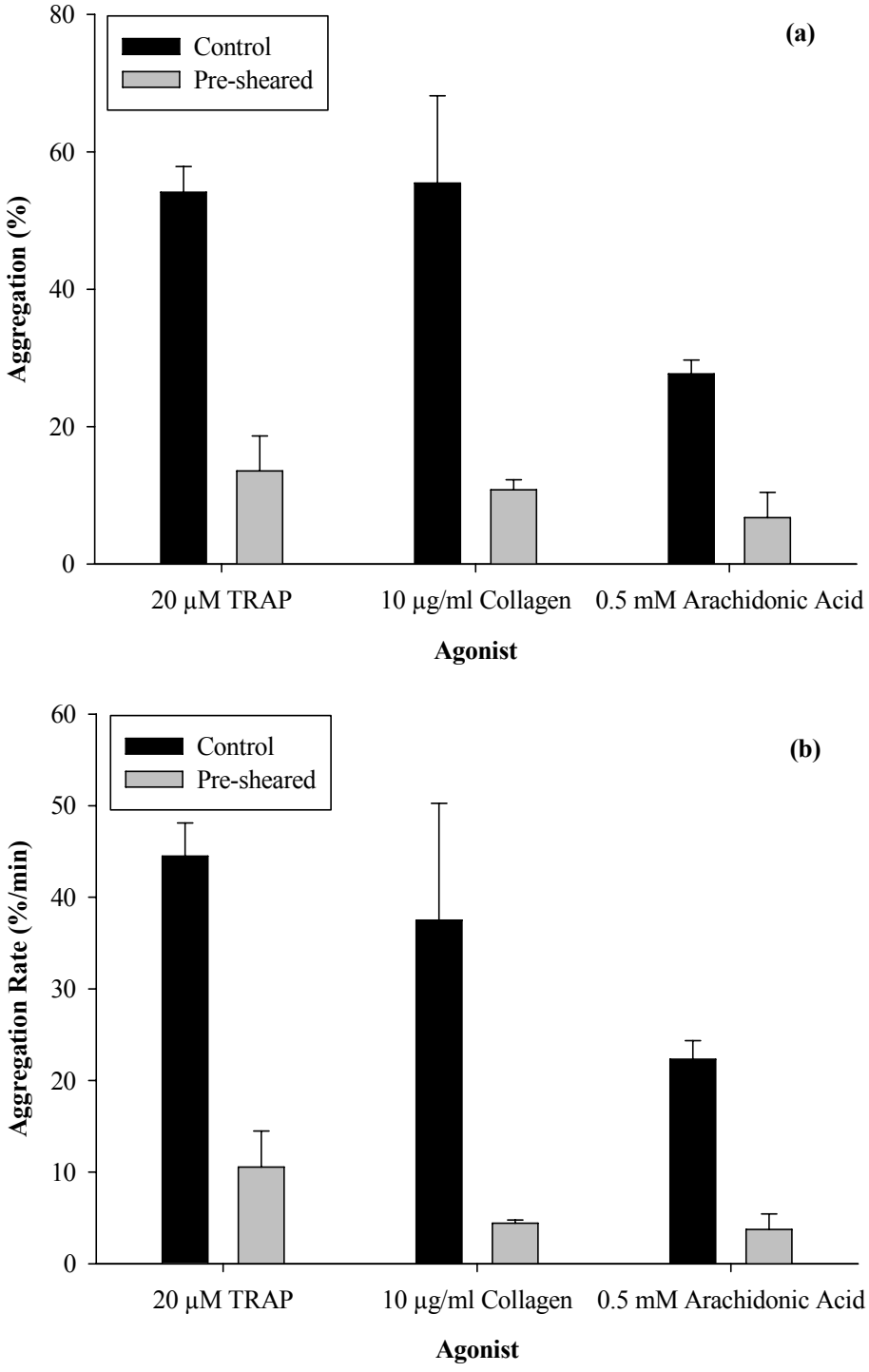

Figure 4.15. Aggregation response of pre-sheared platelets after treatment with agonists. Platelets were pre-exposed to 70 dyne/cm^2 shear stress for 40 s and treated with 20 µm TRAP, 10 µg/ml collagen, or 0.5 mM arachidonic acid. Both the (a) aggregation amplitude and (b) rate of aggregation for the pre-sheared platelets were significantly lower when compared with unsheared, agonist-treated controls ($p < 0.01$).

4.7.2 Platelet Sensitization Modulation after Pre-Treatment with Agonists

The ability of platelet agonists to change the sensitization response of shear-exposed platelets was examined. Platelets at a count of 150,000/μl were pre-treated with 20 μM TRAP, 10 μg/ml collagen, or 0.5 mM arachidonic acid and exposed to 1 dyne/cm^2 for 3 min, 70 dyne/cm^2 for 40 min, and then 1 dyne/cm^2 for an additional 14 min (Section 3.10). For all cases, shear-exposed platelets that were not pre-treated with the biochemical agonists served as the control.

For five pairs of experiments with TRAP-treated platelets, initial exposure to low shear stress generated a small but non-significant increase in PAS when compared to the control (Fig. 4.16). However, exposure to high shear stress caused a doubling in the subsequent low shear stress PAR for TRAP-treated platelets (74.8 ± 19.7 (x 10^{-4}) min^{-1}) when compared to untreated platelets (34.7 ± 11.5 (x 10^{-4}) min^{-1}, $p < 0.05$).

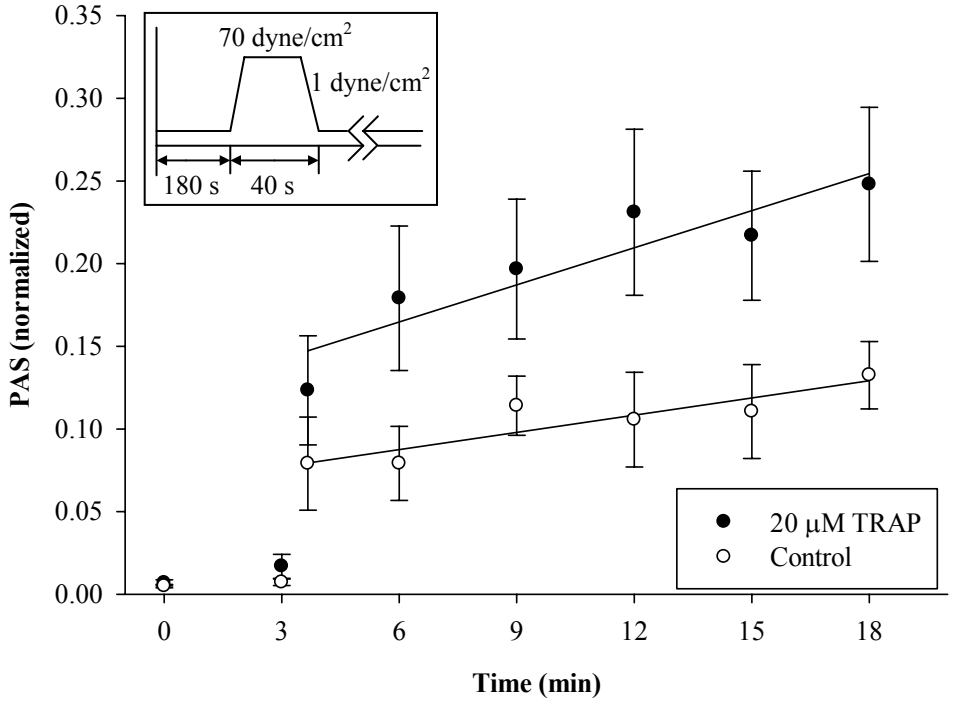

Figure 4.16. Sensitization response of TRAP-treated platelets. Platelets were pre-treated with 20 μM TRAP and exposed to 1 dyne/cm^2 for 3 min, 70 dyne/cm^2 for 40 s, and 1 dyne/cm^2 for 14 min. PAR for TRAP-treated platelets was double of PAR for untreated platelets ($p < 0.05$).

Similar initial low shear stress behavior was observed for eight pairs of experiments with collagen-treated platelets (Fig. 4.17). Exposure to high shear stress nearly doubled the subsequent low shear stress PAR for collagen-treated platelets (103.1 ± 17.7 (x 10^{-4}) min^{-1}) when compared to untreated platelets (54.6 ± 15.7 (x 10^{-4}) min^{-1}, $p < 0.05$).

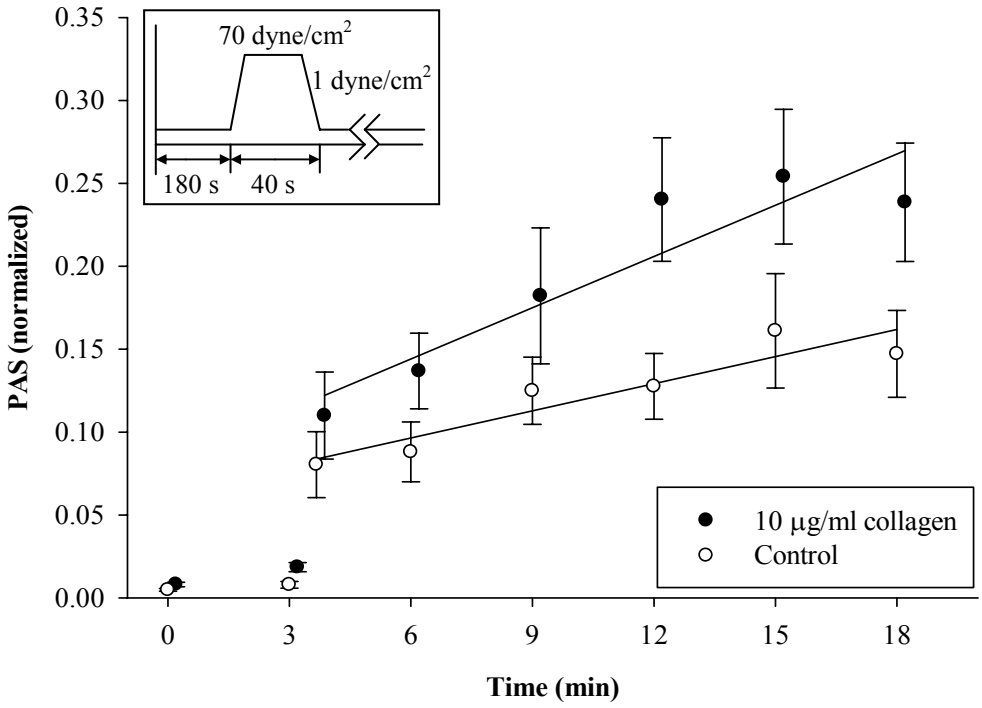

Figure 4.17. Sensitization response of collagen-treated platelets. Platelets were pre-treated with 10 μg/ml collagen and exposed to 1 dyne/cm^2 for 3 min, 70 dyne/cm^2 for 40 s, and 1 dyne/cm^2 for 14 min. PAR for collagen-treated platelets was nearly double of PAR for untreated platelets ($p < 0.05$).

However, the response for the four pairs of arachidonic acid-treated platelets was quite different from that of the TRAP- and collagen-treated platelets. Pre-treatment with arachidonic acid resulted in a PAS over 35% of maximal, with a decrease during the initial 3 min low shear stress phase (Fig. 4.18). High shear stress exposure caused a further drop in PAS, followed a gradual increase in PAS during the subsequent low shear stress phase. PAR for arachidonic acid-treated platelets during this latter phase (31.2 ± 36.3 (x 10^{-4}) min^{-1}) was less than half of the

PAR for untreated platelets (80.6 ± 6.8 (x 10^{-4}) min^{-1}), though this difference was not statistically significant ($p > 0.2$).

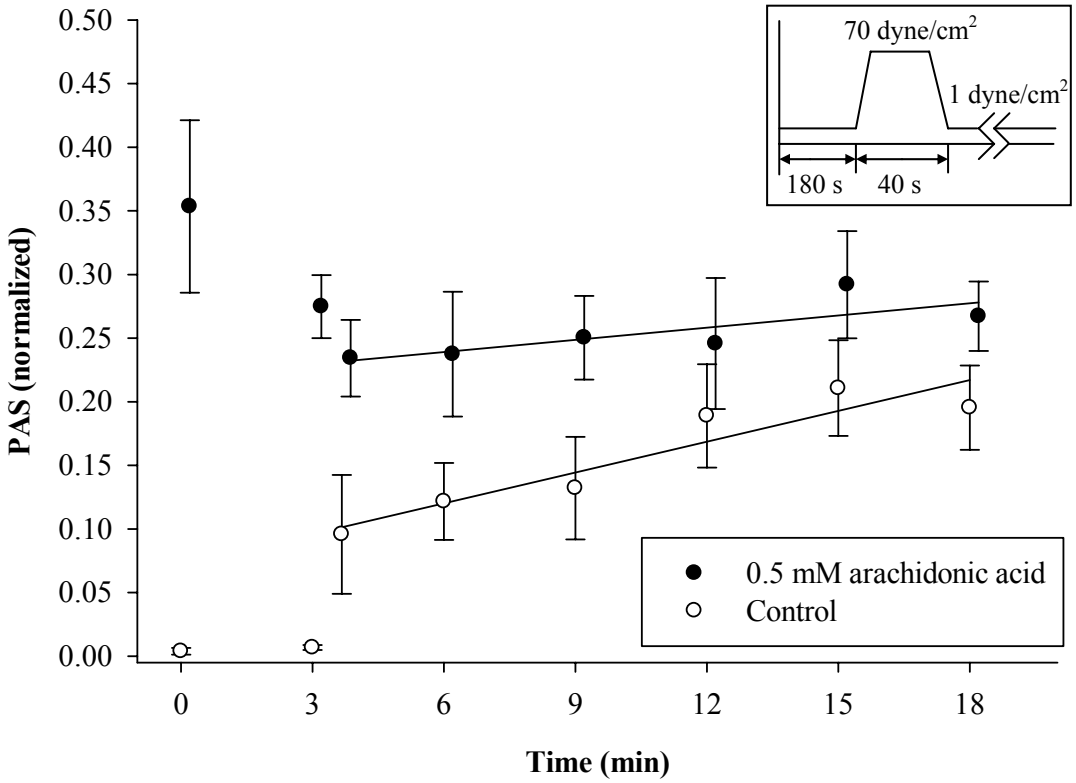

Figure 4.18. Sensitization response of arachidonic acid-treated platelets. Platelets were pre-treated with 0.5 mM arachidonic acid and exposed to 1 dyne/cm^2 for 3 min, 70 dyne/cm^2 for 40 s, and 1 dyne/cm^2 for 14 min. PAR for collagen-treated platelets was less than half of PAR for untreated platelets, but this was not statistically significant ($p > 0.2$).

4.7.3 Platelet Sensitization Modulation after Pre-Treatment with Platelet Inhibitors

The ability of platelet inhibitors to change the sensitization response of shear-exposed platelets was examined. The effects of intracellular Ca^{2+}, which plays a role in amplifying platelet activation response, were blocked by treating platelets 20 μM BAPTA-AM and diluting them to a count of 20,000/μl (Section 3.10.3). Platelets were then exposed to 70 dyne/cm^2 for 40 s, followed by 1 dyne/cm^2. For the five experiments performed, PAS values for BAPTA-treated platelets immediately after high shear stress exposure was lower than that for untreated platelets (Fig. 4.19, $p \sim 0.09$). However, there was no statistically significant difference between

the PAR values for BAPTA-treated platelets (20.9 ± 5.3 (x 10^{-4}) min^{-1}) and untreated platelets (19.3 ± 5.7 (x 10^{-4}) min^{-1}, $p > 0.5$). Thus, while release of intracellular Ca^{2+} helps amplify the thrombin generation of platelets, it does not appear to play a role in the subsequent low shear sensitization response.

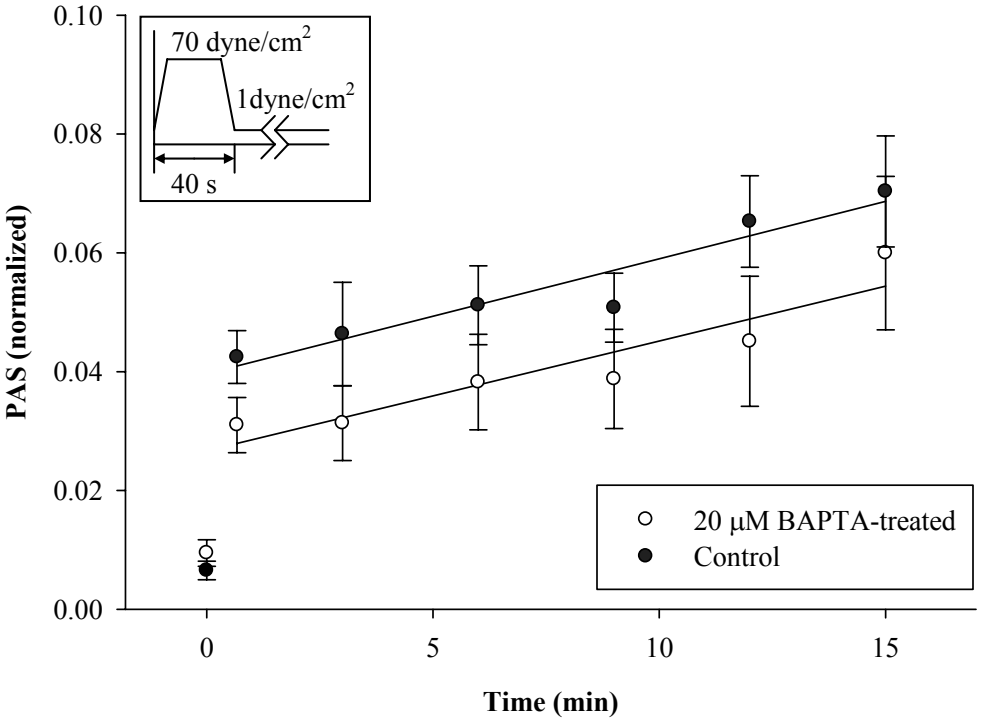

Figure 4.19. Sensitization response of intracellular Ca^{2+}-depleted platelets. Platelets were pre-treated with 20 μM BAPTA-AM and exposed to 70 dyne/cm^2 for 40 s, followed by 1 dyne/cm^2 for 14 min. PAR for BAPTA-treated platelets was similar to PAR for untreated platelets, but this was not statistically significant ($p > 0.5$).

Platelets at a count of 100,000/μl were pre-treated with 1 U/ml apyrase and exposed to 70 dyne/cm^2 for 40 min, followed by 1 dyne/cm^2 for an additional 14 min, to examine whether ADP, a potent platelet agonist, plays a role in shear-induced platelet sensitization (Section 3.10.3). For the four pairs of experiments performed (Fig. 4.20), apyrase-treated platelets (76.9 ± 15.2 (x 10^{-4}) min^{-1}) yielded a 33% reduction in PAR compared to untreated, shear-exposed control (114.6 ± 6.4 (x 10^{-4}) min^{-1}, $p < 0.05$). Therefore, ADP may account for some of the increase in platelet activation during the low shear stress phase.

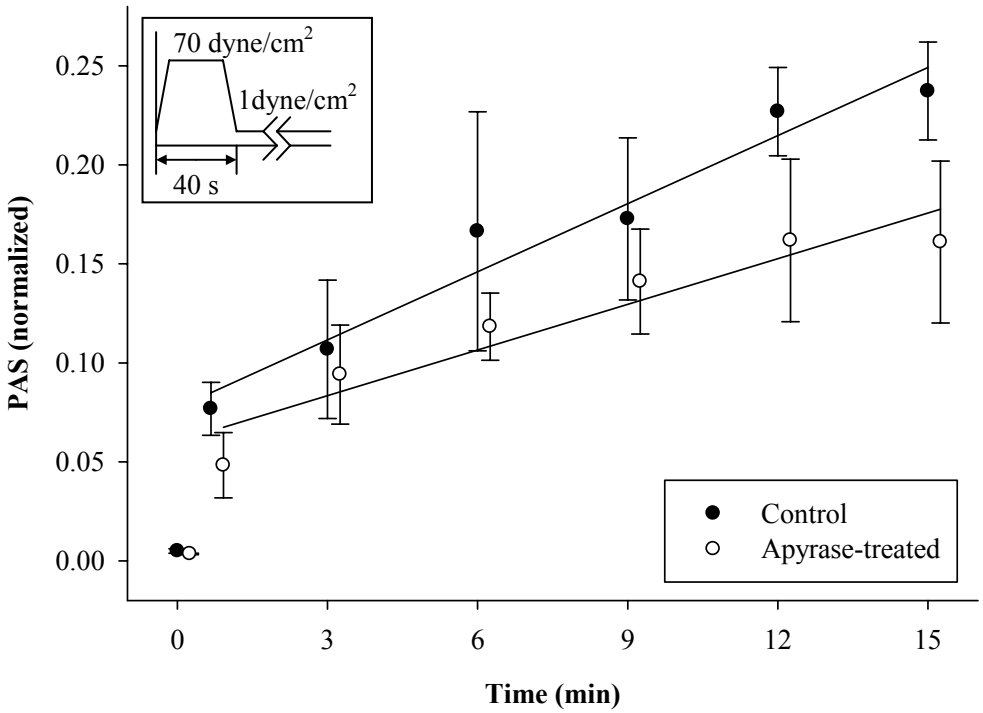

Figure 4.20. Sensitization response of apyrase-treated platelets. Platelets were pre-treated with 1 U/ml apyrase and exposed to 70 dyne/cm^2 for 40 s, followed by 1 dyne/cm^2 for 14 min. PAR for apyrase-treated platelets was significantly lower than the PAR for untreated platelets ($p < 0.05$).

Platelets at a count of 150,000/μl were treated with 1 μM prostacyclin (PGI_2), a platelet inhibitor released from endothelial cells, and exposed to 1 dyne/cm^2 for 3 min, 70 dyne/cm^2 for 40 s, and then 1 dyne/cm^2 for 14 min (Section 3.10.3). A slight but non-significant reduction in PAS after the high shear stress exposure was observed for PGI_2-treated platelets when compared to the untreated control (Fig. 4.21, $p > 0.5$). However, there was no difference in the post-exposure PAR for PGI_2-treated platelets (89.1 ± 23.7 (x 10^{-4}) min^{-1}) when compared to the PAR for untreated platelets (93.9 ± 23.5 (x 10^{-4}) min^{-1}, $p > 0.5$). In physiological circulation, PGI_2 negates the behavior of the platelet agonist thromboxane (TXA_2). The PAR results suggest that PGI_2 does not play a role the platelet sensitization response. The results, in combination with the platelet activation behavior of TXA_2 precursor arachidonic acid (Section 4.7.2), also suggest that TXA_2 is not involved in the sensitization response.

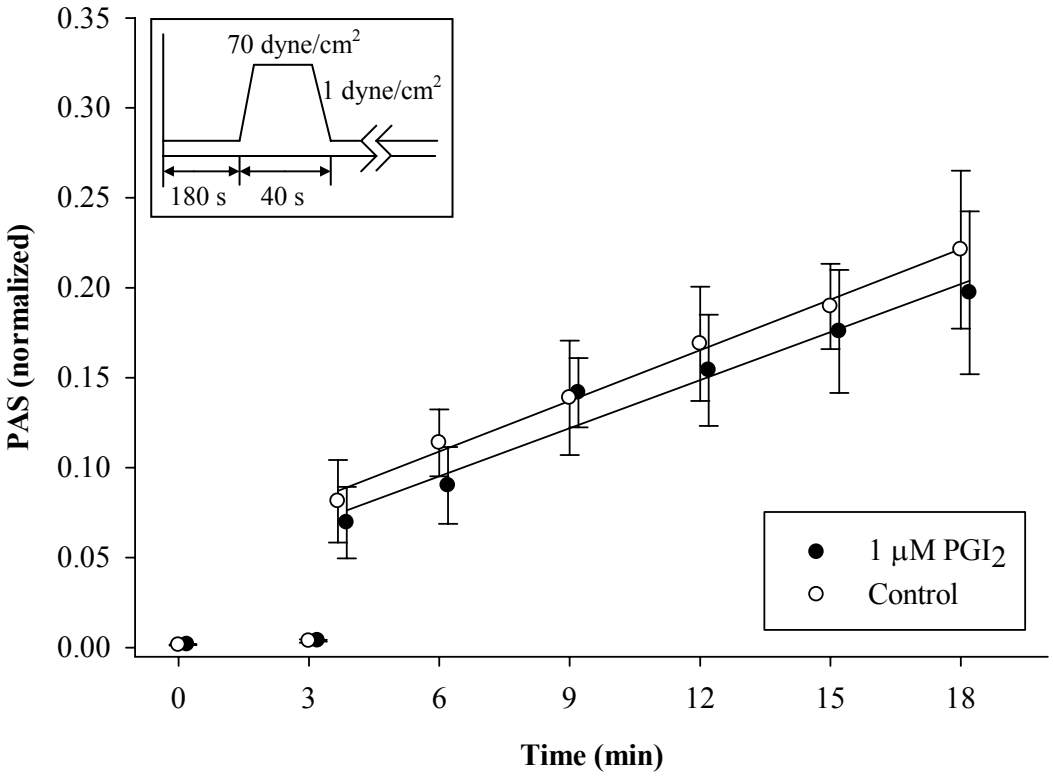

Figure 4.21. Sensitization response of PGI_2-treated platelets. Platelets were pre-treated with 1 μM PGI_2 and exposed to 1 dyne/cm^2 for 3 min, 70 dyne/cm^2 for 40 s, followed by 1 dyne/cm^2 for 14 min. PAR for PGI_2-treated platelets was similar to the PAR for untreated platelets (p > 0.5).

4.8 Model of Platelet Activation Based on Shear-Induced Platelet Sensitization Results

4.8.1 Simple Phenomenological Approach

Table 4.6 shows the model constants for the cases where the shear loading rate is included and omitted, respectively. Figures 4.22 and 4.23 show the model prediction on the same set of axes as experimental results for the variable shear stress and exposure time conditions, respectively, for the case where shear loading rate is included. Including the shear loading rate did not significantly lower the RMS error compared to the case without this term. However, PAS values immediately after the high shear stress phase (40 s) were significantly overestimated when the shear loading rate term was neglected, particularly for the 60 and 70 dyne/cm^2 plots. Therefore the model with the loading rate was selected:

$$PAS(\tau,t) = 1.30\times10^{-14}\left[\int_{t_0}^{t_{total}} 3.99t^{2.99}\tau^{2.89}dt + \int_{t_0}^{t_{total}} 2.89\tau^{1.89}t^{3.99}\,\dot{\tau}dt\right] + PAS_0 \qquad (4.1)$$

Table 4.6. Optimized model constants for the simple phenomenological approach

Case	Model Constants			RMS Error	N
	C (x 10^{-14})	α	β	(x 10^{-3})	
With Shear Loading Rate	1.30	2.89	3.99	6.87	36
Without Shear Loading Rate	2.50	2.89	3.87	6.95	889

Constants are means ± SEM of optimized values corresponding to the lowest RMS errors for the simple phenomenological approach. N is the number of constants combinations yielding the lowest RMS error.

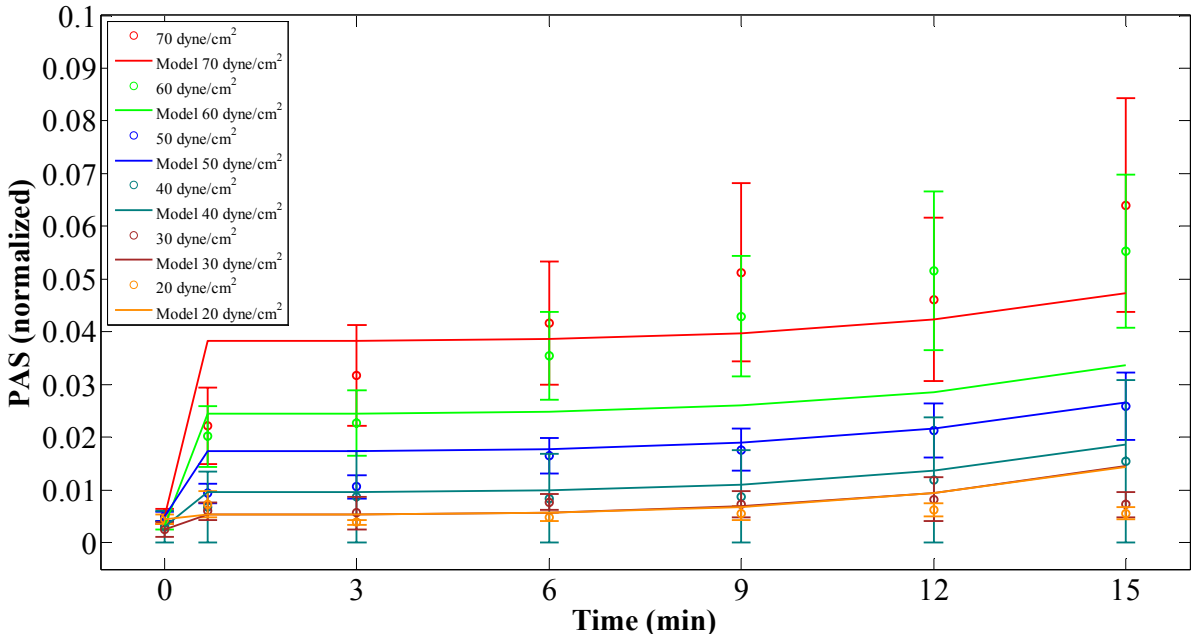

Figure 4.22. Variable shear stress fits for the simple phenomenological approach. Optimized platelet activation model (lines) was fit to shear-induced platelet sensitization experimental PAS values (open circles) for the shear loading case.

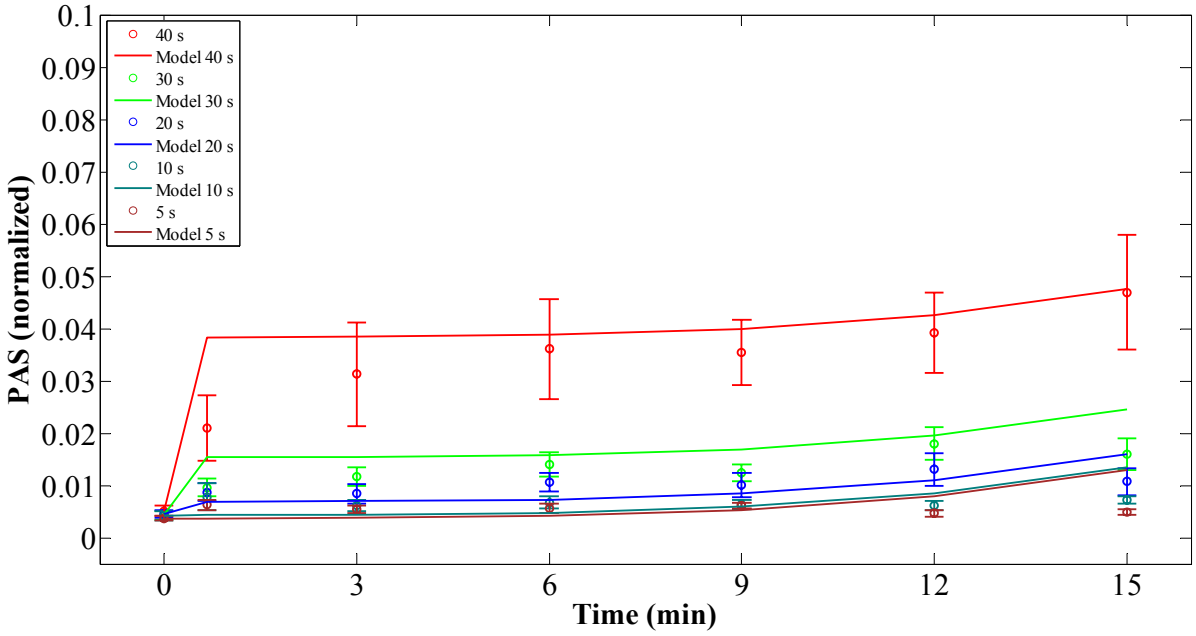

Figure 4.23. Variable duration fits for the simple phenomenological approach. Optimized platelet activation model (lines) was fit to shear-induced platelet sensitization experimental PAS values (open circles) for the shear loading case.

Figures 4.22 and 4.23 show that the model fits may be appropriate for the lower shear stresses, but these fits underestimated the PAS values for the higher shear stresses subsequent to the 40 s time point. Furthermore, all plots subsequent to the initial high shear stress phase (0 – 40 s) show a power law behavior instead of the experimentally observed linear response for PAS. In addition, the fits for the subsequent low shear stress phase are parallel, indicating that this model is solely a function of the shear stress and exposure time, and does not take into account the previous PAS or the initial shear loading rate.

Also analyzed was whether C, α, and β depended on the initial high shear stress, by performing the optimization steps for individual shear stress and exposure time combinations. Collectively, no trend was discernible for all constants. However, for the variable shear stress experiments, an increase in C and a decrease in α and β was observed for shear stresses 40 dyne/cm^2 and higher. This indicates that the constants are functions of shear stress and time when applied to Eqs. 3.9 and 3.10.

4.8.2 Grigioni Approach

Table 4.7 shows the model constants for the cases where the shear loading rate is included and omitted, respectively. Figures 4.24 and 4.25 show the model prediction on the same set of axes as experimental results for the variable shear stress and exposure time conditions, respectively, for only the case where shear loading rate is included. Optimization without the shear loading rate yielded a slightly lower RMS error than for the case with this term. However, PAS values immediately after the high shear stress phase (40 s) were significantly overestimated when the shear loading rate term was neglected, similar to the result for the simple approach. Therefore the model with the loading rate was selected:

$$PAS = 3.79\times10^{-11}\left[\int_{t_0}^{t_{tot}}\left(\int_{t_0}^{t_{tot}}\tau(t)^{1.45}\,dt + 1.45\int_{\tau(t_0)}^{\tau(t_{tot})} t\cdot\tau(t)^{0.45}\,d\tau + \left(\frac{PAS(t_0)}{1.42\times10^{-11}}\right)^{0.37}\right)^{1.67}\tau^{1.45}\,dt\right] \quad (4.2)$$

Table 4.7. Optimized model constants for the Grigioni approach

Case	Model Constants			RMS Error	N
	C (x 10^{-11})	α	β	(x 10^{-3})	
With Shear Loading Rate	1.42 ± 0.01	3.87	2.67	7.13	23
Without Shear Loading Rate	4.35 ± 0.02	3.88	2.55	7.11	74

Constants are means ± SEM of optimized values corresponding to the lowest RMS errors for the Grigioni approach. N is the number of constants combinations yielding the lowest RMS error.

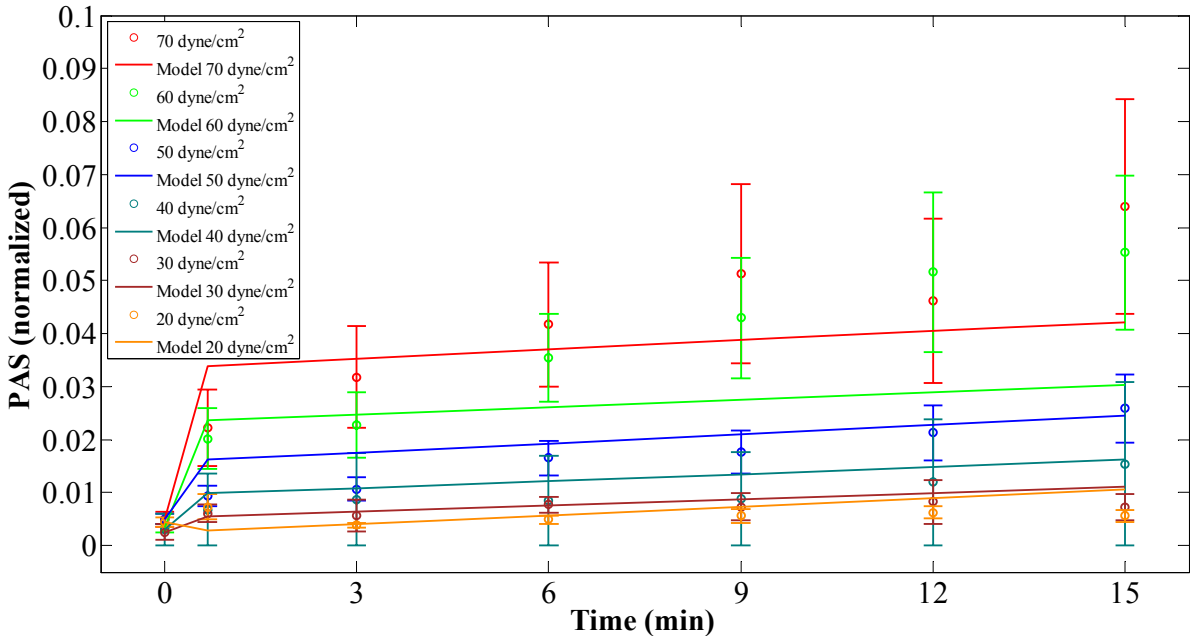

Figure 4.24. Variable shear stress fits for the Grigioni approach. Optimized platelet activation model (lines) was fit to shear-induced platelet sensitization experimental PAS values (open circles) for the shear loading case.

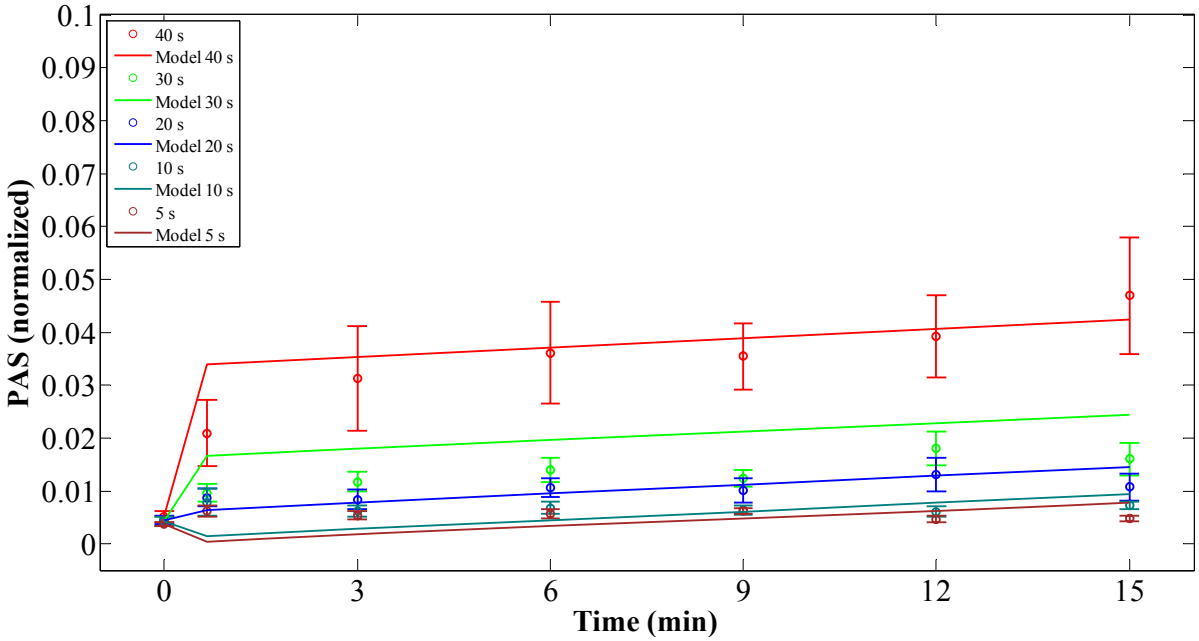

Figure 4.25. Variable duration fits for the Grigioni approach. Optimized platelet activation model (lines) was fit to shear-induced platelet sensitization experimental PAS values (open circles) for the shear loading case.

Similar to the simple model results, Figures 4.24 and 4.25 show that the model fits may be appropriate for the lower shear stresses and durations, but these fits underestimated the PAS values for the higher shear stresses subsequent to the 40 s time point. Unlike for the simple power law approach, the PAS value at 40 s, which is immediately after the high shear stress exposure, was not significantly overestimated for the shear loading case. All plots subsequent to the initial high shear stress phase (0 – 40 s) show a linear behavior, as observed experimentally. However, the slopes for the 60 and 70 dyne/cm^2 cases are lower than experimentally observed, indicating that the PAS values immediately after the high shear stress phase had a minor effect on the predicted results.

4.8.3 Two-Part Optimization Approach

Table 4.8 shows the model constants for the high shear stress and subsequent low shear stress phases when a two-part simple phenomenological optimization scheme was applied.

Figures 4.26 and 4.27 show the model prediction on the same set of axes as experimental results for the variable shear stress and exposure time conditions, respectively. The RMS error was significantly lower for the initial high shear stress phase, and the predicted PAS after the initial high shear stress exposure was more accurate than for the original simple power law model. However, the cumulative RMS error was higher than for the original model, even though the desired linear behavior was observed for the subsequent low shear stress phase. Furthermore, the slope was identical for all fits, and therefore this two-part model does not address the effect of PAS after the initial high shear stress exposure on subsequent values during the low shear stress phase:

$$PAS = 1.2\times10^{-11}\left[2.85\int_{t_0}^{t_1} t^{1.85}\tau^{2.16}dt + 2.16\int_{t_0}^{t_1}\tau^{1.16}t^{2.85}\,\dot{\tau}dt\right] + 2.26\times10^{-5}\int_{t_1}^{t_{total}} t^{-0.07}\tau^{0.5}dt + PAS_0 \tag{4.3}$$

Table 4.8. Optimized model constants for the two-part, simple phenomenological approach

Case	Model Constants			RMS Error	N
	C (x 10^{-7})	α	β	(x 10^{-3})	
High Shear Stress Phase	0.012	2.16	2.85	2.49	996
Low Shear Stress Phase	22300 ± 105	5.25 ± 0.09	0.95	10.28	1040

Constants are means ± SEM of optimized values corresponding to the lowest RMS errors for the two-part simple phenomenological approach. N is the number of constants combinations yielding the lowest RMS error.

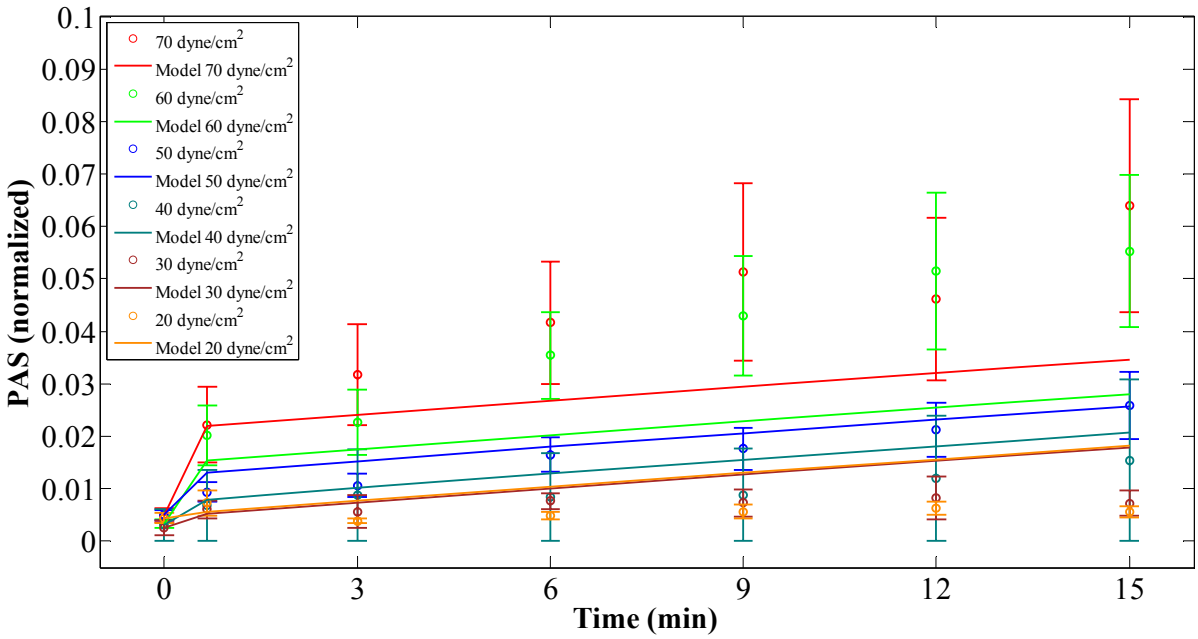

Figure 4.26. Variable shear stress fits for the two-part simple phenomenological approach. Optimized platelet activation model (lines) was fit to shear-induced platelet sensitization experimental PAS values (open circles) for the shear loading case.

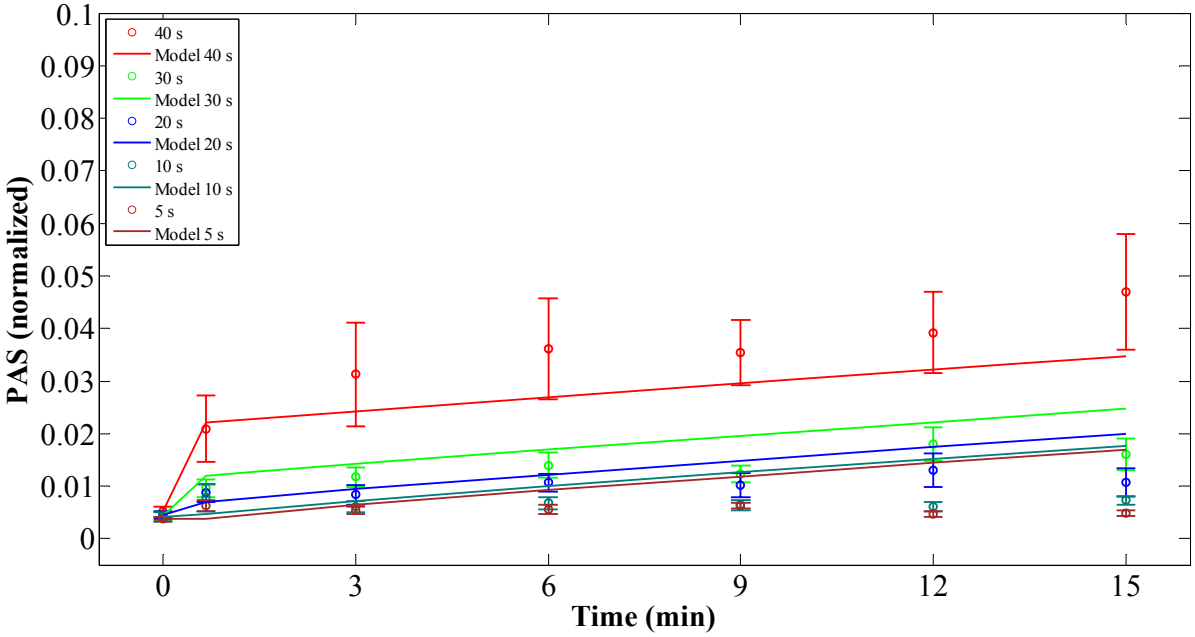

Figure 4.27. Variable duration fits for the two-part simple phenomenological approach. Optimized platelet activation model (lines) was fit to shear-induced platelet sensitization experimental PAS values (open circles) for the shear loading case.

Table 4.9 shows the model constants for the high shear stress and subsequent low shear stress phases when a two-part Grigioni optimization scheme was applied. Figures 4.28 and 4.29

show the model prediction on the same set of axes as experimental results for the variable shear stress and exposure time conditions, respectively. As observed for the simple phenomenological model, the RMS error was significantly lower for the initial high shear stress phase, but the predicted PAS after the initial high shear stress exposure was more accurate than for the one-partl simple model. However, the low shear stress phase PAS values were overestimated for the lower shear stress conditions. While the cumulative RMS error was slightly higher than the one-part Grigioni model, there was an increase in the post-high shear exposure slopes with an increase in the corresponding initial high shear stress. This response resembles the behavior observed experimentally:

$$PAS = 4.73\times10^{-4}\left[\int_{t_0}^{t_1}\left(\int_{t_0}^{t_1}\tau(\xi)^{-0.01}d\xi - 0.01\int_{\tau(t_0)}^{\tau(t_1)}\xi\cdot\tau(\xi)^{-1.01}d\tau + 14.48PAS(t_0)^{1.41}\right)^{-0.29}\tau^{-0.01}dt\right] + 1.08\times10^{-8}\left[\int_{t_1}^{t_{total}}\left(\int_{t_1}^{t_{total}}\tau(\xi)^{2.28}d\xi + 1.03\times10^{4}PAS(t_1)^{0.43}\right)^{1.3}\tau^{2.28}dt\right] \quad (4.4)$$

Table 4.9. Optimized model constants for the two-part, Grigioni approach

Case	Model Constants			RMS Error	N
	C (x 10^{-7})	α	β	(x 10^{-3})	
High Shear Stress Phase	6659.8	-0.01	0.71	2.88	27
Low Shear Stress Phase	0.0047	5.25 ± 0.68	2.30	8.16	20

Constants are means ± SEM of optimized values corresponding to the lowest RMS errors for the two-part Grigioni approach. N is the number of constants combinations yielding the lowest RMS error.

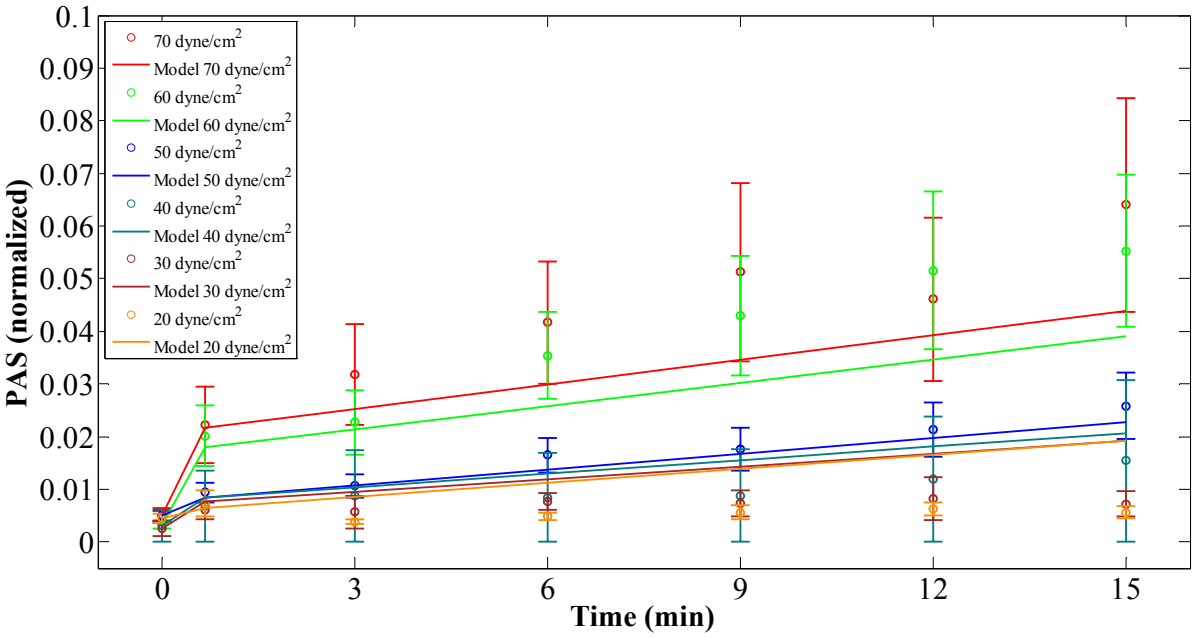

Figure 4.28. Variable shear stress fits for the two-part Grigioni approach. Optimized platelet activation model (lines) was fit to shear-induced platelet sensitization experimental PAS values (open circles) for the shear loading case.

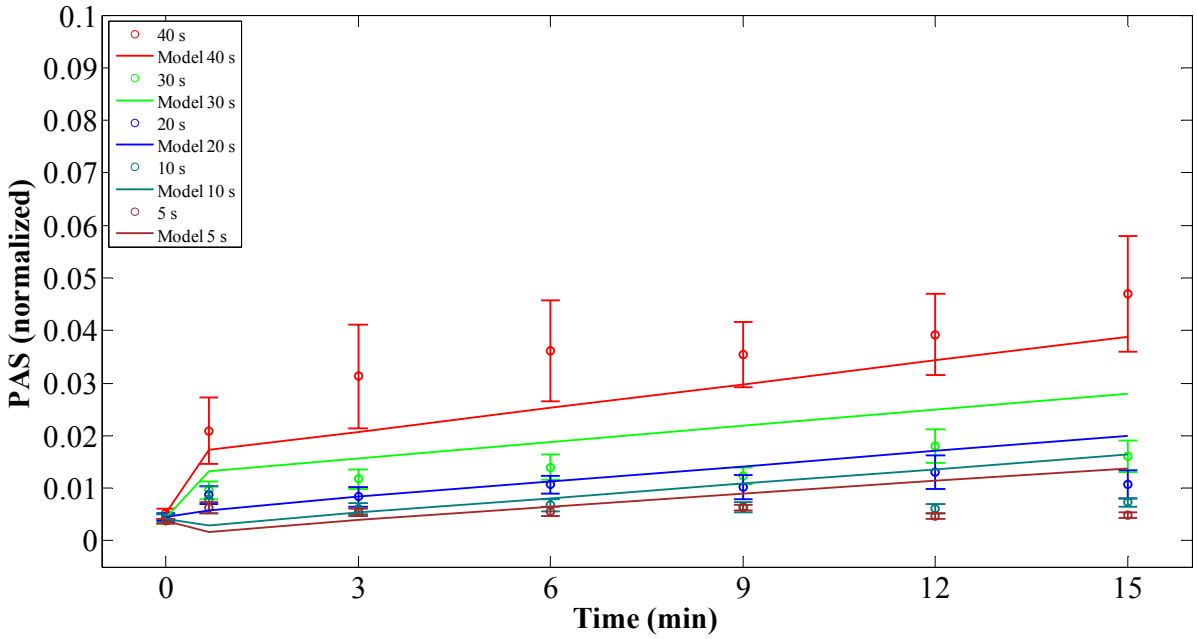

Figure 4.29. Variable duration fits for the two-part Grigioni approach. Optimized platelet activation model (lines) was fit to shear-induced platelet sensitization experimental PAS values (open circles) for the shear loading case.

V. DISCUSSION

5.1 Shear-Induced Platelet Sensitization

Shear-induced platelet activation has been studied extensively since the late 1970s. A multitude of activation markers have been used to examine the response of platelets to shear stress, including the measure of serotonin release [74, 120], β-thromboglobulin release [61, 72], anionic phospholipid exposure [84], P-selectin exposure [24, 63, 64], and prothrombin activation ("PF3" activity) [65, 67].

However, there is little is known about platelet behavior after exposure to pathological shear stress, such as will occur *in vivo* after passage through a blood recirculating device. Do the platelets recover; do they remain stably activated; or do they undergo further activation? Several studies have examined platelet hyperreactivity, defined as increased platelet function with regards to activation and aggregation [121]. However, these studies have focused on platelet response to exogenous agonists such as epinephrine, ADP, collagen, and thrombin-receptor activating peptide (TRAP) [122, 123], rather than the intrinsic activity of the platelets themselves. In this study, we examined the possibility that brief exposure to high shear stress should be considered as a natural physical agonist that sensitizes platelets to later, quite minor, mechanical forces.

Figures 4.2 and 4.3 show that extending the low shear stress period between peak shear stress pulses of 100 dyne/cm^2 causes a decrease in the platelet activation rate, which is particularly significant at a higher platelet count of 100,000/μl. This implies potential platelet-platelet "crosstalk" behavior, although these results lack the nonlinear behavior of prior count-

based experiments [67]. However, it should be noted that the integral shear stress for the two types of shear stress waveforms (short and long low shear stress period) are substantially different, and the platelet activation behavior may actually be a function of the peak shear pulse frequency. To truly understand what is occurring in this instance, the platelet activation behavior subsequent to high shear stress exposure must be examined.

Figures 4.4-7 allow two key conclusions. 1) Platelets are activated a little by short pulses of high shear stress, but they do not recover their normal quiescent activity state under subsequent normal conditions of low shear stress. 2) If the initial exposure is sufficiently severe ($\geq$ 2400 dyne·s/cm^2 integral shear stress), they are become substantially more sensitive to subsequent low shear stress. This sensitization threshold is lower than the platelet activation threshold curve plotted by Hellums (Fig. 2.1), indicating that sensitization behavior may be triggered before any significant platelet activation is observed.

It is relevant to note here that these experiments were done *in vitro* with purified platelets, and in particular that they lacked other blood cells or the presence of endothelial cells. The latter are particularly potent regulators of platelet function, and it is thus feasible that the post-exposure activation that we observe here may be substantially modulated *in vivo* or in the presence of other relevant cell types. This is partially examined in Section 5.3.

The sensitization behavior may partially explain the high risk of thromboembolic complications in patients with implanted blood recirculating devices. Wall shear stresses are typically high in such devices, and in MHVs, they range from 100 to 8,000 dyne/cm^2 [12, 41]. Although exposure to such high shear stress typically lasts only about 10^{-3} to 10^{-1} s [41, 91], the peak shear stress in these situations is substantially higher than we can emulate experimentally. Thus, while this study demonstrated sensitization at a lower (but still pathological) shear stress, it

required a longer exposure time. This issue was partially addressed by the very high shear stress experiments (Figs. 4.8-9). At average shear stress of 1,000 dyne/cm^2 and 25 ms duration, emulating conditions in devices, a large, but non-significant sensitization response was observed. Certainly, more experiments may render this result significant, thus identifying a sensitization threshold at a lower integral shear stress of 25 dyne s/cm^2. However, the lower shear stress conditions have the same integral shear stress, but do not yield such an increase in platelet activation rate. Both shear stress and time obviously play a role, but we do not know if the integral shear stress is in fact the main controlling variable. Based on Figure 4.7 and 4.8, it certainly appears that sensitization is not linearly related to the integral, and that a pathological threshold of exposure must be exceeded. While convenient for identifying shear stress and duration combinations, it is obvious that the linear integral shear stress variable needs to be replaced with a non-linear form based on additional experiments with a multitude of shear stress and exposure time combinations.

5.2 Role of Platelet Count and Activity State

Based on the results of Figures 4.2-3 and prior experiments [67], it was anticipated that platelet count plays a role in the sensitization process. However, Figure 4.11 shows that increasing the platelet count from 20,000/μl to 150,000/μl does not show a significant increase in the post-high shear activation rate, and therefore negates platelet-platelet crosstalk after sensitization. However, sensitized platelets do communicate with quiescent platelets (Fig. 4.12), contradicting the prior observation. This may be partially explained by noting that in the prior case, the entire platelet population is exposed to uniform shear stress, and thus all platelets are similarly activation after the initial high shear stress exposure, and that final platelet

concentrations are equal in the assay. Platelet-platelet collisions may contribute to activation [16], particularly under dynamic shear conditions [67], and the resulting activation rate may be driven by count (i.e. higher count results in more collisions and therefore more activation). However, the platelets in this case are subject to constant shear stress with very brief acceleration and deceleration phases, giving little opportunity for collisions to occur. In the case of quiescent platelets, signals from sensitized platelets may be communicated via agonists released from the latter, and thus effectively activating both subpopulations, and causing a similar subsequent bulk platelet activation rate, despite the count being doubled. While these signaling interactions are partially addressed in Section 5.3, elucidation of specific crosstalk mechanisms requires further study.

5.3 Mechanisms of Shear-Induced Platelet Sensitization

While shear stress is known to activate platelets, the exact mechanism by which such a process occurs in not clearly understood. Before examining the present data and how it guides in the identification of a shear-based mechanism of platelet activation, it is helpful to draw an analogy with endothelial cells, which are exposed to similar physiological and pathological shear stresses, and whose shear-induced activation mechanisms have been extensively studied. In endothelial cells, eight types of stress sensors have been identified: ion channels (including Ca^{2+}-dependent channels), growth factor receptors, G-proteins, calveolae, adhesive proteins, cytoskeleton, glycocalyx, and primary cilia [124-126]. In the present study, we can address Ca^{2+}-dependent signaling, G-proteins (and their associated GPCRs), and adhesive proteins.

We have shown that sensitization is not inhibited by an intracellular Ca^{2+} chelator, BAPTA-AM. Increase in cytosolic calcium concentration, $[Ca^{2+}]_i$, plays a major role in platelet

activation, and introduction of BAPTA-AM abolishes the depolarization and degranulation of platelets caused by thrombin [127], and reduces activation in a constant-shear flow loop [128]. Additional experiments also demonstrate that $[Ca^{2+}]_i$ depletion in platelets exposed to high shear stress still form spheres and membrane projections, indicating Ca^{2+}-independent cytoskeletal rearrangement [129]. Our results indicate that while BAPTA-AM causes a small reduction in platelet activation over the initial 40 s exposure to 70 dyne/cm^2, as expected, subsequent platelet activation at low shear stress was unaffected (Fig. 4.19). It therefore seems unlikely that $[Ca^{2+}]_i$ is involved in activation during the extended low-shear phase.

GPCRs appear to play a role in the modulation of the sensitization behavior. TRAP, a powerful thrombin analog, acts through the PAR1 receptor, which is coupled to G-proteins G_q, G_{12}/G_{13}, and G_i [9], and appears to amplify the sensitization response (Fig. 4.16). TRAP was used in lieu of thrombin as the latter is a powerful agonist that interferes with prothrombinase activity measurements. The PAS Assay [66] utilized in this study offers an advantage over prior prothrombinase assays [130-133] in that it uses acetylated prothrombin that is activated at near-normal rates by the prothrombinase complex and produces modified thrombin that cannot activate platelets. Arachidonic acid, whose conversion byproduct TXA_2 acts through the TXA_2 receptor (TP) coupled to G_q and G_{12}/G_{13}, activates the platelets prior to shear stress application (Fig. 4.18). A reduced post-high shear sensitization response is observed, which indicates that the activated TP receptors are unable to amplify the subsequent shear-induced signal. Previous studies [134, 135] have shown that activation of the TP receptor by the TXA_2 mimetic U46619 causes subsequent desensitization of the TP receptor as well as $P2Y_1$, an ADP receptor, which may explain the initial drop in Figure 4.18. Another study has shown that arachidonic acid and its metabolites play a critical role in causing platelet activation but their continued presence is

not essential for irreversible aggregation [136]. Arachidonic acid is also found in platelet-derived microparticles (PMP or microvesicles) and may further upregulate platelet activation [137]. This may partly explain the subsequent sensitization response, albeit reduced (Figure 4.18). The endothelium-derived inhibitor, PGI_2, which acts through the G_s-coupled IP receptor and stimulates adenylyl cyclase and cAMP production [9], does not appear to attenuate the sensitization response (Fig. 4.21). ADP, which was not directly studied, acts via the $P2Y_{12}$ receptor coupled to G_{12}, as well as causes platelet shape change via the $P2Y_1$ receptor coupled to G_q [17]. However, the ADP scavenger apyrase attenuated the sensitization response (Fig. 4.20), indicating a role for ADP in sensitization. Thus, among the GPCRs, only the PAR1 receptor is substantially involved in modulation of the sensitization response, with further elucidation needed on the role of the ADP receptors $P2Y_1$ and $P2Y_{12}$.

Collagen amplifies the sensitization response (Fig. 4.17). It is exposed from the subendothelial extracellular matrix after endothelial denudation or plaque rupture. Collagen interacts with platelets via the GPVI receptor through a tyrosine kinase-dependent pathway [138] to increase $[Ca^{2+}]_i$ and activate protein kinase C, leading to secretion of ADP and TXA_2 [17, 117].

Prior studies have promoted the GPIbα constituent of the GPIb-IX-V complex as a mechanoreceptor that senses shear stress and induces cytoskeletal remodeling [129, 139]. However, this process requires vWF immobilized either on subendothelial extracellular matrix components or on adjacent platelets under fluid shear stress [129, 140]. In this study, it is unknown if GPIbα is a potential mechanoreceptor since smaller monomers of vWF have most likely been removed by gel-filtration and replaced with vWF- and fibrinogen-free platelet buffer.

Platelet-derived fibrinogen and vWF may be able to participate in later activation, but this requires activation-induced α-granule release.

Aggregation response with and without pre-exposure to high shear stress was also examined. Pre-sheared platelets show a marked decrease in aggregation response when compared to unsheared platelets (Fig. 4.15). This contradicts earlier experiments that indicate that shear stress enhances the aggregation response in PRP [15] and washed platelets [141]. However, in the latter, fibrinogen was added prior to shear stress exposure, while fibrinogen was added post-high shear stress exposure in the present study. This indicates a shear-induced desensitization of the integrin $\alpha_{IIb}\beta_3$ (GPIIb-IIIa). Aggregation and activation desensitization has been observed when platelets are pre-exposed to one biochemical agonist, followed by the same or different biochemical agonist a short time later [134, 142, 143]. Few studies have addressed desensitization with shear stress. Low shear stress (via stirring) caused a desensitization in response to challenges with ADP [69]. Impairment of ADP-induced aggregation was previously observed after exposure to a pathologic shear stress of 204 dyne/cm^2 [24]. While GPIIb-IIIa is activated under shear stress via binding to vWF or fibrinogen, it also acts a "stabilizer" for adhesion to prevent dislocation from the endothelial surface [144]. It is possible that shear stress strengthens the bond between GPIIb-IIIa and fibrinogen through a conformational change, but this behavior needs to be studied in the absence of ligands such as vWF and fibrinogen.

Because lysis is a well known result of high shear, we also examined whether lysis is correlated with subsequent activation. Platelets are more prone to lysis, compared to RBCs, as they have less flexible membranes and experience a higher strain when exposed to shear stress [25]. Wurzinger et al. [27] showed that platelet activation and lysis (marked by LDH release) correlate well, but the conditions studied involved much higher shear stress (2,550 dyne/cm^2 for

7 ms and 1,700 dyne/cm^2 for 113 ms). Under the conditions in this study, lysis is minor in the high-shear phase (approx. 5% of maximal), and this correlates with a minor increase in platelet activation state as measured by prothrombinase activity (approx. 6% maximal). However, in the latter low-shear phase, while the platelets undergo continuing activation, no further lysis occurs (Fig. 4.13).

Shear-sensitized platelets appear to show hallmarks of apoptosis, or programmed cell death. Apoptotic platelets exhibit morphological changes such as shrinkage, cytoplasmic condensation, granule fusion with the plasma membrane, blebbing, filopod extension, and PMP formation [24]. The latter was examined in this study. Figure 4.14 demonstrates that PMP activity is evident immediately after high shear stress exposure and continually increases during the low shear stress phase. This activity constitutes about 50% of the combined platelet and PMP activity at both immediately after the high shear stress exposure and at the end of the low shear stress phase. The prothrombinase activity (Section 5.1) and PMP activity agrees with a prior study that showed marked phosphatidylserine (anionic phospholipid) and microparticle response (as measured by the anti-GPIIb-IIIa antibody, anti-CD41) after exposure to shear stresses between 117 and 204 dyne/cm^2 [24]. Prior studies have made the observation that PMP shedding is completely dependent on GPIbα interaction with vWF [145], but vWF activity was expected to be minimal due to plasma gel-filtration. However, the Sepharose 2B beads (filtration size > 40,000 kDa) may have allowed larger vWF multimers (>250,000 kDa [146]) to pass with platelets. The enhanced sensitization response to TRAP (Fig. 4.16) may also be explained by the fact that TRAP potentiates shear-induced PMP formation, although this behavior was not observed for agonists such as ADP, collagen, or TXA_2 [116]. Whether these behaviors are due to apoptosis is unknown, as other apoptotic responses [24] were not examined.

These results allow us to propose a mechanism whereby shear stress induces platelet sensitization response observed in fibrinogen- and vWF-free washed platelets post- high shear stress exposure. Briefly, the high shear stress causes minimal lysis (approximately 5% observed for 40 s exposure to 70 dyne/cm^2). This liberates granular contents, including ADP, Ca^{2+}, FV, fibrinogen, and vWF, which allows for the initiation of activation during the high shear stress phase. The combination of these chemical agonists and high shear stress then induce PMP formation and further granular release, while impairing aggregation, even during the low shear stress phase. This results in the observation of increasing activation behavior, despite removal of the high shear stress insult, in what is termed as *shear-induced platelet sensitization*. The validation of this proposed mechanism (Fig. 5.1) awaits further study.

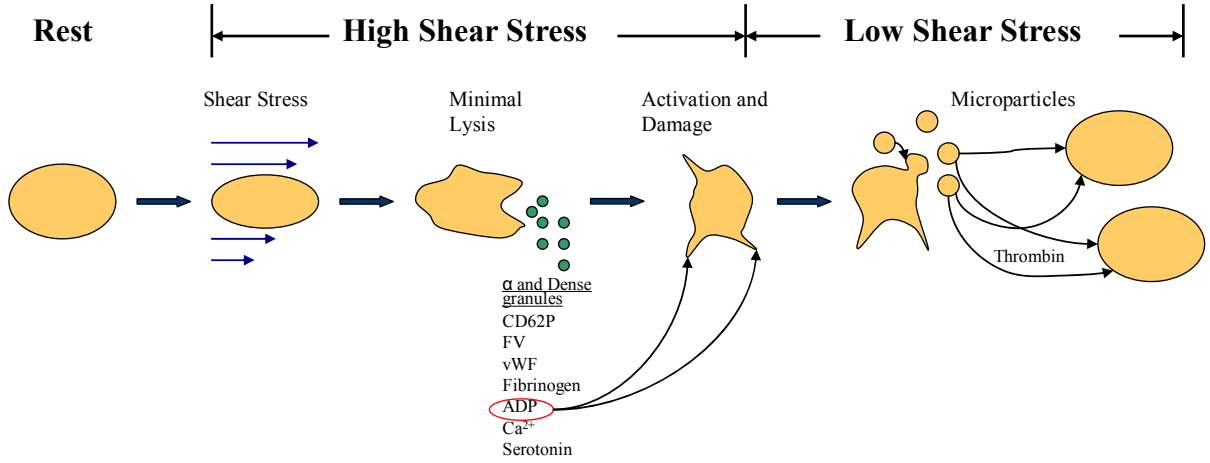

Figure 5.1. Proposed mechanism of shear-induced platelet sensitization.

5.4 Development of a Platelet Activation Model

While several researchers have broached the concept of predictive platelet activation models, only two groups have developed such models based on direct experimental results [2, 68]. Of these two, only the Nobili model [68], optimized with experiments conducted by our group, addresses the three conditions of blood damage power law formulations, as identified by

Grigioni [102]: (1) it should not violate the causality principle (i.e. decreasing shear stress does not equal decreasing activation); (2) it must be validated by experimental results based on shear stress magnitude and exposure time; and (3) it must account for prior shear stress history. The present models provide improvements over previous models by accounting for dynamic shear stresses, such as those found in blood-recirculating devices. The present predictive approaches are key to a combined design optimization framework that couples numerical simulations to experimental platelet activation state (PAS) measurements in order to reduce thrombogenic complications associated with blood-recirculating devices [89].

These conditions were addressed using two models: the simple phenomenological and Grigioni approaches. Both the approaches used offer an advantage over the Nobili model in that they include the shear loading rate, which accounts for acceleration and deceleration of flow and allows for platelet activation prediction under more dynamic conditions. The simple phenomenological approach fell short in that it overestimated the PAS due to the high shear stress and produced a nonlinear behavior for the subsequent low shear stress phase (Figs. 4.22-23). The Grigioni approach offered a slight improvement in that it recreated the linear platelet activation response during the low shear stress phase, but it overestimated the high shear stress PAS and underestimated the low shear stress PAS (Figs. 4.24-25). Dividing both approaches into a two-step model, where the results of the high shear stress phase drive the behavior of the low shear stress phase, provided a better fit for the high shear stress phase. The Grigioni approach recreated the low shear stress platelet activation response observed in experiments, where the subsequent platelet activation rate was dependent on the PAS at the conclusion of the high shear stress phase (Figs. 4.28-29).

Unlike the one-part simple and Grigioni approaches, and two-part simple approach, the two-part Grigioni approach yields predicted platelet activation rates that emulate experimental behavior during the subsequent low shear stress phase. This indicates a dependence on post-high shear stress PAS and shear loading rate. This phenomenological model is most appropriate of the studied approaches for describing shear-induced platelet sensitization behavior. While the one-part simple and Grigioni approaches with a shear-loading rate term do not appear to take into account the effect of the high shear stress PAS on the subsequent low shear stress platelet activation rates, they may be appropriate for constant or dynamic shear stress patterns, as used by Nobili [68]. However, this approach needs to be further validated by a wider array of experiments involving dynamic waveforms such as those that are present in blood recirculating devices.

The Nobili model used the genetic algorithm method, which is a global nonlinear least squares (NLS) approach and is more robust in minimization of error between experimental results and numerical predictions [68]. While the Levenburg-Marquardt optimization scheme uses a local NLS approach, which can be mired in local minima, the constants to be determined were initialized over a large range of values to reduce the risk of obtaining a non-desirable set of optimized constants.

While these approaches are phenomenological (or shear stress- and duration-dependent) in nature, the contribution of biochemical interactions, particularly those of agonists that amplify the activation response and vascular inhibitors that limit this response, should not be neglected Future improvements in these modeling approaches should include contributions from these interactions in order to provide robust predictive tools for the design optimization of blood recirculating devices [89].

The present predictive platelet activation models provide an improved alternative to prior platelet activation models [2, 68, 91] by introducing terms that express previous platelet activation history and shear-loading rate terms that account for the dynamic nature of shear stress waveforms, such as those found in blood-recirculating devices [4]. Our group previously introduced the Device Thrombogenicity Emulator (DTE) approach, consisting of numerical simulation of devices, extraction of shear stress behavior along specific platelet trajectories, experimental emulation of these conditions in a hemodynamic shearing device, and measurement of platelet activation. The present predictive modeling approaches provide a robust platelet damage quantification tool that can be used in combination with modeling approaches [89] to map device-specific thrombogenicity footprints in the thrombogenic optimization of blood-recirculating devices.

VI. SUMMARY AND FUTURE WORK

Platelets exposed to high shear stress for brief durations are substantially sensitized to subsequent, much lower levels of shear stress, but this does not occur unless the initial high-shear exposure exceeds a threshold. Under the conditions of this study (maximal shear stress of 70 dyne/cm^2), this threshold was 2,400 dyne s/cm^2. Exposure to 1,000 dyne/cm^2 for 25 ms, which is similar to conditions in devices, recreated this sensitization behavior, although not significantly.

The sensitization response was amplified with the addition of platelet agonists TRAP, a thrombin analog, and collagen; this response was attenuated with the ADP scavenger apyrase. The aggregation response to various platelet agonists was impaired after pre-exposure to shear. While lysis was minimal and restricted to the high shear stress exposure, increasing microparticle activity and the potential for sensitized-quiescent platelet-platelet crosstalk was observed in the subsequent low shear stress phase. These observations suggest that shear-induced platelet lysis triggers granular release of agonists, and the combination of these agonists with high shear stress cause platelet microparticle formation. This results in the sensitization response observed in the subsequent low shear stress exposure.

A phenomenological platelet activation model based solely on shear stress, exposure time, and shear-loading rate was derived and fitted to results obtained from the sensitization experiments. While several models were optimized with experimental results, the Grigioni approach with separate evaluations of the high and low shear stress phases provided the best fit.

Future work should address whether the sensitization response is observed under more complex and dynamic conditions, and whether this behavior can be modulated by a larger variety of synthetic platelet agents. Furthermore, platelet treatment with a variety of platelet agonists and inhibitors will allow further elucidation of platelet activation and sensitization mechanisms. These observations will then allow for the formulation of a more robust platelet activation model that takes both phenomenological and biochemical factors into account. Such a model may provide a useful tool for both scientists and device manufacturers to increase understanding of platelet activation mechanisms and enhance design optimization of blood recirculating devices in order to limit or eliminate thrombogenic complications.

REFERENCES

1. Sutera, S.P. and M.H. Mehrjardi, *Deformation and fragmentation of human red blood cells in turbulent shear flow.* Biophys J, 1975. **15**(1): p. 1-10.

2. Ramstack, J.M., L. Zuckerman, and L.F. Mockros, *Shear-induced activation of platelets.* J Biomech, 1979. **12**(2): p. 113-25.

3. Bluestein, D., *Towards optimization of the thrombogenic potential of blood recirculating cardiovascular devices using modeling approaches.* Expert Rev Med Devices, 2006. **3**(3): p. 267-70.

4. Bluestein, D., K.B. Chandran, and K.B. Manning, *Towards non-thrombogenic performance of blood recirculating devices.* Ann Biomed Eng, 2010. **38**(3): p. 1236-56.

5. Hartwig, J.H., *The platelet: form and function.* Semin Hematol, 2006. **43**(1 Suppl 1): p. S94-100.

6. White, J.G., *Platelet Structure*, in *Platelets*, A.D. Michelson, Editor. 2007, Academic Press: San Diego, CA. p. 45-73.

7. *Haemotological Diseases*, in *Clinical Medicine*, P. Kumar and M. Clark, Editors. 2005, Elsevier Saunders: London, U.K. p. 469.

8. Clemetson, K.J., *Platelet Receptors*, in *Platelets*, A.D. Michelson, Editor. 2002, Academic Press: San Diego, CA. p. 65-84.

9. Offermanns, S., *Activation of platelet function through G protein-coupled receptors.* Circ Res, 2006. **99**(12): p. 1293-304.

10. Reed, G.L., *Platelet Secretion*, in *Platelets*, A.D. Michelson, Editor. 2002, Academic Press: San Diego, CA. p. 181-195.

11. Fuster, V., L. Badimon, J.J. Badimon, and J.H. Chesebro, *The pathogenesis of coronary artery disease and the acute coronary syndromes (2).* N Engl J Med, 1992. **326**(5): p. 310-8.

12. Kroll, M.H., J.D. Hellums, L.V. McIntire, A.I. Schafer, and J.L. Moake, *Platelets and shear stress.* Blood, 1996. **88**(5): p. 1525-41.

13. Lowe, G.D., *Virchow's triad revisited: abnormal flow.* Pathophysiol Haemost Thromb, 2003. **33**(5-6): p. 455-7.

14. Clemetson, K.J., *Platelet Receptors*, in *Platelets*, A.D. Michelson, Editor. 2007, Academic Press: San Diego, CA.

15. Hellums, J.D., D.M. Peterson, N.A. Stathopoulos, and J. Moake, *Studies on the Mechanisms of Shear-Induced Platelet Activation*, in *Cerebral Ischemia and Hemorheology*, A. Hartmann and W. Kuschinsky, Editors. 1987, Springer-Verlag: Heidelberg. p. 80-89.

16. Hellums, J.D., *1993 Whitaker Lecture: biorheology in thrombosis research.* Ann Biomed Eng, 1994. **22**(5): p. 445-55.

17. Woulfe, D.S., J. Yang, N. Prevost, P.J. O'Brien, and L.F. Brass, *Signal Transduction During the Initiation, Extension, and Perpetuation of Platelet Plug Formation*, in *Platelets*, A.D. Michelson, Editor. 2002, Academic Press: San Diego, CA. p. 197-213.

18. Tracy, P.B., L.L. Eide, and K.G. Mann, *Human prothrombinase complex assembly and function on isolated peripheral blood cell populations.* J Biol Chem, 1985. **260**(4): p. 2119-24.

19. Bouchard, B.A., S. Butenas, K.G. Mann, and P.B. Tracy, *Interaction Between Platelets and the Coagulation System*, in *Platelets*, A.D. Michelson, Editor. 2002, Academic Press: San Diego, CA. p. 229-253.

20. Alevriadou, B.R., J.L. Moake, N.A. Turner, Z.M. Ruggeri, B.J. Folie, M.D. Phillips, A.B. Schreiber, M.E. Hrinda, and L.V. McIntire, *Real-time analysis of shear-dependent thrombus formation and its blockade by inhibitors of von Willebrand factor binding to platelets.* Blood, 1993. **81**(5): p. 1263-76.

21. McCrary, J.K., L.H. Nolasco, J.D. Hellums, M.H. Kroll, N.A. Turner, and J.L. Moake, *Direct demonstration of radiolabeled von Willebrand factor binding to platelet glycoprotein Ib and IIb-IIIa in the presence of shear stress.* Ann Biomed Eng, 1995. **23**(6): p. 787-93.

22. Goto, S., Y. Ikeda, E. Saldivar, and Z.M. Ruggeri, *Distinct mechanisms of platelet aggregation as a consequence of different shearing flow conditions.* J Clin Invest, 1998. **101**(2): p. 479-86.

23. Merten, M., T. Chow, J.D. Hellums, and P. Thiagarajan, *A new role for P-selectin in shear-induced platelet aggregation.* Circulation, 2000. **102**(17): p. 2045-50.

24. Leytin, V., D.J. Allen, S. Mykhaylov, L. Mis, E.V. Lyubimov, B. Garvey, and J. Freedman, *Pathologic high shear stress induces apoptosis events in human platelets.* Biochem Biophys Res Commun, 2004. **320**(2): p. 303-10.

25. Travis, B.R., U.M. Marzec, H.L. Leo, T. Momin, C. Sanders, S.R. Hanson, and A.P. Yoganathan, *Bileaflet aortic valve prosthesis pivot geometry influences platelet secretion and anionic phospholipid exposure.* Ann Biomed Eng, 2001. **29**(8): p. 657-64.

26. Bluestein, D., W. Yin, K. Affeld, and J. Jesty, *Flow-induced platelet activation in mechanical heart valves.* J Heart Valve Dis, 2004. **13**(3): p. 501-8.

27. Wurzinger, L.J., P. Blasberg, and H. Schmid-Schonbein, *Towards a concept of thrombosis in accelerated flow: rheology, fluid dynamics, and biochemistry.* Biorheology, 1985. **22**(5): p. 437-50.

28. Bluestein, D., Y.M. Li, and I.B. Krukenkamp, *Free emboli formation in the wake of bi-leaflet mechanical heart valves and the effects of implantation techniques.* J Biomech, 2002. **35**(12): p. 1533-40.

29. Lloyd-Jones, D., R.J. Adams, T.M. Brown, M. Carnethon, S. Dai, G. De Simone, T.B. Ferguson, E. Ford, K. Furie, C. Gillespie, A. Go, K. Greenlund, N. Haase, S. Hailpern, P.M. Ho, V. Howard, B. Kissela, S. Kittner, D. Lackland, L. Lisabeth, A. Marelli, M.M. McDermott, J. Meigs, D. Mozaffarian, M. Mussolino, G. Nichol, V.L. Roger, W. Rosamond, R. Sacco, P. Sorlie, T. Thom, S. Wasserthiel-Smoller, N.D. Wong, and J. Wylie-Rosett, *Heart disease and stroke statistics--2010 update: a report from the American Heart Association.* Circulation, 2010. **121**(7): p. e46-e215.

30. Lietz, K. and L.W. Miller, *Destination therapy: current results and future promise.* Semin Thorac Cardiovasc Surg, 2008. **20**(3): p. 225-33.

31. Stevenson, L.W. and G. Couper, *On the fledgling field of mechanical circulatory support.* J Am Coll Cardiol, 2007. **50**(8): p. 748-51.

32. Simon, M.A., J. Watson, J.T. Baldwin, W.R. Wagner, and H.S. Borovetz, *Current and future considerations in the use of mechanical circulatory support devices.* Annu Rev Biomed Eng, 2008. **10**: p. 59-84.

33. Christiansen, S., A. Klocke, and R. Autschbach, *Past, present, and future of long-term mechanical cardiac support in adults.* J Card Surg, 2008. **23**(6): p. 664-76.

34. Rose, E.A., H.R. Levin, M.C. Oz, O.H. Frazier, Q. Macmanus, N.A. Burton, and E.A. Lefrak, *Artificial circulatory support with textured interior surfaces. A counterintuitive approach to minimizing thromboembolism.* Circulation, 1994. **90**(5 Pt 2): p. II87-91.

35. Rose, E.A., A.C. Gelijns, A.J. Moskowitz, D.F. Heitjan, L.W. Stevenson, W. Dembitsky, J.W. Long, D.D. Ascheim, A.R. Tierney, R.G. Levitan, J.T. Watson, P. Meier, N.S. Ronan, P.A. Shapiro, R.M. Lazar, L.W. Miller, L. Gupta, O.H. Frazier, P. Desvigne-Nickens, M.C. Oz, and V.L. Poirier, *Long-term mechanical left ventricular assistance for end-stage heart failure.* N Engl J Med, 2001. **345**(20): p. 1435-43.

36. Lietz, K., J.W. Long, A.G. Kfoury, M.S. Slaughter, M.A. Silver, C.A. Milano, J.G. Rogers, Y. Naka, D. Mancini, and L.W. Miller, *Outcomes of left ventricular assist device implantation as destination therapy in the post-REMATCH era: implications for patient selection.* Circulation, 2007. **116**(5): p. 497-505.

37. Slater, J.P., E.A. Rose, H.R. Levin, O.H. Frazier, J.K. Roberts, A.D. Weinberg, and M.C. Oz, *Low thromboembolic risk without anticoagulation using advanced-design left ventricular assist devices.* Ann Thorac Surg, 1996. **62**(5): p. 1321-7; discussion 1328.

38. Nielsen, V.G., J.K. Kirklin, W.L. Holman, B.L. Steenwyk, J.F. George, F. Zhou, D.A. Parks, and T.C. Ellis, *Mechanical circulatory device thrombosis: a new paradigm linking hypercoagulation and hypofibrinolysis.* ASAIO J, 2008. **54**(4): p. 351-8.

39. Vural, K.M., *Ventricular assist device applications.* Anadolu Kardiyol Derg, 2008. **8 Suppl 2**: p. 117-30.

40. Friedewald, V.E., R.O. Bonow, J.S. Borer, B.A. Carabello, P.P. Kleine, C.W. Akins, and W.C. Roberts, *The Editor's Roundtable: cardiac valve surgery.* Am J Cardiol, 2007. **99**(9): p. 1269-78.

41. Yoganathan, A.P., Z. He, and S. Casey Jones, *Fluid mechanics of heart valves.* Annu Rev Biomed Eng, 2004. **6**: p. 331-62.

42. Yacoub, M.H. and J.J. Takkenberg, *Will heart valve tissue engineering change the world?* Nat Clin Pract Cardiovasc Med, 2005. **2**(2): p. 60-1.

43. Akins, C.W., *Results with mechanical cardiac valvular prostheses.* Ann Thorac Surg, 1995. **60**(6): p. 1836-44.

44. Kidane, A.G., G. Burriesci, P. Cornejo, A. Dooley, S. Sarkar, P. Bonhoeffer, M. Edirisinghe, and A.M. Seifalian, *Current developments and future prospects for heart valve replacement therapy.* J Biomed Mater Res B Appl Biomater, 2009. **88**(1): p. 290-303.

45. Rahimtoola, S.H., *Choice of prosthetic heart valve in adults an update.* J Am Coll Cardiol, 2010. **55**(22): p. 2413-26.

46. Bonow, R.O., B.A. Carabello, K. Chatterjee, A.C. de Leon, Jr., D.P. Faxon, M.D. Freed, W.H. Gaasch, B.W. Lytle, R.A. Nishimura, P.T. O'Gara, R.A. O'Rourke, C.M. Otto, P.M. Shah, and J.S. Shanewise, *2008 focused update incorporated into the ACC/AHA 2006 guidelines for the management of patients with valvular heart disease: a report of the American College of Cardiology/American Heart Association Task Force on Practice Guidelines (Writing Committee to revise the 1998 guidelines for the management of patients with valvular heart disease). Endorsed by the Society of Cardiovascular Anesthesiologists, Society for Cardiovascular Angiography and Interventions, and Society of Thoracic Surgeons.* J Am Coll Cardiol, 2008. **52**(13): p. e1-142.

47. Butchart, E.G., P.A. Lewis, E.N. Kulatilake, and I.M. Breckenridge, *Anticoagulation variability between centres: implications for comparative prosthetic valve assessment.* Eur J Cardiothorac Surg, 1988. **2**(2): p. 72-81.

48. Butchart, E.G., A. Ionescu, N. Payne, J. Giddings, G.L. Grunkemeier, and A.G. Fraser, *A new scoring system to determine thromboembolic risk after heart valve replacement.* Circulation, 2003. **108 Suppl 1**: p. II68-74.

49. Goldsmith, I., A.G. Turpie, and G.Y. Lip, *Valvar heart disease and prosthetic heart valves.* BMJ, 2002. **325**(7374): p. 1228-31.

50. Dasi, L.P., H.A. Simon, P. Sucosky, and A.P. Yoganathan, *Fluid mechanics of artificial heart valves.* Clin Exp Pharmacol Physiol, 2009. **36**(2): p. 225-37.

51. Paul, R., O. Marseille, E. Hintze, L. Huber, H. Schima, H. Reul, and G. Rau, *In vitro thrombogenicity testing of artificial organs.* Int J Artif Organs, 1998. **21**(9): p. 548-52.

52. Schima, H. and G. Wieselthaler, *Mechanically induced blood trauma: are the relevant questions already solved, or is it still an important field to be investigated?* Artif Organs, 1995. **19**(7): p. 563-4.

53. Sallam, A.M. and N.H. Hwang, *Human red blood cell hemolysis in a turbulent shear flow: contribution of Reynolds shear stresses.* Biorheology, 1984. **21**(6): p. 783-97.

54. Grigioni, M., C. Daniele, G. D'Avenio, and V. Barbaro, *A discussion on the threshold limit for hemolysis related to Reynolds shear stress.* J Biomech, 1999. **32**(10): p. 1107-12.

55. Leverett, L.B., J.D. Hellums, C.P. Alfrey, and E.C. Lynch, *Red blood cell damage by shear stress.* Biophys J, 1972. **12**(3): p. 257-73.

56. Brown, C.H., 3rd, R.F. Lemuth, J.D. Hellums, L.B. Leverett, and C.P. Alfrey, *Response of human platelets to shear stress.* Trans Am Soc Artif Intern Organs, 1975. **21**: p. 35-9.

57. Brown, C.H., 3rd, L.B. Leverett, C.W. Lewis, C.P. Alfrey, Jr., and J.D. Hellums, *Morphological, biochemical, and functional changes in human platelets subjected to shear stress.* J Lab Clin Med, 1975. **86**(3): p. 462-71.

58. Lamson, T.C., G. Rosenberg, D.B. Geselowitz, S. Deutsch, D.R. Stinebring, J.A. Frangos, and J.M. Tarbell, *Relative blood damage in the three phases of a prosthetic heart valve flow cycle.* ASAIO J, 1993. **39**(3): p. M626-33.

59. Wootton, D.M. and D.N. Ku, *Fluid mechanics of vascular systems, diseases, and thrombosis.* Annu Rev Biomed Eng, 1999. **1**: p. 299-329.

60. Ku, D.N., *Blood flow in arteries.* Annual Review of Fluid Mechanics, 1997. **29**: p. 399-434.

61. Wurzinger, L.J., R. Opitz, P. Blasberg, and H. Schmid-Schonbein, *Platelet and coagulation parameters following millisecond exposure to laminar shear stress.* Thromb Haemost, 1985. **54**(2): p. 381-6.

62. Wurzinger, L.J., R. Opitz, M. Wolf, and H. Schmid-Schonbein, *"Shear induced platelet activation"--a critical reappraisal.* Biorheology, 1985. **22**(5): p. 399-413.

63. Zhang, J.N., A.L. Bergeron, Q. Yu, C. Sun, L.V. McIntire, J.A. Lopez, and J.F. Dong, *Platelet aggregation and activation under complex patterns of shear stress.* Thromb Haemost, 2002. **88**(5): p. 817-21.

64. Zhang, J.N., A.L. Bergeron, Q. Yu, C. Sun, L. McBride, P.F. Bray, and J.F. Dong, *Duration of exposure to high fluid shear stress is critical in shear-induced platelet activation-aggregation.* Thromb Haemost, 2003. **90**(4): p. 672-8.

65. Jesty, J., W. Yin, P. Perrotta, and D. Bluestein, *Platelet activation in a circulating flow loop: combined effects of shear stress and exposure time.* Platelets, 2003. **14**(3): p. 143-9.

66. Jesty, J. and D. Bluestein, *Acetylated prothrombin as a substrate in the measurement of the procoagulant activity of platelets: elimination of the feedback activation of platelets by thrombin.* Anal Biochem, 1999. **272**(1): p. 64-70.

67. Schulz-Heik, K., J. Ramachandran, D. Bluestein, and J. Jesty, *The extent of platelet activation under shear depends on platelet count: differential expression of anionic phospholipid and factor Va.* Pathophysiol Haemost Thromb, 2005. **34**(6): p. 255-62.

68. Nobili, M., J. Sheriff, U. Morbiducci, A. Redaelli, and D. Bluestein, *Platelet activation due to hemodynamic shear stresses: damage accumulation model and comparison to in vitro measurements.* Asaio J, 2008. **54**(1): p. 64-72.

69. Aursnes, I., J. Sundal, and T. Nome, *Shear stress activation of platelets with subsequent refractoriness.* Thromb Res, 1987. **45**(1): p. 29-37.

70. Born, G.V., *Aggregation of blood platelets by adenosine diphosphate and its reversal.* Nature, 1962. **194**: p. 927-9.

71. Weiss, H.J., V.T. Turitto, and H.R. Baumgartner, *Effect of shear rate on platelet interaction with subendothelium in citrated and native blood. I. Shear rate--dependent decrease of adhesion in von Willebrand's disease and the Bernard-Soulier syndrome.* J Lab Clin Med, 1978. **92**(5): p. 750-64.

72. Voisin, P., C. Guimont, and J.F. Stoltz, *Experimental investigation of the rheological activation of blood platelets.* Biorheology, 1985. **22**(5): p. 425-35.

73. Bernstein, E.F., U. Marzec, and G.G. Johnston, *Structural correlates of platelet functional damage by physical forces.* Trans Am Soc Artif Intern Organs, 1977. **23**: p. 617-25.

74. Colantuoni, G., J.D. Hellums, J.L. Moake, and C.P. Alfrey, Jr., *The response of human platelets to shear stress at short exposure times.* Trans Am Soc Artif Intern Organs, 1977. **23**: p. 626-31.

75. Anderson, G.H., J.D. Hellums, J.L. Moake, and C.P. Alfrey, Jr., *Platelet lysis and aggregation in shear fields.* Blood Cells, 1978. **4**(3): p. 499-511.

76. Belval, T.K. and J.D. Hellums, *Rapid reactions of platelets studied by a quenched-flow approach: aggregation kinetics.* J Lab Clin Med, 1984. **103**(3): p. 485-7.

77. Sutera, S.P., M.D. Nowak, J.H. Joist, D.J. Zeffren, and J.E. Bauman, *A programmable, computer-controlled cone-plate viscometer for the application of pulsatile shear stress to platelet suspensions.* Biorheology, 1988. **25**(3): p. 449-59.

78. Wurzinger, L.J., R. Opitz, M. Wolf, and H. Schmid-Schonbein, *Ultrastructural investigations on the question of mechanical activation of blood platelets.* Blut, 1987. **54**(2): p. 97-107.

79. Giorgio, T.D. and J.D. Hellums, *A cone and plate viscometer for the continuous measurement of blood platelet activation.* Biorheology, 1988. **25**(4): p. 605-24.

80. Sutera, S.P., M.D. Nowak, J.H. Joist, D.J. Zeffren, and J.E. Bauman, *A Programmable, Computer-Controlled Cone Plate Viscometer for the Application of Pulsatile Shear-Stress to Platelet Suspensions.* Biorheology, 1988. **25**(3): p. 449-459.

81. Schnittler, H.J., R.P. Franke, U. Akbay, C. Mrowietz, and D. Drenckhahn, *Improved in vitro rheological system for studying the effect of fluid shear stress on cultured cells.* Am J Physiol, 1993. **265**(1 Pt 1): p. C289-98.

82. Grad, Y. and S. Einav, *Spectral and instantaneous flow field characteristics of the laminar to turbulent transition in a cone and plate apparatus.* Experiments in Fluids, 2000. **28**(4): p. 336-343.

83. Buschmann, M.H., P. Dieterich, N.A. Adams, and H.J. Schnittler, *Analysis of flow in a cone-and-plate apparatus with respect to spatial and temporal effects on endothelial cells.* Biotechnol Bioeng, 2005. **89**(5): p. 493-502.

84. Shankaran, H., P. Alexandridis, and S. Neelamegham, *Aspects of hydrodynamic shear regulating shear-induced platelet activation and self-association of von Willebrand factor in suspension.* Blood, 2003. **101**(7): p. 2637-45.

85. Shankaran, H. and S. Neelamegham, *Effect of secondary flow on biological experiments in the cone-plate viscometer: methods for estimating collision frequency, wall shear stress and inter-particle interactions in non-linear flow.* Biorheology, 2001. **38**(4): p. 275-304.

86. Shankaran, H. and S. Neelamegham, *Nonlinear flow affects hydrodynamic forces and neutrophil adhesion rates in cone-plate viscometers.* Biophys J, 2001. **80**(6): p. 2631-48.

87. Sdougos, H.P., S.R. Bussolari, and C.F. Dewey, *Secondary Flow and Turbulence in a Cone-and-Plate Device.* Journal of Fluid Mechanics, 1984. **138**(Jan): p. 379-404.

88. Chung, C.A., M.R. Tzou, and R.W. Ho, *Oscillatory flow in a cone-and-plate bioreactor.* J Biomech Eng, 2005. **127**(4): p. 601-10.

89. Xenos, M., G. Girdhar, Y. Alemu, J. Jesty, M. Slepian, S. Einav, and D. Bluestein, *Device Thrombogenicity Emulator (DTE) - Design optimization methodology for cardiovascular devices: A study in two bileaflet MHV designs.* J Biomech, 2010.

90. Girdhar, G. and D. Bluestein, *Biological effects of dynamic shear stress in cardiovascular pathologies and devices.* Expert Rev Med Devices, 2008. **5**(2): p. 167-81.

91. Boreda, R., R.S. Fatemi, and S.E. Rittgers, *Potential for platelet stimulation in critically stenosed carotid and coronary arteries.* J Vasc Invest, 1995. **1**: p. 26-37.

92. Giersiepen, M., L.J. Wurzinger, R. Opitz, and H. Reul, *Estimation of shear stress-related blood damage in heart valve prostheses--in vitro comparison of 25 aortic valves.* Int J Artif Organs, 1990. **13**(5): p. 300-6.

93. Blackshear, P.L., Jr., F.D. Dorman, and J.H. Steinbach, *Some Mechanical Effects That Influence Hemolysis.* Trans Am Soc Artif Intern Organs, 1965. **11**: p. 112-7.

94. Bluestein, D., L. Niu, R.T. Schoephoerster, and M.K. Dewanjee, *Fluid mechanics of arterial stenosis: relationship to the development of mural thrombus.* Ann Biomed Eng, 1997. **25**(2): p. 344-56.

95. Dumont, K., J. Vierendeels, R. Kaminsky, G. van Nooten, P. Verdonck, and D. Bluestein, *Comparison of the hemodynamic and thrombogenic performance of two bileaflet mechanical heart valves using a CFD/FSI model.* J Biomech Eng, 2007. **129**(4): p. 558-65.

96. Tambasco, M. and D.A. Steinman, *Path-dependent hemodynamics of the stenosed carotid bifurcation.* Ann Biomed Eng, 2003. **31**(9): p. 1054-65.

97. Simon, H.A., L. Ge, F. Sotiropoulos, and A.P. Yoganathan, *Numerical investigation of the performance of three hinge designs of bileaflet mechanical heart valves.* Ann Biomed Eng, 2010. **38**(11): p. 3295-310.

98. Wu, J., B.M. Yun, A.M. Fallon, S.R. Hanson, C.K. Aidun, and A.P. Yoganathan, *Numerical Investigation of the Effects of Channel Geometry on Platelet Activation and Blood Damage.* Ann Biomed Eng, 2010.

99. Alemu, Y. and D. Bluestein, *Flow-induced platelet activation and damage accumulation in a mechanical heart valve: numerical studies.* Artif Organs, 2007. **31**(9): p. 677-88.

100. Yeleswarapu, K.K., J.F. Antaki, M.V. Kameneva, and K.R. Rajagopal, *A mathematical model for shear-induced hemolysis.* Artif Organs, 1995. **19**(7): p. 576-82.

101. Grigioni, M., C. Daniele, U. Morbiducci, G. D'Avenio, G. Di Benedetto, and V. Barbaro, *The power-law mathematical model for blood damage prediction: analytical developments and physical inconsistencies.* Artif Organs, 2004. **28**(5): p. 467-75.

102. Grigioni, M., U. Morbiducci, G. D'Avenio, G.D. Benedetto, and C.D. Gaudio, *A novel formulation for blood trauma prediction by a modified power-law mathematical model.* Biomech Model Mechanobiol, 2005. **4**(4): p. 249-60.

103. Purvis, N.B., Jr. and T.D. Giorgio, *The effects of elongational stress exposure on the activation and aggregation of blood platelets.* Biorheology, 1991. **28**(5): p. 355-67.

104. Neuenschwander, P. and J. Jesty, *A comparison of phospholipid and platelets in the activation of human factor VIII by thrombin and factor Xa, and in the activation of factor X.* Blood, 1988. **72**(5): p. 1761-70.

105. Blackman, B.R., G. Garcia-Cardena, and M.A. Gimbrone, Jr., *A new in vitro model to evaluate differential responses of endothelial cells to simulated arterial shear stress waveforms.* J Biomech Eng, 2002. **124**(4): p. 397-407.

106. Sheriff, J., D. Bluestein, G. Girdhar, and J. Jesty, *High-shear stress sensitizes platelets to subsequent low-shear conditions.* Ann Biomed Eng, 2010. **38**(4): p. 1442-50.

107. Miyazaki, Y., S. Nomura, T. Miyake, H. Kagawa, C. Kitada, H. Taniguchi, Y. Komiyama, Y. Fujimura, Y. Ikeda, and S. Fukuhara, *High shear stress can initiate both platelet aggregation and shedding of procoagulant containing microparticles.* Blood, 1996. **88**(9): p. 3456-64.

108. Nomura, S., *Function and clinical significance of platelet-derived microparticles.* Int J Hematol, 2001. **74**(4): p. 397-404.

109. Pontiggia, L., B. Steiner, H. Ulrichts, H. Deckmyn, M. Forestier, and J.H. Beer, *Platelet microparticle formation and thrombin generation under high shear are effectively suppressed by a monoclonal antibody against GPIba.* Thromb Haemost, 2006. **96**(6): p. 774-80.

110. Sakariassen, K.S., P.A. Holme, U. Orvim, R.M. Barstad, N.O. Solum, and F.R. Brosstad, *Shear-induced platelet activation and platelet microparticle formation in native human blood.* Thromb Res, 1998. **92**(6 Suppl 2): p. S33-41.

111. Holme, P.A., U. Orvim, M.J. Hamers, N.O. Solum, F.R. Brosstad, R.M. Barstad, and K.S. Sakariassen, *Shear-induced platelet activation and platelet microparticle formation at blood flow conditions as in arteries with a severe stenosis.* Arterioscler Thromb Vasc Biol, 1997. **17**(4): p. 646-53.

112. Horstman, L.L. and Y.S. Ahn, *Platelet microparticles: a wide-angle perspective.* Crit Rev Oncol Hematol, 1999. **30**(2): p. 111-42.

113. Malek, L.A., M. Spiewak, K.J. Filipiak, M. Grabowski, M. Szpotanska, M. Rosiak, R. Glowczynska, T. Imiela, Z. Huczek, and G. Opolski, *Persistent platelet activation is related to very early cardiovascular events in patients with acute coronary syndromes.* Kardiol Pol, 2007. **65**(1): p. 40-5; discussion 46.

114. Davi, G. and C. Patrono, *Platelet activation and atherothrombosis.* N Engl J Med, 2007. **357**(24): p. 2482-94.

115. Penz, S.M., I. Bernlochner, O. Toth, R. Lorenz, A. Calatzis, and W. Siess, *Selective and rapid monitoring of dual platelet inhibition by aspirin and P2Y12 antagonists by using multiple electrode aggregometry.* Thromb J, 2010. **8**: p. 9.

116. Chow, T.W., J.D. Hellums, and P. Thiagarajan, *Thrombin receptor activating peptide (SFLLRN) potentiates shear-induced platelet microvesiculation.* J Lab Clin Med, 2000. **135**(1): p. 66-72.

117. Roberts, D.E., A. McNicol, and R. Bose, *Mechanism of collagen activation in human platelets.* J Biol Chem, 2004. **279**(19): p. 19421-30.

118. Levenberg, K., *A method for the solution of certain non-linear problems in least squares.* Quart Appl Math, 1944. **2**: p. 164-168.

119. Marquardt, D., *An Algorithm for Least-Squares Estimation of Nonlinear Parameters.* SIAM J Appl Math, 1963. **11**: p. 431-441.

120. Anderson, G.H., J.D. Hellums, J. Moake, and C.P. Alfrey, Jr., *Platelet response to shear stress: changes in serotonin uptake, serotonin release, and ADP induced aggregation.* Thromb Res, 1978. **13**(6): p. 1039-47.

121. Kottke-Marchant, K., *Importance of platelets and platelet response in acute coronary syndromes.* Cleve Clin J Med, 2009. **76 Suppl 1**: p. S2-7.

122. Yee, D.L., C.W. Sun, A.L. Bergeron, J.F. Dong, and P.F. Bray, *Aggregometry detects platelet hyperreactivity in healthy individuals.* Blood, 2005. **106**(8): p. 2723-9.

123. Yee, D.L., A.L. Bergeron, C.W. Sun, J.F. Dong, and P.F. Bray, *Platelet hyperreactivity generalizes to multiple forms of stimulation.* J Thromb Haemost, 2006. **4**(9): p. 2043-50.

124. Ando, J. and K. Yamamoto, *Vascular mechanobiology: endothelial cell responses to fluid shear stress.* Circ J, 2009. **73**(11): p. 1983-92.

125. Chien, S., *Mechanotransduction and endothelial cell homeostasis: the wisdom of the cell.* Am J Physiol Heart Circ Physiol, 2007. **292**(3): p. H1209-24.

126. Davies, P.F., *Hemodynamic shear stress and the endothelium in cardiovascular pathophysiology.* Nat Clin Pract Cardiovasc Med, 2009. **6**(1): p. 16-26.

127. Davies, T.A., D.L. Drotts, G.J. Weil, and E.R. Simons, *Cytoplasmic Ca2+ is necessary for thrombin-induced platelet activation.* J Biol Chem, 1989. **264**(33): p. 19600-6.

128. Bahou, W.F., L. Scudder, D. Rubenstein, and J. Jesty, *A shear-restricted pathway of platelet procoagulant activity is regulated by IQGAP1.* J Biol Chem, 2004. **279**(21): p. 22571-7.

129. Maxwell, M.J., S.M. Dopheide, S.J. Turner, and S.P. Jackson, *Shear induces a unique series of morphological changes in translocating platelets: effects of morphology on translocation dynamics.* Arterioscler Thromb Vasc Biol, 2006. **26**(3): p. 663-9.

130. Bevers, E.M., P. Comfurius, and R.F. Zwaal, *Platelet procoagulant activity: physiological significance and mechanisms of exposure.* Blood Rev, 1991. **5**(3): p. 146-54.

131. Martin, D.W. and J. Jesty, *Calcium stimulation of procoagulant activity in human erythrocytes. ATP dependence and the effects of modifiers of stimulation and recovery.* J Biol Chem, 1995. **270**(18): p. 10468-74.

132. Rosing, J., J.L. van Rijn, E.M. Bevers, G. van Dieijen, P. Comfurius, and R.F. Zwaal, *The role of activated human platelets in prothrombin and factor X activation.* Blood, 1985. **65**(2): p. 319-32.

133. Schroit, A.J. and R.F. Zwaal, *Transbilayer movement of phospholipids in red cell and platelet membranes.* Biochim Biophys Acta, 1991. **1071**(3): p. 313-29.

134. Barton, J.F., A.R. Hardy, A.W. Poole, and S.J. Mundell, *Reciprocal regulation of platelet responses to P2Y and thromboxane receptor activation.* J Thromb Haemost, 2008. **6**(3): p. 534-43.

135. Murray, R. and G.A. FitzGerald, *Regulation of thromboxane receptor activation in human platelets.* Proc Natl Acad Sci U S A, 1989. **86**(1): p. 124-8.

136. Rao, G.H. and J.G. White, *Role of arachidonic acid metabolism in human platelet activation and irreversible aggregation.* Am J Hematol, 1985. **19**(4): p. 339-47.

137. Barry, O.P., M.G. Kazanietz, D. Pratico, and G.A. FitzGerald, *Arachidonic acid in platelet microparticles up-regulates cyclooxygenase-2-dependent prostaglandin formation via a protein kinase C/mitogen-activated protein kinase-dependent pathway.* J Biol Chem, 1999. **274**(11): p. 7545-56.

138. Moroi, M., S.M. Jung, K. Shinmyozu, Y. Tomiyama, A. Ordinas, and M. Diaz-Ricart, *Analysis of platelet adhesion to a collagen-coated surface under flow conditions: the involvement of glycoprotein VI in the platelet adhesion.* Blood, 1996. **88**(6): p. 2081-92.

139. Kuwahara, M., M. Sugimoto, S. Tsuji, H. Matsui, T. Mizuno, S. Miyata, and A. Yoshioka, *Platelet shape changes and adhesion under high shear flow.* Arterioscler Thromb Vasc Biol, 2002. **22**(2): p. 329-34.

140. Mazzucato, M., P. Pradella, M.R. Cozzi, L. De Marco, and Z.M. Ruggeri, *Sequential cytoplasmic calcium signals in a 2-stage platelet activation process induced by the glycoprotein Ibalpha mechanoreceptor.* Blood, 2002. **100**(8): p. 2793-800.

141. Moritz, M.W., R.C. Reimers, R.K. Baker, S.P. Sutera, and J.H. Joist, *Role of cytoplasmic and releasable ADP in platelet aggregation induced by laminar shear stress.* J Lab Clin Med, 1983. **101**(4): p. 537-44.

142. Baurand, A., A. Eckly, N. Bari, C. Leon, B. Hechler, J.P. Cazenave, and C. Gachet, *Desensitization of the platelet aggregation response to ADP: differential down-regulation of the P2Y1 and P2cyc receptors.* Thromb Haemost, 2000. **84**(3): p. 484-91.

143. Keuren, J.F., S.J. Wielders, H. Ulrichts, T. Hackeng, J.W. Heemskerk, H. Deckmyn, E.M. Bevers, and T. Lindhout, *Synergistic effect of thrombin on collagen-induced platelet procoagulant activity is mediated through protease-activated receptor-1.* Arterioscler Thromb Vasc Biol, 2005. **25**(7): p. 1499-505.

144. Tsuji, S., M. Sugimoto, S. Miyata, M. Kuwahara, S. Kinoshita, and A. Yoshioka, *Real-time analysis of mural thrombus formation in various platelet aggregation disorders: distinct shear-dependent roles of platelet receptors and adhesive proteins under flow.* Blood, 1999. **94**(3): p. 968-75.

145. Reininger, A.J., H.F. Heijnen, H. Schumann, H.M. Specht, W. Schramm, and Z.M. Ruggeri, *Mechanism of platelet adhesion to von Willebrand factor and microparticle formation under high shear stress.* Blood, 2006. **107**(9): p. 3537-45.

146. Sadler, J.E., *Biochemistry and genetics of von Willebrand factor.* Annu Rev Biochem, 1998. **67**: p. 395-424.

APPENDIX A

BASIC PROGRAMS FOR THE HEMODYNAMIC SHEARING DEVICE

A1. Basic Program for Repeating Triangular Waveforms (Section 3.6.1)

```
DEL test4
DEF test4

LH0
COMEXC1
COMEXS1
MC1

; PARAMETERS FOR A TWO DEGREE CONE ONLY!
; Cycle 2000 times to obtain run time of 30 minutes
; This program valid only for T2 = 0 seconds and relaxation for 60 seconds, using Dextran!
; Viscosity= 0.03 Poise, Acceleration/Deceleration time= 0.5 seconds
; Peak Shear Stress = 100 dynes/sq. cm.

L2000

V0.278  ;Starts at shear stress of 1.5 dynes/sq.cm and maintains for 60 s
TIMST0
GO
WAIT(TIM>=60000)
TIMSTP
TTIM

V18.52 ;Accelerate to Shear Stress of 100 dynes/sq.cm, accelerating at 35.926 revolutions/s^2
A35.926
TIMST0
GO
WAIT(as.4=b1)
TIMSTP
TTIM

V0.278  ;Decelerate to shear stress of 1.5 dynes/sq.cm at 35.926 revolutions/s^2
AD35.926
TIMST0
GO
WAIT(as.4=b1)
TIMSTP
TTIM

LN

;End Cycle

END
```

A2. Basic Program for Initial High Shear Stress Exposure (Sections 3.6.2-3)

```
DEL test4
DEF test4

LH0
COMEXC1
COMEXS1
MC1

; PARAMETERS FOR A TWO DEGREE CONE ONLY!
; Cycle 2000 times to obtain run time of 30 minutes
; This program valid only without Dextran!
; Viscosity= 0.01 Poise, Acceleration/Deceleration time = 0.767 seconds (a = 50 revolution/s^2)
; Recovery where 1 dyn/cm^2 for first 15 seconds, 70 dyn/cm^2 for 40 seconds and then 1 dyn/cm^2 thereafter

L2000

V0.556 ;Maintain shear stress of 1 dyn/cm^2 for 15 seconds
TIMST0
GO
WAIT(TIM>=15000)

V38.889 ;Accelerate to 70 dyn/cm^2
A49.978
GO
WAIT(as 0.4=b1)
TIMSTP
TTIM

V38.889 ;Maintain Shear Stress of 70 dyn/cm^2, and maintain for 40 seconds
TIMST0
GO
WAIT(TIM>=40000)
TIMSTP
TTIM

V0.556  ;Decelerate to 1 dyn/cm^2
AD49.978
TIMST0
GO
WAIT(as 0.4=b1)
TIMSTP
TTIM

V0.556 ;Maintain shear stress of 1 dyn/cm^2 for 120 minutes
TIMST0
GO
WAIT(TIM>=7200000)
TIMSTP
TTIM

LN
;End Cycle
END
```

APPENDIX B

DERIVATION AND OPTIMIZATION OF THE PLATELET ACTIVATION MODEL

B1. Derivation of the Simple Phenomenological Platelet Activation Model

We wish to derive a power-law formulation that includes a shear-loading term, $\dot{\tau}$, that accounts for the change in shear stress as opposed to assuming the shear stress is applied in a stepwise manner. We start with the simple equation that accounts for shear stress and time (Eq. B1):

$$PAS(\tau,t) = C\tau^{\alpha}t^{\beta} \tag{B1}$$

Taking the derivative with respect to time and shear stress yields:

$$\frac{d(C\tau^{\alpha}t^{\beta})}{dt} = C\beta\tau^{\alpha}t^{\beta-1} + C\alpha\tau^{\alpha-1}t^{\beta}\frac{d\tau(t)}{dt} \tag{B2}$$

The final term $\frac{d\tau(t)}{dt}$ is the shear-loading rate term. Multiplying both sides by *dt* and applying the integral over the duration of the experiment, we get Eq. B3:

$$PAS(\tau,t) = C\tau^{\alpha}t^{\beta} = C\underbrace{\int_{t_0}^{t_{total}} \beta t^{\beta-1}\tau^{\alpha}dt}_{\text{Constant shear stress}} + C\underbrace{\int_{t_0}^{t_{total}} \alpha\tau^{\alpha-1}t^{\beta}\,\dot{\tau}dt}_{\text{Shear loading rate}} + \underbrace{PAS_0}_{\text{Prior activation history}} \tag{B3}$$

The final term is the constant of integration and accounts for a non-zero initial activation. For utilization in a computational tool, such as MATLAB, the above equation is discretized:

$$PAS(\tau,t) = C\beta\sum_{i=1}^{n} t_i^{\beta-1}\tau_i^{\alpha}\Delta t + C\alpha\sum_{i=1}^{n}\tau_i^{\alpha-1}t_i^{\beta}\frac{\Delta\tau_i}{\cancel{\Delta t}}\cancel{\Delta t} + PAS_0$$

Rewriting $\Delta\tau_i$, we get Eq. B4:

$$PAS(\tau,t) = C\beta\sum_{i=1}^{n} t_i^{\beta-1}\tau_i^{\alpha}\Delta t + C\alpha\sum_{i=1}^{n}\tau_i^{\alpha-1}t_i^{\beta}\left|\tau_i - \tau_{i-1}\right| + PAS_0 \tag{B4}$$

B2. Derivation of the Grigioni Platelet Activation Model

As in the previous section, we want to derive a power-law formulation that includes a shear-loading term, $\dot{\tau}$, that accounts for the change in shear stress as opposed to assuming the shear stress is applied in a stepwise manner. However, we want to truly account for loading history, where two groups of platelets exposed to different mechanical loadings are expected to show different responses in a subsequent loading, even if the latter is the same for both groups. That means that the PAS at each loading stage is dependent on the PAS of a previous loading scheme. Equations B3 and B4 do not satisfy these requirements, since only the initial activity, PAS_0, is considered. Thus, we need to follow the Grigioni approach [102], with modification for PAS [68]. We start with the simple equation that accounts for shear stress and time (Eq. B5):

$$PAS(\tau, t) = C\tau^{\alpha} t^{\beta} \tag{B5}$$

Grouping the independent variables τ and t on one side, we get:

$$\frac{PAS}{C} = \tau^{\alpha} t^{\beta} \tag{B6}$$

Here, we define a mechanical dose function, D:

$$D = \sqrt[\beta]{\frac{PAS}{C}} = \tau^{\alpha/\beta} t \tag{B7}$$

Thus, the function for PAS can be rewritten as:

$$PAS = C \cdot D^{\beta} \tag{B8}$$

Applying the chain rule, we get the form:

$$\frac{dD}{dt} = \frac{\partial D}{\partial t} + \frac{\partial D}{\partial \tau} \cdot \frac{d\tau}{dt} = \tau^{\alpha/\beta} + \alpha/\beta \, t \cdot \tau^{\alpha/\beta - 1} \dot{\tau} \tag{B9}$$

Grigioni et al. neglected the shear loading rate term, $\dot{\tau}$, claiming that it violates the principle of causality and causes a reduction in damage if shear stress is decreasing [102]. Here we diverge

from this approach, adopted previously for PAS [68], by accounting for the shear loading rate and taking its absolute value so that its effect is always additive. In partial differential form, the above equation becomes:

$$dD = \tau^{\alpha/\beta} dt + \alpha/\beta \, t \cdot \tau^{\alpha/\beta - 1} d\tau \tag{B10}$$

Integrating with respect to time and shear stress, the above equation can be written:

$$D(t) - D(t_0) = \int_{t_0}^{t_{total}} \tau(\phi)^{\alpha/\beta} d\phi + \alpha/\beta \int_{\tau(t_0)}^{\tau(t_{total})} \phi \cdot \tau(\phi)^{\alpha/\beta - 1} d\tau \tag{B11}$$

We must rewrite $D(t_0)$ in terms of the initial platelet activity state, PAS_0 (Eq. B12):

$$\begin{aligned} PAS(t_0) &= C \cdot D(t_0)^{\beta} \\ D(t_0) &= \left(\frac{PAS(t_0)}{C} \right)^{1/\beta} \end{aligned} \tag{B12}$$

Taking the derivative of the PAS function in terms of the dose D, we obtain:

$$d(PAS) = d(C \cdot D^{\beta}) = C d(D^{\beta}) = C\beta D^{\beta - 1} dD \tag{B13}$$

Putting this equation in integral form yields:

$$d(PAS) = C\beta \left(\int_{t_0}^{t_{total}} \tau(\xi)^{\alpha/\beta} d\xi + \alpha/\beta \int_{\tau(t_0)}^{\tau(t_{total})} \xi \cdot \tau(\xi)^{\alpha/\beta - 1} d\tau + D(t_0) \right)^{\beta - 1} dD \tag{B14}$$

Substituting the expression for dD yields:

$$d(PAS) = C\beta \left(\int_{t_0}^{t_{total}} \tau(\xi)^{\alpha/\beta} d\xi + \alpha/\beta \int_{\tau(t_0)}^{\tau(t_{total})} \xi \cdot \tau(\xi)^{\alpha/\beta - 1} d\tau + D(t_0) \right)^{\beta - 1} \left(\tau^{\alpha/\beta} dt + \frac{\alpha}{\beta} t \cdot \tau^{\alpha/\beta - 1} d\tau \right) \tag{B15}$$

Expressing the PAS as the integral sum of the infinitesimal contributions represented by the above equation yields:

$$PAS = C\beta\left[\int_{t_0}^{t_{total}}\left(\int_{t_0}^{t_{total}}\tau(\xi)^{\alpha/\beta}d\xi + \alpha/\beta\int_{\tau(t_0)}^{\tau(t_{total})}\xi\cdot\tau(\xi)^{\alpha/\beta-1}d\tau + D(t_0)\right)^{\beta-1}\tau^{\alpha/\beta}dt\right.$$
$$\left.+\int_{\tau(t_0)}^{\tau(t_{total})}\alpha/\beta\left(\int_{t_0}^{t_{total}}\tau(\xi)^{\alpha/\beta}d\xi + \alpha/\beta\int_{\tau(t_0)}^{\tau(t_{total})}\xi\cdot\tau(\xi)^{\alpha/\beta-1}d\tau + D(t_0)\right)^{\beta-1}t\cdot\tau^{\alpha/\beta-1}d\tau\right] \quad \text{(B16)}$$

PAS can be numerically computed by adding the mechanical doses acting on a platelet moving on a fluid pathline. The discrete elemental dose $\Delta(PAS)_i$ is sustained by a platelet in the *i*-th interval, from the instant t_{i-1} to t_i, and is expressed as:

$$\Delta(PAS)_i = C\beta\left[\left(\sum_{j=1}^{i}\tau(t_j)^{\alpha/\beta}\Delta t_j + \alpha/\beta\sum_{j=1}^{i}t_j\cdot\tau(t_j)^{\alpha/\beta-1}\left|\Delta\tau_j\right| + D(t_0)\right)^{\beta-1}\tau(t_i)^{\alpha/\beta}\Delta t_i\right.$$
$$\left.+\alpha/\beta\left(\sum_{j=1}^{i}\tau(t_j)^{\alpha/\beta}\Delta t_j + \alpha/\beta\sum_{j=1}^{i}t_j\cdot\tau(t_j)^{\alpha/\beta-1}\left|\Delta\tau_j\right| + D(t_0)\right)^{\beta-1}t_i\cdot\tau(t_i)^{\alpha/\beta-1}\left|\Delta\tau_i\right|\right] \quad \text{(B17)}$$

The time period Δt_i refers to the duration between experimental observations. Unlike previous derivations of this formula, we no longer assume the shear stress is constant in this interval, as we now have a shear loading term. The starting observation time, t_0, is conventionally assumed to be equal to 0. The mechanical dose, if complex, is broken into multiple sub-intervals (referred to as the *j*-th interval in the above equation). Each sub-interval can be a constant shear stress dose if applied as such, or an approximation, where the dose is approximated as a constant shear stress part and a linearly ramped part, which includes the change in shear stress $\Delta\tau_j$. Note that for the latter, the absolute value is taken in order not to violate the principle of causality [102]. Thus, for each *i*-th interval, multiple *j*-th intervals may be present. From the integral form for the PAS function, we derive the discrete form:

$$PAS = C\beta\sum_{i=1}^{N}\left[\left(\sum_{j=1}^{i}\tau(t_j)^{\alpha/\beta}\Delta t_j + \alpha/\beta\sum_{j=1}^{i}t_j\cdot\tau(t_j)^{\alpha/\beta-1}\left|\Delta\tau_j\right| + D(t_0)\right)^{\beta-1}\tau(t_i)^{\alpha/\beta}\Delta t_i\right.$$
$$\left. + \alpha/\beta\left(\sum_{j=1}^{i}\tau(t_j)^{\alpha/\beta}\Delta t_j + \alpha/\beta\sum_{j=1}^{i}t_j\cdot\tau(t_j)^{\alpha/\beta-1}\left|\Delta\tau_j\right| + D(t_0)\right)^{\beta-1}t_i\cdot\tau(t_i)^{\alpha/\beta-1}\left|\Delta\tau_i\right|\right] \quad \text{(B18)}$$

This represents the sum of PAS values over *N* intervals. In our experiments, PAS measurements were only taken during constant shear stress phases. Therefore, we can neglect the second part of the above equation. In addition, the term for $D(t_0)$ can also be substituted, yielding:

$$PAS = C\beta\sum_{i=1}^{N}\left(\sum_{j=1}^{i}\tau(t_j)^{\alpha/\beta}\Delta t_j + \alpha/\beta\sum_{j=1}^{i}t_j\cdot\tau(t_j)^{\alpha/\beta-1}\left|\Delta\tau_j\right| + \left(\frac{PAS(t_0)}{C}\right)^{1/\beta}\right)^{\beta-1}\tau(t_i)^{\alpha/\beta}\Delta t_i \quad \text{(B19)}$$

Making a similar simplification for Eq. B16 yields:

$$PAS = C\beta\left[\int_{t_0}^{t_{total}}\left(\underbrace{\int_{t_0}^{t_{total}}\tau(\xi)^{\alpha/\beta}d\xi}_{\text{Constant shear stress}} + \alpha/\beta\underbrace{\int_{\tau(t_0)}^{\tau(t_{total})}\xi\cdot\tau(\xi)^{\alpha/\beta-1}d\tau}_{\text{Shear loading rate}} + \underbrace{\left(\frac{PAS(t_0)}{C}\right)^{1/\beta}}_{\text{Prior activation history}}\right)^{\beta-1}\tau^{\alpha/\beta}dt\right] \quad \text{(B20)}$$

Thus, we have a model that accounts for previous shear stress history and platelet activity, as well as the effect of the shear-loading rate, the latter which was not addressed in prior models [2, 68, 91].

B3. Levenberg-Marquardt Optimization for the Simple Phenomenological Approach (in MATLAB)

```
% ----- Start of main ----------------------
function Main
clear; clc;
% Initialization for constants C, a, and b where 0 <= C, a, b <= 1, and constants increment by 0.05 or 0.5 each
% iteration. In differential form, a and b are alpha and beta, respectively.
MaxIter = 20;
iter    = 1;

for i = 1 : MaxIter
   for j = 1 : MaxIter
      for k = 1 : MaxIter

x0(1) = 0.05 * i;
x0(2) = 0.5  * j;
x0(3) = 0.5  * k;
% Levenberg-Marquadt non-linear optimization for all equations with shear-loading rate
   options0=optimset('Display','iter','NonlEqnAlgorithm','lm', 'MaxFunEval', 20000);
   [xsolu, residual] = fsolve(@optimize, x0, options0);

   xsolu;
   sum_residual = sqrt(sum(residual(:).^2));

   result(1,iter) = xsolu(1);
   result(2,iter) = xsolu(2);
   result(3,iter) = xsolu(3);
   result(4,iter) = sum_residual;

   iter = iter + 1;

      end
   end
end
% --- Output C, a, b for each set of iterations with its related residual
fileDAT = fopen(sprintf('%s.dat','fsolveresults_all_wload_lm_simple_noctl'),'w');
      fprintf(fileDAT,'C-value, a-value, b-value, residual\n');
    for i = 1 : iter - 1
      fprintf(fileDAT, '%5.2e %5.2e %5.2e %5.2e\n', result(1,i), result(2,i), result(3,i), result(4,i));
    end
fclose(fileDAT)
% --- Figure with distribution of C, a, and b on one set of axes
figure(1)
hold on
for i = 1 : iter - 1
   c = result(1,i);
   a = result(2,i);
   b = result(3,i);
if c <= 1.0 && c >= 0.0 && a <= 1.0 && a >= 0.0 && b <=1.0 && a >= 0.0
   plot3(result(1,i),result(2,i),result(3,i),'*r')
else
   plot3(result(1,i),result(2,i),result(3,i),'+b')
end
```

```
end
%---Output C, a, and b linked with lowes residual in Matlab window
opti_result = min(result(4,:));
optsize = size(result(1,:)); ops = optsize(2);

for i = 1 : ops
   if  abs(opti_result - result(4,i)) <= 10e-20
      C   = result(1,i)
      a   = result(2,i)
      b   = result(3,i)
      LSE = result(4,i)
   end
end

% ----- End of main ------------------------
   function eq = optimize(x0)

% ---- Constant values of the system ----
c = x0(1);
a = x0(2);
b = x0(3);

% ---- System of Equations ---------------------------------------------------
% The equations below are residual error equations, where eq (t) = Experimental PAS (t) - Model PAS (t) -
% PAS (0).  Model PAS is written in the form of Eq. 3.10.
% ---- 70 dyne/cm^2, 40 s (variable Shear Stress) -------------------------
eq1 = 0.02220194 - c * (a * (70-1) * ((0.5*(70+1))^(a-1)) * (0.77^b + 41.54^b) + b * ((0.5*(70+1))^a * 0.77 *
(0.77^(b-1) + 41.54^(b-1)) + 40.77^(b-1) * 70^a * 40)) - 0.00496477;
eq2 = 0.03177084 - c * (a * (70-1) * ((0.5*(70+1))^(a-1)) * (0.77^b + 41.54^b) + b * ((0.5*(70+1))^a * 0.77 *
(0.77^(b-1) + 41.54^(b-1)) + 40.77^(b-1) * 70^a * 40 + 180^(b-1) * 1^a * 140)) - 0.00496477;
eq3 = 0.04168683 - c * (a * (70-1) * ((0.5*(70+1))^(a-1)) * (0.77^b + 41.54^b) + b * ((0.5*(70+1))^a * 0.77 *
(0.77^(b-1) + 41.54^(b-1)) + 40.77^(b-1) * 70^a * 40 + 180^(b-1) * 1^a * 140 + 360^(b-1) * 1^a * 180)) -
0.00496477;
eq4 = 0.0512601  - c * (a * (70-1) * ((0.5*(70+1))^(a-1)) * (0.77^b + 41.54^b) + b * ((0.5*(70+1))^a * 0.77 *
(0.77^(b-1) + 41.54^(b-1)) + 40.77^(b-1) * 70^a * 40 + 180^(b-1) * 1^a * 140 + 360^(b-1) * 1^a * 180 + 540^(b-1)
* 1^a * 180)) - 0.00496477;
eq5 = 0.04612707 - c * (a * (70-1) * ((0.5*(70+1))^(a-1)) * (0.77^b + 41.54^b) + b * ((0.5*(70+1))^a * 0.77 *
(0.77^(b-1) + 41.54^(b-1)) + 40.77^(b-1) * 70^a * 40 + 180^(b-1) * 1^a * 140 + 360^(b-1) * 1^a * 180 + 540^(b-1)
* 1^a * 180 + 720^(b-1) * 1^a * 180)) - 0.00496477;
eq6 = 0.06400678 - c * (a * (70-1) * ((0.5*(70+1))^(a-1)) * (0.77^b + 41.54^b) + b * ((0.5*(70+1))^a * 0.77 *
(0.77^(b-1) + 41.54^(b-1)) + 40.77^(b-1) * 70^a * 40 + 180^(b-1) * 1^a * 140 + 360^(b-1) * 1^a * 180 + 540^(b-1)
* 1^a * 180 + 720^(b-1) * 1^a * 180 + 900^(b-1) * 1^a * 180)) - 0.00496477;
% ---- 60 dyne/cm^2, 40 s (variable Shear Stress) -------------------------
eq7  = 0.02018382 - c * (a * (60-1) * ((0.5*(60+1))^(a-1)) * (0.655^b + 41.31^b) + b * ((0.5*(60+1))^a * 0.655 *
(0.655^(b-1) + 41.31^(b-1)) + 40.655^(b-1) * 60^a * 40)) - 0.00331667;
eq8  = 0.02267312 - c * (a * (60-1) * ((0.5*(60+1))^(a-1)) * (0.655^b + 41.31^b) + b * ((0.5*(60+1))^a * 0.655 *
(0.655^(b-1) + 41.31^(b-1)) + 40.655^(b-1) * 60^a * 40 + 180^(b-1) * 1^a * 140)) - 0.00331667;
eq9  = 0.03542513 - c * (a * (60-1) * ((0.5*(60+1))^(a-1)) * (0.655^b + 41.31^b) + b * ((0.5*(60+1))^a * 0.655 *
(0.655^(b-1) + 41.31^(b-1)) + 40.655^(b-1) * 60^a * 40 + 180^(b-1) * 1^a * 140 + 360^(b-1) * 1^a * 180)) -
0.00331667;
eq10 = 0.0429566  - c * (a * (60-1) * ((0.5*(60+1))^(a-1)) * (0.655^b + 41.31^b) + b * ((0.5*(60+1))^a * 0.655 *
(0.655^(b-1) + 41.31^(b-1)) + 40.655^(b-1) * 60^a * 40 + 180^(b-1) * 1^a * 140 + 360^(b-1) * 1^a * 180 + 540^(b-
1) * 1^a * 180)) - 0.00331667;
eq11 = 0.05155452 - c * (a * (60-1) * ((0.5*(60+1))^(a-1)) * (0.655^b + 41.31^b) + b * ((0.5*(60+1))^a * 0.655 *
(0.655^(b-1) + 41.31^(b-1)) + 40.655^(b-1) * 60^a * 40 + 180^(b-1) * 1^a * 140 + 360^(b-1) * 1^a * 180 + 540^(b-
1) * 1^a * 180 + 720^(b-1) * 1^a * 180)) - 0.00331667;
```

```
eq12 = 0.05526862 - c * (a * (60-1) * ((0.5*(60+1))^(a-1)) * (0.655^b + 41.31^b) + b * ((0.5*(60+1))^a * 0.655 *
(0.655^(b-1) + 41.31^(b-1)) + 40.655^(b-1) * 60^a * 40 + 180^(b-1) * 1^a * 140 + 360^(b-1) * 1^a * 180 + 540^(b-
1) * 1^a * 180 + 720^(b-1) * 1^a * 180 + 900^(b-1) * 1^a * 180)) - 0.00331667;
% ---- 50 dyne/cm^2, 40 s (variable Shear Stress) -------------------------
eq13 = 0.00938  - c * (a * (50-1) * ((0.5*(50+1))^(a-1)) * (0.545^b + 41.09^b) + b * ((0.5*(50+1))^a * 0.545 *
(0.545^(b-1) + 41.09^(b-1)) + 40.545^(b-1) * 50^a * 40))- 0.004998;
eq14 = 0.010634 - c * (a * (50-1) * ((0.5*(50+1))^(a-1)) * (0.545^b + 41.09^b) + b * ((0.5*(50+1))^a * 0.545 *
(0.545^(b-1) + 41.09^(b-1)) + 40.545^(b-1) * 50^a * 40 + 180^(b-1) * 1^a * 140)) - 0.004998;
eq15 = 0.016517 - c * (a * (50-1) * ((0.5*(50+1))^(a-1)) * (0.545^b + 41.09^b) + b * ((0.5*(50+1))^a * 0.545 *
(0.545^(b-1) + 41.09^(b-1)) + 40.545^(b-1) * 50^a * 40 + 180^(b-1) * 1^a * 140 + 360^(b-1) * 1^a * 180)) -
0.004998;
eq16 = 0.017617 - c * (a * (50-1) * ((0.5*(50+1))^(a-1)) * (0.545^b + 41.09^b) + b * ((0.5*(50+1))^a * 0.545 *
(0.545^(b-1) + 41.09^(b-1)) + 40.545^(b-1) * 50^a * 40 + 180^(b-1) * 1^a * 140 + 360^(b-1) * 1^a * 180 + 540^(b-
1) * 1^a * 180)) - 0.004998;
eq17 = 0.021294 - c * (a * (50-1) * ((0.5*(50+1))^(a-1)) * (0.545^b + 41.09^b) + b * ((0.5*(50+1))^a * 0.545 *
(0.545^(b-1) + 41.09^(b-1)) + 40.545^(b-1) * 50^a * 40 + 180^(b-1) * 1^a * 140 + 360^(b-1) * 1^a * 180 + 540^(b-
1) * 1^a * 180 + 720^(b-1) * 1^a * 180)) - 0.004998;
eq18 = 0.02586  - c * (a * (50-1) * ((0.5*(50+1))^(a-1)) * (0.545^b + 41.09^b) + b * ((0.5*(50+1))^a * 0.545 *
(0.545^(b-1) + 41.09^(b-1)) + 40.545^(b-1) * 50^a * 40 + 180^(b-1) * 1^a * 140 + 360^(b-1) * 1^a * 180 + 540^(b-
1) * 1^a * 180 + 720^(b-1) * 1^a * 180 + 900^(b-1) * 1^a * 180)) - 0.004998;
% ---- 40 dyne/cm^2, 40 s (variable Shear Stress) -------------------------
eq19 = 0.006783 - c * (a * (40-1) * ((0.5*(40+1))^(a-1)) * (0.435^b + 40.87^b) + b * ((0.5*(40+1))^a * 0.435 *
(0.435^(b-1) + 40.87^(b-1)) + 40.435^(b-1) * 40^a * 40)) - 0.00304;
eq20 = 0.008724 - c * (a * (40-1) * ((0.5*(40+1))^(a-1)) * (0.435^b + 40.87^b) + b * ((0.5*(40+1))^a * 0.435 *
(0.435^(b-1) + 40.87^(b-1)) + 40.435^(b-1) * 40^a * 40 + 180^(b-1) * 1^a * 140)) - 0.00304;
eq21 = 0.008433 - c * (a * (40-1) * ((0.5*(40+1))^(a-1)) * (0.435^b + 40.87^b) + b * ((0.5*(40+1))^a * 0.435 *
(0.435^(b-1) + 40.87^(b-1)) + 40.435^(b-1) * 40^a * 40 + 180^(b-1) * 1^a * 140 + 360^(b-1) * 1^a * 180)) -
0.00304;
eq22 = 0.008808 - c * (a * (40-1) * ((0.5*(40+1))^(a-1)) * (0.435^b + 40.87^b) + b * ((0.5*(40+1))^a * 0.435 *
(0.435^(b-1) + 40.87^(b-1)) + 40.435^(b-1) * 40^a * 40 + 180^(b-1) * 1^a * 140 + 360^(b-1) * 1^a * 180 + 540^(b-
1) * 1^a * 180)) - 0.00304;
eq23 = 0.011919 - c * (a * (40-1) * ((0.5*(40+1))^(a-1)) * (0.435^b + 40.87^b) + b * ((0.5*(40+1))^a * 0.435 *
(0.435^(b-1) + 40.87^(b-1)) + 40.435^(b-1) * 40^a * 40 + 180^(b-1) * 1^a * 140 + 360^(b-1) * 1^a * 180 + 540^(b-
1) * 1^a * 180 + 720^(b-1) * 1^a * 180)) - 0.00304;
eq24 = 0.01541  - c * (a * (40-1) * ((0.5*(40+1))^(a-1)) * (0.435^b + 40.87^b) + b * ((0.5*(40+1))^a * 0.435 *
(0.435^(b-1) + 40.87^(b-1)) + 40.435^(b-1) * 40^a * 40 + 180^(b-1) * 1^a * 140 + 360^(b-1) * 1^a * 180 + 540^(b-
1) * 1^a * 180 + 720^(b-1) * 1^a * 180 + 900^(b-1) * 1^a * 180)) - 0.00304;
% ---- 30 dyne/cm^2, 40 s (variable Shear Stress) -------------------------
eq25 = 0.006034 - c * (a * (30-1) * ((0.5*(30+1))^(a-1)) * (0.32^b + 40.64^b) + b * ((0.5*(30+1))^a * 0.32 *
(0.32^(b-1) + 40.64^(b-1)) + 40.32^(b-1) * 30^a * 40)) - 0.002547;
eq26 = 0.005656 - c * (a * (30-1) * ((0.5*(30+1))^(a-1)) * (0.32^b + 40.64^b) + b * ((0.5*(30+1))^a * 0.32 *
(0.32^(b-1) + 40.64^(b-1)) + 40.32^(b-1) * 30^a * 40 + 180^(b-1) * 1^a * 140)) - 0.002547;
eq27 = 0.007692 - c * (a * (30-1) * ((0.5*(30+1))^(a-1)) * (0.32^b + 40.64^b) + b * ((0.5*(30+1))^a * 0.32 *
(0.32^(b-1) + 40.64^(b-1)) + 40.32^(b-1) * 30^a * 40 + 180^(b-1) * 1^a * 140 + 360^(b-1) * 1^a * 180)) - 0.002547;
eq28 = 0.007306 - c * (a * (30-1) * ((0.5*(30+1))^(a-1)) * (0.32^b + 40.64^b) + b * ((0.5*(30+1))^a * 0.32 *
(0.32^(b-1) + 40.64^(b-1)) + 40.32^(b-1) * 30^a * 40 + 180^(b-1) * 1^a * 140 + 360^(b-1) * 1^a * 180 + 540^(b-1)
* 1^a * 180)) - 0.002547;
eq29 = 0.008229 - c * (a * (30-1) * ((0.5*(30+1))^(a-1)) * (0.32^b + 40.64^b) + b * ((0.5*(30+1))^a * 0.32 *
(0.32^(b-1) + 40.64^(b-1)) + 40.32^(b-1) * 30^a * 40 + 180^(b-1) * 1^a * 140 + 360^(b-1) * 1^a * 180 + 540^(b-1)
* 1^a * 180 + 720^(b-1) * 1^a * 180)) - 0.002547;
eq30 = 0.007232 - c * (a * (30-1) * ((0.5*(30+1))^(a-1)) * (0.32^b + 40.64^b) + b * ((0.5*(30+1))^a * 0.32 *
(0.32^(b-1) + 40.64^(b-1)) + 40.32^(b-1) * 30^a * 40 + 180^(b-1) * 1^a * 140 + 360^(b-1) * 1^a * 180 + 540^(b-1)
* 1^a * 180 + 720^(b-1) * 1^a * 180 + 900^(b-1) * 1^a * 180)) - 0.002547;
% ---- 20 dyne/cm^2, 40 s (variable Shear Stress) -------------------------
eq31 = 0.0073216 - c * (a * (20-1) * ((0.5*(20+1))^(a-1)) * (0.21^b + 40.42^b) + b * ((0.5*(20+1))^a * 0.21 *
(0.21^(b-1) + 40.42^(b-1)) + 40.21^(b-1) * 20^a * 40)) - 0.0044259;
```

```
eq32 = 0.0038632 - c * (a * (20-1) * ((0.5*(20+1))^(a-1)) * (0.21^b + 40.42^b) + b * ((0.5*(20+1))^a * 0.21 *
(0.21^(b-1) + 40.42^(b-1)) + 40.21^(b-1) * 20^a * 40 + 180^(b-1) * 1^a * 140)) - 0.0044259;
eq33 = 0.0048832 - c * (a * (20-1) * ((0.5*(20+1))^(a-1)) * (0.21^b + 40.42^b) + b * ((0.5*(20+1))^a * 0.21 *
(0.21^(b-1) + 40.42^(b-1)) + 40.21^(b-1) * 20^a * 40 + 180^(b-1) * 1^a * 140 + 360^(b-1) * 1^a * 180)) -
0.0044259;
eq34 = 0.0056049 - c * (a * (20-1) * ((0.5*(20+1))^(a-1)) * (0.21^b + 40.42^b) + b * ((0.5*(20+1))^a * 0.21 *
(0.21^(b-1) + 40.42^(b-1)) + 40.21^(b-1) * 20^a * 40 + 180^(b-1) * 1^a * 140 + 360^(b-1) * 1^a * 180 + 540^(b-1)
* 1^a * 180)) - 0.0044259;
eq35 = 0.0062744 - c * (a * (20-1) * ((0.5*(20+1))^(a-1)) * (0.21^b + 40.42^b) + b * ((0.5*(20+1))^a * 0.21 *
(0.21^(b-1) + 40.42^(b-1)) + 40.21^(b-1) * 20^a * 40 + 180^(b-1) * 1^a * 140 + 360^(b-1) * 1^a * 180 + 540^(b-1)
* 1^a * 180 + 720^(b-1) * 1^a * 180)) - 0.0044259;
eq36 = 0.0056099 - c * (a * (20-1) * ((0.5*(20+1))^(a-1)) * (0.21^b + 40.42^b) + b * ((0.5*(20+1))^a * 0.21 *
(0.21^(b-1) + 40.42^(b-1)) + 40.21^(b-1) * 20^a * 40 + 180^(b-1) * 1^a * 140 + 360^(b-1) * 1^a * 180 + 540^(b-1)
* 1^a * 180 + 720^(b-1) * 1^a * 180 + 900^(b-1) * 1^a * 180)) - 0.0044259;
% ---- 1 dyne/cm^2 control (variable Shear Stress) ------------------------
% eq37 = 0.0043   - c * b * (40^(b-1) * 1^a * 40) - 0.005184;
% eq38 = 0.005583 - c * b * (40^(b-1) * 1^a * 40 + 180^(b-1) * 1^a * 140) - 0.005184;
% eq39 = 0.006812 - c * b * (40^(b-1) * 1^a * 40 + 180^(b-1) * 1^a * 140 + 360^(b-1) * 1^a * 180) - 0.005184;
% eq40 = 0.005953 - c * b * (40^(b-1) * 1^a * 40 + 180^(b-1) * 1^a * 140 + 360^(b-1) * 1^a * 180 + 540^(b-1) *
1^a * 180) - 0.005184;
% eq41 = 0.006804 - c * b * (40^(b-1) * 1^a * 40 + 180^(b-1) * 1^a * 140 + 360^(b-1) * 1^a * 180 + 540^(b-1) *
1^a * 180 + 720^(b-1) * 1^a * 180) - 0.005184;
% eq42 = 0.00708  - c * b * (40^(b-1) * 1^a * 40 + 180^(b-1) * 1^a * 140 + 360^(b-1) * 1^a * 180 + 540^(b-1) *
1^a * 180 + 720^(b-1) * 1^a * 180 + 900^(b-1) * 1^a * 180) - 0.005184;
% ---- 70 dyne/cm^2, 40 s (variable Exposure Time) ------------------------
eq37 = 0.0209221 - c * (a * (70-1) * ((0.5*(70+1))^(a-1)) * (0.77^b + 41.54^b) + b * ((0.5*(70+1))^a * 0.77 *
(0.77^(b-1) + 41.54^(b-1)) + 40.77^(b-1) * 70^a * 40)) - 0.005131;
eq38 = 0.0312898 - c * (a * (70-1) * ((0.5*(70+1))^(a-1)) * (0.77^b + 41.54^b) + b * ((0.5*(70+1))^a * 0.77 *
(0.77^(b-1) + 41.54^(b-1)) + 40.77^(b-1) * 70^a * 40 + 180^(b-1) * 1^a * 140)) - 0.005131;
eq39 = 0.0361134 - c * (a * (70-1) * ((0.5*(70+1))^(a-1)) * (0.77^b + 41.54^b) + b * ((0.5*(70+1))^a * 0.77 *
(0.77^(b-1) + 41.54^(b-1)) + 40.77^(b-1) * 70^a * 40 + 180^(b-1) * 1^a * 140 + 360^(b-1) * 1^a * 180)) - 0.005131;
eq40 = 0.0354258 - c * (a * (70-1) * ((0.5*(70+1))^(a-1)) * (0.77^b + 41.54^b) + b * ((0.5*(70+1))^a * 0.77 *
(0.77^(b-1) + 41.54^(b-1)) + 40.77^(b-1) * 70^a * 40 + 180^(b-1) * 1^a * 140 + 360^(b-1) * 1^a * 180 + 540^(b-1)
* 1^a * 180)) - 0.005131;
eq41 = 0.0392182 - c * (a * (70-1) * ((0.5*(70+1))^(a-1)) * (0.77^b + 41.54^b) + b * ((0.5*(70+1))^a * 0.77 *
(0.77^(b-1) + 41.54^(b-1)) + 40.77^(b-1) * 70^a * 40 + 180^(b-1) * 1^a * 140 + 360^(b-1) * 1^a * 180 + 540^(b-1)
* 1^a * 180 + 720^(b-1) * 1^a * 180)) - 0.005131;
eq42 = 0.0468981 - c * (a * (70-1) * ((0.5*(70+1))^(a-1)) * (0.77^b + 41.54^b) + b * ((0.5*(70+1))^a * 0.77 *
(0.77^(b-1) + 41.54^(b-1)) + 40.77^(b-1) * 70^a * 40 + 180^(b-1) * 1^a * 140 + 360^(b-1) * 1^a * 180 + 540^(b-1)
* 1^a * 180 + 720^(b-1) * 1^a * 180 + 900^(b-1) * 1^a * 180)) - 0.005131;
% ---- 70 dyne/cm^2, 30 s (variable Exposure Time) ------------------------
eq43 = 0.0096355 - c * (a * (70-1) * ((0.5*(70+1))^(a-1)) * (0.77^b + 31.54^b) + b * ((0.5*(70+1))^a * 0.77 *
(0.77^(b-1) + 31.54^(b-1)) + 30.77^(b-1) * 70^a * 30)) - 0.004289;
eq44 = 0.0117141 - c * (a * (70-1) * ((0.5*(70+1))^(a-1)) * (0.77^b + 31.54^b) + b * ((0.5*(70+1))^a * 0.77 *
(0.77^(b-1) + 31.54^(b-1)) + 30.77^(b-1) * 70^a * 30 + 180^(b-1) * 1^a * 150)) - 0.004289;
eq45 = 0.0139984 - c * (a * (70-1) * ((0.5*(70+1))^(a-1)) * (0.77^b + 31.54^b) + b * ((0.5*(70+1))^a * 0.77 *
(0.77^(b-1) + 31.54^(b-1)) + 30.77^(b-1) * 70^a * 30 + 180^(b-1) * 1^a * 150 + 360^(b-1) * 1^a * 180)) - 0.004289;
eq46 = 0.0123609 - c * (a * (70-1) * ((0.5*(70+1))^(a-1)) * (0.77^b + 31.54^b) + b * ((0.5*(70+1))^a * 0.77 *
(0.77^(b-1) + 31.54^(b-1)) + 30.77^(b-1) * 70^a * 30 + 180^(b-1) * 1^a * 150 + 360^(b-1) * 1^a * 180 + 540^(b-1)
* 1^a * 180)) - 0.004289;
eq47 = 0.0180173 - c * (a * (70-1) * ((0.5*(70+1))^(a-1)) * (0.77^b + 31.54^b) + b * ((0.5*(70+1))^a * 0.77 *
(0.77^(b-1) + 31.54^(b-1)) + 30.77^(b-1) * 70^a * 30 + 180^(b-1) * 1^a * 150 + 360^(b-1) * 1^a * 180 + 540^(b-1)
* 1^a * 180 + 720^(b-1) * 1^a * 180)) - 0.004289;
eq48 = 0.0160206 - c * (a * (70-1) * ((0.5*(70+1))^(a-1)) * (0.77^b + 31.54^b) + b * ((0.5*(70+1))^a * 0.77 *
(0.77^(b-1) + 31.54^(b-1)) + 30.77^(b-1) * 70^a * 30 + 180^(b-1) * 1^a * 150 + 360^(b-1) * 1^a * 180 + 540^(b-1)
* 1^a * 180 + 720^(b-1) * 1^a * 180 + 900^(b-1) * 1^a * 180)) - 0.004289;
```

```
% ---- 70 dyne/cm^2, 20 s (variable Exposure Time) ----------
eq49 = 0.0087302 - c * (a * (70-1) * ((0.5*(70+1))^(a-1)) * (0.77^b + 21.54^b) + b * ((0.5*(70+1))^a * 0.77 *
(0.77^(b-1) + 21.54^(b-1)) + 20.77^(b-1) * 70^a * 20)) - 0.004525;
eq50 = 0.0083986 - c * (a * (70-1) * ((0.5*(70+1))^(a-1)) * (0.77^b + 21.54^b) + b * ((0.5*(70+1))^a * 0.77 *
(0.77^(b-1) + 21.54^(b-1)) + 20.77^(b-1) * 70^a * 20 + 180^(b-1) * 1^a * 160)) - 0.004525;
eq51 = 0.0106598 - c * (a * (70-1) * ((0.5*(70+1))^(a-1)) * (0.77^b + 21.54^b) + b * ((0.5*(70+1))^a * 0.77 *
(0.77^(b-1) + 21.54^(b-1)) + 20.77^(b-1) * 70^a * 20 + 180^(b-1) * 1^a * 160 + 360^(b-1) * 1^a * 180)) - 0.004525;
eq52 = 0.0101414 - c * (a * (70-1) * ((0.5*(70+1))^(a-1)) * (0.77^b + 21.54^b) + b * ((0.5*(70+1))^a * 0.77 *
(0.77^(b-1) + 21.54^(b-1)) + 20.77^(b-1) * 70^a * 20 + 180^(b-1) * 1^a * 160 + 360^(b-1) * 1^a * 180 + 540^(b-1)
* 1^a * 180)) - 0.004525;
eq53 = 0.0130556 - c * (a * (70-1) * ((0.5*(70+1))^(a-1)) * (0.77^b + 21.54^b) + b * ((0.5*(70+1))^a * 0.77 *
(0.77^(b-1) + 21.54^(b-1)) + 20.77^(b-1) * 70^a * 20 + 180^(b-1) * 1^a * 160 + 360^(b-1) * 1^a * 180 + 540^(b-1)
* 1^a * 180 + 720^(b-1) * 1^a * 180)) - 0.004525;
eq54 = 0.0107269 - c * (a * (70-1) * ((0.5*(70+1))^(a-1)) * (0.77^b + 21.54^b) + b * ((0.5*(70+1))^a * 0.77 *
(0.77^(b-1) + 21.54^(b-1)) + 20.77^(b-1) * 70^a * 20 + 180^(b-1) * 1^a * 160 + 360^(b-1) * 1^a * 180 + 540^(b-1)
* 1^a * 180 + 720^(b-1) * 1^a * 180 + 900^(b-1) * 1^a * 180)) - 0.004525;
% ---- 70 dyne/cm^2, 10 s (variable Exposure Time) ----------
eq55 = 0.0078392 - c * (a * (70-1) * ((0.5*(70+1))^(a-1)) * (0.77^b + 11.54^b) + b * ((0.5*(70+1))^a * 0.77 *
(0.77^(b-1) + 11.54^(b-1)) + 10.77^(b-1) * 70^a * 10)) - 0.004214;
eq56 = 0.0061542 - c * (a * (70-1) * ((0.5*(70+1))^(a-1)) * (0.77^b + 11.54^b) + b * ((0.5*(70+1))^a * 0.77 *
(0.77^(b-1) + 11.54^(b-1)) + 10.77^(b-1) * 70^a * 10 + 180^(b-1) * 1^a * 170)) - 0.004214;
eq57 = 0.0067483 - c * (a * (70-1) * ((0.5*(70+1))^(a-1)) * (0.77^b + 11.54^b) + b * ((0.5*(70+1))^a * 0.77 *
(0.77^(b-1) + 11.54^(b-1)) + 10.77^(b-1) * 70^a * 10 + 180^(b-1) * 1^a * 170 + 360^(b-1) * 1^a * 180)) - 0.004214;
eq58 = 0.0063858 - c * (a * (70-1) * ((0.5*(70+1))^(a-1)) * (0.77^b + 11.54^b) + b * ((0.5*(70+1))^a * 0.77 *
(0.77^(b-1) + 11.54^(b-1)) + 10.77^(b-1) * 70^a * 10 + 180^(b-1) * 1^a * 170 + 360^(b-1) * 1^a * 180 + 540^(b-1)
* 1^a * 180)) - 0.004214;
eq59 = 0.0061095 - c * (a * (70-1) * ((0.5*(70+1))^(a-1)) * (0.77^b + 11.54^b) + b * ((0.5*(70+1))^a * 0.77 *
(0.77^(b-1) + 11.54^(b-1)) + 10.77^(b-1) * 70^a * 10 + 180^(b-1) * 1^a * 170 + 360^(b-1) * 1^a * 180 + 540^(b-1)
* 1^a * 180 + 720^(b-1) * 1^a * 180)) - 0.004214;
eq60 = 0.0072843 - c * (a * (70-1) * ((0.5*(70+1))^(a-1)) * (0.77^b + 11.54^b) + b * ((0.5*(70+1))^a * 0.77 *
(0.77^(b-1) + 11.54^(b-1)) + 10.77^(b-1) * 70^a * 10 + 180^(b-1) * 1^a * 170 + 360^(b-1) * 1^a * 180 + 540^(b-1)
* 1^a * 180 + 720^(b-1) * 1^a * 180 + 900^(b-1) * 1^a * 180)) - 0.004214;
% ---- 70 dyne/cm^2, 5 s (variable Exposure Time) ----------
eq61 = 0.0062505 - c * c * (a * (70-1) * ((0.5*(70+1))^(a-1)) * (0.77^b + 6.54^b) + b * ((0.5*(70+1))^a * 0.77 *
(0.77^(b-1) + 6.54^(b-1)) + 5.77^(b-1) * 70^a * 5)) - 0.003708;
eq62 = 0.0053974 - c * c * (a * (70-1) * ((0.5*(70+1))^(a-1)) * (0.77^b + 6.54^b) + b * ((0.5*(70+1))^a * 0.77 *
(0.77^(b-1) + 6.54^(b-1)) + 5.77^(b-1) * 70^a * 5 + 180^(b-1) * 1^a * 175)) - 0.003708;
eq63 = 0.0055954 - c * c * (a * (70-1) * ((0.5*(70+1))^(a-1)) * (0.77^b + 6.54^b) + b * ((0.5*(70+1))^a * 0.77 *
(0.77^(b-1) + 6.54^(b-1)) + 5.77^(b-1) * 70^a * 5 + 180^(b-1) * 1^a * 175 + 360^(b-1) * 1^a * 180)) - 0.003708;
eq64 = 0.0062308 - c * c * (a * (70-1) * ((0.5*(70+1))^(a-1)) * (0.77^b + 6.54^b) + b * ((0.5*(70+1))^a * 0.77 *
(0.77^(b-1) + 6.54^(b-1)) + 5.77^(b-1) * 70^a * 5 + 180^(b-1) * 1^a * 175 + 360^(b-1) * 1^a * 180 + 540^(b-1) *
1^a * 180)) - 0.003708;
eq65 = 0.0046747 - c * c * (a * (70-1) * ((0.5*(70+1))^(a-1)) * (0.77^b + 6.54^b) + b * ((0.5*(70+1))^a * 0.77 *
(0.77^(b-1) + 6.54^(b-1)) + 5.77^(b-1) * 70^a * 5 + 180^(b-1) * 1^a * 175 + 360^(b-1) * 1^a * 180 + 540^(b-1) *
1^a * 180 + 720^(b-1) * 1^a * 180)) - 0.003708;
eq66 = 0.0048517 - c * c * (a * (70-1) * ((0.5*(70+1))^(a-1)) * (0.77^b + 6.54^b) + b * ((0.5*(70+1))^a * 0.77 *
(0.77^(b-1) + 6.54^(b-1)) + 5.77^(b-1) * 70^a * 5 + 180^(b-1) * 1^a * 175 + 360^(b-1) * 1^a * 180 + 540^(b-1) *
1^a * 180 + 720^(b-1) * 1^a * 180 + 900^(b-1) * 1^a * 180)) - 0.003708;
% ---- 1 dyne/cm^2 control (variable Exposure Time) ----------
% eq73 = 0.0055100 - c * b * (40^(b-1) * 1^a * 40) - 0.004716;
% eq74 = 0.0049060 - c * b * (40^(b-1) * 1^a * 40 + 180^(b-1) * 1^a * 140) - 0.004716;
% eq75 = 0.0042023 - c * b * (40^(b-1) * 1^a * 40 + 180^(b-1) * 1^a * 140 + 360^(b-1) * 1^a * 180) - 0.004716;
% eq76 = 0.0038300 - c * b * (40^(b-1) * 1^a * 40 + 180^(b-1) * 1^a * 140 + 360^(b-1) * 1^a * 180 + 540^(b-1) *
1^a * 180) - 0.004716;
% eq77 = 0.0039658 - c * b * (40^(b-1) * 1^a * 40 + 180^(b-1) * 1^a * 140 + 360^(b-1) * 1^a * 180 + 540^(b-1) *
1^a * 180 + 720^(b-1) * 1^a * 180) - 0.004716;
```

```
% eq78 = 0.0034444 - c * b * (40^(b-1) * 1^a * 40 + 180^(b-1) * 1^a * 140 + 360^(b-1) * 1^a * 180 + 540^(b-1) *
1^a * 180 + 720^(b-1) * 1^a * 180 + 900^(b-1) * 1^a * 180) - 0.004716;
% ---- System of Equations ---------------------------------------------------
% This section assembles all the residual equations into a single vector "eq".
eq(1)  = eq1(1);  eq(2)  = eq2(1);  eq(3)  = eq3(1);  eq(4)  = eq4(1);  eq(5)  = eq5(1);  eq(6)  = eq6(1);
eq(7)  = eq7(1);  eq(8)  = eq8(1);  eq(9)  = eq9(1);  eq(10) = eq10(1); eq(11) = eq11(1); eq(12) = eq12(1);
eq(13) = eq13(1); eq(14) = eq14(1); eq(15) = eq15(1); eq(16) = eq16(1); eq(17) = eq17(1); eq(18) = eq18(1);
eq(19) = eq19(1); eq(20) = eq20(1); eq(21) = eq21(1); eq(22) = eq22(1); eq(23) = eq23(1); eq(24) = eq24(1);
eq(25) = eq25(1); eq(26) = eq26(1); eq(27) = eq27(1); eq(28) = eq28(1); eq(29) = eq29(1); eq(30) = eq30(1);
eq(31) = eq31(1); eq(32) = eq32(1); eq(33) = eq33(1); eq(34) = eq34(1); eq(35) = eq35(1); eq(36) = eq36(1);
eq(37) = eq37(1); eq(38) = eq38(1); eq(39) = eq39(1); eq(40) = eq40(1); eq(41) = eq41(1); eq(42) = eq42(1);
eq(43) = eq43(1); eq(44) = eq44(1); eq(45) = eq45(1); eq(46) = eq46(1); eq(47) = eq47(1); eq(48) = eq48(1);
eq(49) = eq49(1); eq(50) = eq50(1); eq(51) = eq51(1); eq(52) = eq52(1); eq(53) = eq53(1); eq(54) = eq54(1);
eq(55) = eq55(1); eq(56) = eq56(1); eq(57) = eq57(1); eq(58) = eq58(1); eq(59) = eq59(1); eq(60) = eq60(1);
eq(61) = eq61(1); eq(62) = eq62(1); eq(63) = eq63(1); eq(64) = eq64(1); eq(65) = eq65(1); eq(66) = eq66(1);
% ----------------------------------------------------------------
```

B4. Levenberg-Marquardt Optimization for the Grigioni Approach (in MATLAB)

```
% ----- Start of main ----------------------
function Main
clear; clc;
% Initialization for constants C, a, and b where 0 <= a, b <= 10, and  0 <= C <= 1, and constants increment by
% 0.5 each iteration for a and b. and by 0.05 for C.  In differential form, a and b are alpha and beta, respectively.
MaxIncrement = 20;
iter    = 1;

for i = 1 : MaxIncrement
   for j = 1 : MaxIncrement
      for k = 1 : MaxIncrement

x0(1) = 0.05 * i;
x0(2) = 0.5  * j;
x0(3) = 0.5  * k;
% Levenberg-Marquadt non-linear optimization for all equations with shear-loading rate
   options0=optimset('Display','iter','NonlEqnAlgorithm','lm','MaxFunEval',20000);
   [xsolu, residual] = fsolve(@optimize, x0, options0);

   xsolu;
   sum_residual = sqrt(sum(residual(:).^2));

   result(1,iter) = xsolu(1);
   result(2,iter) = xsolu(2);
   result(3,iter) = xsolu(3);
   result(4,iter) = sum_residual;

   iter = iter + 1;

      end
   end
end
% --- Output C, a, b for each set of iterations with its related residual
fileDAT = fopen(sprintf('%s.dat','fsolveresults_all_wload_lm_Grig_102710_noctl'),'w');
      fprintf(fileDAT,'Re_C-value, Im_C-value, Re_a-value, Im_a-value, Re_b-value, Im_b-value, Re_residual,
Im_residual\n');

    for i = 1 : iter - 1
      if imag(result(1,i)) <= 10e-20 &&  imag(result(2,i)) <= 10e-20 && imag(result(3,i)) <= 10e-20 &&
imag(result(4,i)) <= 10e-20
         fprintf(fileDAT, '%5.2e %5.2e %5.2e %5.2e %5.2e %5.2e %5.2e %5.2e\n', real(result(1,i)), imag(result(1,i)),
...
                                                  real(result(2,i)), imag(result(2,i)), ...
                                                  real(result(3,i)), imag(result(3,i)), ...
                                                  real(result(4,i)), imag(result(4,i)) );
      end
    end

fclose(fileDAT)
% --- Figure with distribution of C, a, and b on one set of axes
figure(1)
hold on
for i = 1 : iter - 1
   c = result(1,i);
```

```
    a = result(2,i);
    b = result(3,i);
if c <= 1.0 && c >= 0.0 && a <= 1.0 && a >= 0.0 && b <=1.0 && a >= 0.0
    plot3(result(1,i),result(2,i),result(3,i),'*r')
else
    plot3(result(1,i),result(2,i),result(3,i),'+b')
end
end
%---Output C, a, and b linked with lowes residual in Matlab window
opti_result = min(result(4,:));
optsize = size(result(1,:)); ops = optsize(2);

for i = 1 : ops
   if  abs(opti_result - result(4,i)) <= 10e-20
       C   = result(1,i)
       a   = result(2,i)
       b   = result(3,i)
       LSE = result(4,i)
   end
end


% ----- End of main ------------------------
   function eq = optimize(x0)

% ---- Constant values of the system ----
c = x0(1);
a = x0(2);
b = x0(3);

% ---- System of Equations ---------------------------------------------------
% The equations below are residual error equations, where eq (t) = Experimental PAS (t) - Model PAS (t) –
% PAS (0).  Model PAS is written in the form of Eq. 3.14.
% ---- 70 dyne/cm^2, 40 s (variable Shear Stress) -------------------------
eq1 = 0.02220194 - c * b * ((2 * 0.77 * ((71/2)^(a/b)) + 40 * (70^(a/b)) + (a/b) * (70-1) * (0.77 * 70^((a/b)-1) +
41.54 * 1) + (0.00496477/c)^(1/b))^(b-1) * 41.54);
eq2 = 0.03177084 - c * b * ((2 * 0.77 * ((71/2)^(a/b)) + 40 * (70^(a/b)) + (a/b) * (70-1) * (0.77 * 70^((a/b)-1) +
41.54 * 1) + (0.00496477/c)^(1/b))^(b-1) * 41.54 + (138.46 * (1) + (0.00496477/c)^(1/b))^(b-1) * 138.46);
eq3 = 0.04168683 - c * b * ((2 * 0.77 * ((71/2)^(a/b)) + 40 * (70^(a/b)) + (a/b) * (70-1) * (0.77 * 70^((a/b)-1) +
41.54 * 1) + (0.00496477/c)^(1/b))^(b-1) * 41.54 + (138.46 * (1) + (0.00496477/c)^(1/b))^(b-1) * 138.46 + (180 *
(1) + (0.00496477/c)^(1/b))^(b-1) * 180);
eq4 = 0.0512601  - c * b * ((2 * 0.77 * ((71/2)^(a/b)) + 40 * (70^(a/b)) + (a/b) * (70-1) * (0.77 * 70^((a/b)-1) +
41.54 * 1) + (0.00496477/c)^(1/b))^(b-1) * 41.54 + (138.46 * (1) + (0.00496477/c)^(1/b))^(b-1) * 138.46 + (180 *
(1) + (0.00496477/c)^(1/b))^(b-1) * 180 + (180 * (1) + (0.00496477/c)^(1/b))^(b-1) * 180);
eq5 = 0.04612707 - c * b * ((2 * 0.77 * ((71/2)^(a/b)) + 40 * (70^(a/b)) + (a/b) * (70-1) * (0.77 * 70^((a/b)-1) +
41.54 * 1) + (0.00496477/c)^(1/b))^(b-1) * 41.54 + (138.46 * (1) + (0.00496477/c)^(1/b))^(b-1) * 138.46 + (180 *
(1) + (0.00496477/c)^(1/b))^(b-1) * 180 + (180 * (1) + (0.00496477/c)^(1/b))^(b-1) * 180 + (180 * (1) +
(0.00496477/c)^(1/b))^(b-1) * 180);
eq6 = 0.06400678 - c * b * ((2 * 0.77 * ((71/2)^(a/b)) + 40 * (70^(a/b)) + (a/b) * (70-1) * (0.77 * 70^((a/b)-1) +
41.54 * 1) + (0.00496477/c)^(1/b))^(b-1) * 41.54 + (138.46 * (1) + (0.00496477/c)^(1/b))^(b-1) * 138.46 + (180 *
(1) + (0.00496477/c)^(1/b))^(b-1) * 180 + (180 * (1) + (0.00496477/c)^(1/b))^(b-1) * 180 + (180 * (1) +
(0.00496477/c)^(1/b))^(b-1) * 180 + (180 * (1) + (0.00496477/c)^(1/b))^(b-1) * 180);
% % ---- 60 dyne/cm^2, 40 s (variable Shear Stress) -------------------------
eq7  = 0.02018382 - c * b * ((2 * 0.655 * ((61/2)^(a/b)) + 40 * (60^(a/b)) + (a/b) * (60-1) * (0.655 * 60^((a/b)-1) +
41.31 * 1) + (0.00331667/c)^(1/b))^(b-1) * 41.31);
```

```
eq8  = 0.02267312 - c * b * ((2 * 0.655 * ((61/2)^(a/b)) + 40 * (60^(a/b)) + (a/b) * (60-1) * (0.655 * 60^((a/b)-1) +
41.31 * 1) + (0.00331667/c)^(1/b))^(b-1) * 41.31 + (138.69 * (1) + (0.00331667/c)^(1/b))^(b-1) * 138.69);
eq9  = 0.03542513 - c * b * ((2 * 0.655 * ((61/2)^(a/b)) + 40 * (60^(a/b)) + (a/b) * (60-1) * (0.655 * 60^((a/b)-1) +
41.31 * 1) + (0.00331667/c)^(1/b))^(b-1) * 41.31 + (138.69 * (1) + (0.00331667/c)^(1/b))^(b-1) * 138.69 + (180 *
(1) + (0.00331667/c)^(1/b))^(b-1) * 180);
eq10 = 0.0429566  - c * b * ((2 * 0.655 * ((61/2)^(a/b)) + 40 * (60^(a/b)) + (a/b) * (60-1) * (0.655 * 60^((a/b)-1) +
41.31 * 1) + (0.00331667/c)^(1/b))^(b-1) * 41.31 + (138.69 * (1) + (0.00331667/c)^(1/b))^(b-1) * 138.69 + (180 *
(1) + (0.00331667/c)^(1/b))^(b-1) * 180 + (180 * (1) + (0.00331667/c)^(1/b))^(b-1) * 180);
eq11 = 0.05155452 - c * b * ((2 * 0.655 * ((61/2)^(a/b)) + 40 * (60^(a/b)) + (a/b) * (60-1) * (0.655 * 60^((a/b)-1) +
41.31 * 1) + (0.00331667/c)^(1/b))^(b-1) * 41.31 + (138.69 * (1) + (0.00331667/c)^(1/b))^(b-1) * 138.69 + (180 *
(1) + (0.00331667/c)^(1/b))^(b-1) * 180 + (180 * (1) + (0.00331667/c)^(1/b))^(b-1) * 180 + (180 * (1) +
(0.00331667/c)^(1/b))^(b-1) * 180);
eq12 = 0.05526862 - c * b * ((2 * 0.655 * ((61/2)^(a/b)) + 40 * (60^(a/b)) + (a/b) * (60-1) * (0.655 * 60^((a/b)-1) +
41.31 * 1) + (0.00331667/c)^(1/b))^(b-1) * 41.31 + (138.69 * (1) + (0.00331667/c)^(1/b))^(b-1) * 138.69 + (180 *
(1) + (0.00331667/c)^(1/b))^(b-1) * 180 + (180 * (1) + (0.00331667/c)^(1/b))^(b-1) * 180 + (180 * (1) +
(0.00331667/c)^(1/b))^(b-1) * 180 + (180 * (1) + (0.00331667/c)^(1/b))^(b-1) * 180);
% % ---- 50 dyne/cm^2, 40 s (variable Shear Stress) -------------------------
eq13 = 0.00938  - c * b * ((2 * 0.545 * ((51/2)^(a/b)) + 40 * (50^(a/b)) + (a/b) * (50-1) * (0.545 * 50^((a/b)-1) +
41.09 * 1) + (0.004998/c)^(1/b))^(b-1) * 41.09);
eq14 = 0.010634 - c * b * ((2 * 0.545 * ((51/2)^(a/b)) + 40 * (50^(a/b)) + (a/b) * (50-1) * (0.545 * 50^((a/b)-1) +
41.09 * 1) + (0.004998/c)^(1/b))^(b-1) * 41.09 + (138.91 * (1) + (0.004998/c)^(1/b))^(b-1) * 138.91);
eq15 = 0.016517 - c * b * ((2 * 0.545 * ((51/2)^(a/b)) + 40 * (50^(a/b)) + (a/b) * (50-1) * (0.545 * 50^((a/b)-1) +
41.09 * 1) + (0.004998/c)^(1/b))^(b-1) * 41.09 + (138.91 * (1) + (0.004998/c)^(1/b))^(b-1) * 138.91 + (180 * (1) +
(0.004998/c)^(1/b))^(b-1) * 180);
eq16 = 0.017617 - c * b * ((2 * 0.545 * ((51/2)^(a/b)) + 40 * (50^(a/b)) + (a/b) * (50-1) * (0.545 * 50^((a/b)-1) +
41.09 * 1) + (0.004998/c)^(1/b))^(b-1) * 41.09 + (138.91 * (1) + (0.004998/c)^(1/b))^(b-1) * 138.91 + (180 * (1) +
(0.004998/c)^(1/b))^(b-1) * 180 + (180 * (1) + (0.004998/c)^(1/b))^(b-1) * 180);
eq17 = 0.021294 - c * b * ((2 * 0.545 * ((51/2)^(a/b)) + 40 * (50^(a/b)) + (a/b) * (50-1) * (0.545 * 50^((a/b)-1) +
41.09 * 1) + (0.004998/c)^(1/b))^(b-1) * 41.09 + (138.91 * (1) + (0.004998/c)^(1/b))^(b-1) * 138.91 + (180 * (1) +
(0.004998/c)^(1/b))^(b-1) * 180 + (180 * (1) + (0.004998/c)^(1/b))^(b-1) * 180 + (180 * (1) +
(0.004998/c)^(1/b))^(b-1) * 180);
eq18 = 0.02586  - c * b * ((2 * 0.545 * ((51/2)^(a/b)) + 40 * (50^(a/b)) + (a/b) * (50-1) * (0.545 * 50^((a/b)-1) +
41.09 * 1) + (0.004998/c)^(1/b))^(b-1) * 41.09 + (138.91 * (1) + (0.004998/c)^(1/b))^(b-1) * 138.91 + (180 * (1) +
(0.004998/c)^(1/b))^(b-1) * 180 + (180 * (1) + (0.004998/c)^(1/b))^(b-1) * 180 + (180 * (1) +
(0.004998/c)^(1/b))^(b-1) * 180 + (180 * (1) + (0.004998/c)^(1/b))^(b-1) * 180);
% % ---- 40 dyne/cm^2, 40 s (variable Shear Stress) -------------------------
eq19 = 0.006783 - c * b * ((2 * 0.435 * ((41/2)^(a/b)) + 40 * (40^(a/b)) + (a/b) * (40-1) * (0.435 * 40^((a/b)-1) +
40.87 * 1) + (0.00304/c)^(1/b))^(b-1) * 40.87);
eq20 = 0.008724 - c * b * ((2 * 0.435 * ((41/2)^(a/b)) + 40 * (40^(a/b)) + (a/b) * (40-1) * (0.435 * 40^((a/b)-1) +
40.87 * 1) + (0.00304/c)^(1/b))^(b-1) * 40.87 + (139.13 * (1) + (0.00304/c)^(1/b))^(b-1) * 139.13);
eq21 = 0.008433 - c * b * ((2 * 0.435 * ((41/2)^(a/b)) + 40 * (40^(a/b)) + (a/b) * (40-1) * (0.435 * 40^((a/b)-1) +
40.87 * 1) + (0.00304/c)^(1/b))^(b-1) * 40.87 + (139.13 * (1) + (0.00304/c)^(1/b))^(b-1) * 139.13 + (180 * (1) +
(0.00304/c)^(1/b))^(b-1) * 180);
eq22 = 0.008808 - c * b * ((2 * 0.435 * ((41/2)^(a/b)) + 40 * (40^(a/b)) + (a/b) * (40-1) * (0.435 * 40^((a/b)-1) +
40.87 * 1) + (0.00304/c)^(1/b))^(b-1) * 40.87 + (139.13 * (1) + (0.00304/c)^(1/b))^(b-1) * 139.13 + (180 * (1) +
(0.00304/c)^(1/b))^(b-1) * 180 + (180 * (1) + (0.00304/c)^(1/b))^(b-1) * 180);
eq23 = 0.011919 - c * b * ((2 * 0.435 * ((41/2)^(a/b)) + 40 * (40^(a/b)) + (a/b) * (40-1) * (0.435 * 40^((a/b)-1) +
40.87 * 1) + (0.00304/c)^(1/b))^(b-1) * 40.87 + (139.13 * (1) + (0.00304/c)^(1/b))^(b-1) * 139.13 + (180 * (1) +
(0.00304/c)^(1/b))^(b-1) * 180 + (180 * (1) + (0.00304/c)^(1/b))^(b-1) * 180 + (180 * (1) + (0.00304/c)^(1/b))^(b-
1) * 180);
eq24 = 0.01541  - c * b * ((2 * 0.435 * ((41/2)^(a/b)) + 40 * (40^(a/b)) + (a/b) * (40-1) * (0.435 * 40^((a/b)-1) +
40.87 * 1) + (0.00304/c)^(1/b))^(b-1) * 40.87 + (139.13 * (1) + (0.00304/c)^(1/b))^(b-1) * 139.13 + (180 * (1) +
(0.00304/c)^(1/b))^(b-1) * 180 + (180 * (1) + (0.00304/c)^(1/b))^(b-1) * 180 + (180 * (1) + (0.00304/c)^(1/b))^(b-
1) * 180 + (180 * (1) + (0.00304/c)^(1/b))^(b-1) * 180);
% % ---- 30 dyne/cm^2, 40 s (variable Shear Stress) -------------------------
```

```
eq25 = 0.006034 - c * b * ((2 * 0.32 * ((31/2)^(a/b)) + 40 * (30^(a/b)) + (a/b) * (30-1) * (0.32 * 30^((a/b)-1) + 40.64
* 1) + (0.002547/c)^(1/b))^(b-1) * 40.64);
eq26 = 0.005656 - c * b * ((2 * 0.32 * ((31/2)^(a/b)) + 40 * (30^(a/b)) + (a/b) * (30-1) * (0.32 * 30^((a/b)-1) + 40.64
* 1) + (0.002547/c)^(1/b))^(b-1) * 40.64 + (139.36 * (1) + (0.002547/c)^(1/b))^(b-1) * 139.36);
eq27 = 0.007692 - c * b * ((2 * 0.32 * ((31/2)^(a/b)) + 40 * (30^(a/b)) + (a/b) * (30-1) * (0.32 * 30^((a/b)-1) + 40.64
* 1) + (0.002547/c)^(1/b))^(b-1) * 40.64 + (139.36 * (1) + (0.002547/c)^(1/b))^(b-1) * 139.36 + (180 * (1) +
(0.002547/c)^(1/b))^(b-1) * 180);
eq28 = 0.007306 - c * b * ((2 * 0.32 * ((31/2)^(a/b)) + 40 * (30^(a/b)) + (a/b) * (30-1) * (0.32 * 30^((a/b)-1) + 40.64
* 1) + (0.002547/c)^(1/b))^(b-1) * 40.64 + (139.36 * (1) + (0.002547/c)^(1/b))^(b-1) * 139.36 + (180 * (1) +
(0.002547/c)^(1/b))^(b-1) * 180 + (180 * (1) + (0.002547/c)^(1/b))^(b-1) * 180);
eq29 = 0.008229 - c * b * ((2 * 0.32 * ((31/2)^(a/b)) + 40 * (30^(a/b)) + (a/b) * (30-1) * (0.32 * 30^((a/b)-1) + 40.64
* 1) + (0.002547/c)^(1/b))^(b-1) * 40.64 + (139.36 * (1) + (0.002547/c)^(1/b))^(b-1) * 139.36 + (180 * (1) +
(0.002547/c)^(1/b))^(b-1) * 180 + (180 * (1) + (0.002547/c)^(1/b))^(b-1) * 180 + (180 * (1) +
(0.002547/c)^(1/b))^(b-1) * 180);
eq30 = 0.007232 - c * b * ((2 * 0.32 * ((31/2)^(a/b)) + 40 * (30^(a/b)) + (a/b) * (30-1) * (0.32 * 30^((a/b)-1) + 40.64
* 1) + (0.002547/c)^(1/b))^(b-1) * 40.64 + (139.36 * (1) + (0.002547/c)^(1/b))^(b-1) * 139.36 + (180 * (1) +
(0.002547/c)^(1/b))^(b-1) * 180 + (180 * (1) + (0.002547/c)^(1/b))^(b-1) * 180 + (180 * (1) +
(0.002547/c)^(1/b))^(b-1) * 180 + (180 * (1) + (0.002547/c)^(1/b))^(b-1) * 180);
% % ---- 20 dyne/cm^2, 40 s (variable Shear Stress) ------------------------
eq31 = 0.0073216 - c * b * ((2 * 0.21 * ((21/2)^(a/b)) + 40 * (20^(a/b)) + (a/b) * (20-1) * (0.21 * 20^((a/b)-1) +
40.42 * 1) + (0.0044259/c)^(1/b))^(b-1) * 40.42);
eq32 = 0.0038632 - c * b * ((2 * 0.21 * ((21/2)^(a/b)) + 40 * (20^(a/b)) + (a/b) * (20-1) * (0.21 * 20^((a/b)-1) +
40.42 * 1) + (0.0044259/c)^(1/b))^(b-1) * 40.42 + (139.58 * (1) + (0.0044259/c)^(1/b))^(b-1) * 139.58);
eq33 = 0.0048832 - c * b * ((2 * 0.21 * ((21/2)^(a/b)) + 40 * (20^(a/b)) + (a/b) * (20-1) * (0.21 * 20^((a/b)-1) +
40.42 * 1) + (0.0044259/c)^(1/b))^(b-1) * 40.42 + (139.58 * (1) + (0.0044259/c)^(1/b))^(b-1) * 139.58 + (180 * (1)
+ (0.0044259/c)^(1/b))^(b-1) * 180);
eq34 = 0.0056049 - c * b * ((2 * 0.21 * ((21/2)^(a/b)) + 40 * (20^(a/b)) + (a/b) * (20-1) * (0.21 * 20^((a/b)-1) +
40.42 * 1) + (0.0044259/c)^(1/b))^(b-1) * 40.42 + (139.58 * (1) + (0.0044259/c)^(1/b))^(b-1) * 139.58 + (180 * (1)
+ (0.0044259/c)^(1/b))^(b-1) * 180 + (180 * (1) + (0.0044259/c)^(1/b))^(b-1) * 180) - 0.0044259;
eq35 = 0.0062744 - c * b * ((2 * 0.21 * ((21/2)^(a/b)) + 40 * (20^(a/b)) + (a/b) * (20-1) * (0.21 * 20^((a/b)-1) +
40.42 * 1) + (0.0044259/c)^(1/b))^(b-1) * 40.42 + (139.58 * (1) + (0.0044259/c)^(1/b))^(b-1) * 139.58 + (180 * (1)
+ (0.0044259/c)^(1/b))^(b-1) * 180 + (180 * (1) + (0.0044259/c)^(1/b))^(b-1) * 180 + (180 * (1) +
(0.0044259/c)^(1/b))^(b-1) * 180) - 0.0044259;
eq36 = 0.0056099 - c * b * ((2 * 0.21 * ((21/2)^(a/b)) + 40 * (20^(a/b)) + (a/b) * (20-1) * (0.21 * 20^((a/b)-1) +
40.42 * 1) + (0.0044259/c)^(1/b))^(b-1) * 40.42 + (139.58 * (1) + (0.0044259/c)^(1/b))^(b-1) * 139.58 + (180 * (1)
+ (0.0044259/c)^(1/b))^(b-1) * 180 + (180 * (1) + (0.0044259/c)^(1/b))^(b-1) * 180 + (180 * (1) +
(0.0044259/c)^(1/b))^(b-1) * 180 + (180 * (1) + (0.0044259/c)^(1/b))^(b-1) * 180) - 0.0044259;
% % ---- 1 dyne/cm^2 control (variable Shear Stress) ------------------------
% eq37 = 0.0043   - c * b * ((40 * 1 + (0.005184/c)^(1/b))^(b-1) * 40);
% eq38 = 0.005583 - c * b * ((40 * 1 + (0.005184/c)^(1/b))^(b-1) * 40 + (140 * (1) + (0.005184/c)^(1/b))^(b-1) *
140);
% eq39 = 0.006812 - c * b * ((40 * 1 + (0.005184/c)^(1/b))^(b-1) * 40 + (140 * (1) + (0.005184/c)^(1/b))^(b-1) *
140 + (180 * (1) + (0.005184/c)^(1/b))^(b-1) * 180);
% eq40 = 0.005953 - c * b * ((40 * 1 + (0.005184/c)^(1/b))^(b-1) * 40 + (140 * (1) + (0.005184/c)^(1/b))^(b-1) *
140 + (180 * (1) + (0.005184/c)^(1/b))^(b-1) * 180 + (180 * (1) + (0.005184/c)^(1/b))^(b-1) * 180);
% eq41 = 0.006804 - c * b * ((40 * 1 + (0.005184/c)^(1/b))^(b-1) * 40 + (140 * (1) + (0.005184/c)^(1/b))^(b-1) *
140 + (180 * (1) + (0.005184/c)^(1/b))^(b-1) * 180 + (180 * (1) + (0.005184/c)^(1/b))^(b-1) * 180 + (180 * (1) +
(0.005184/c)^(1/b))^(b-1) * 180);
% eq42 = 0.00708  - c * b * ((40 * 1 + (0.005184/c)^(1/b))^(b-1) * 40 + (140 * (1) + (0.005184/c)^(1/b))^(b-1) *
140 + (180 * (1) + (0.005184/c)^(1/b))^(b-1) * 180 + (180 * (1) + (0.005184/c)^(1/b))^(b-1) * 180 + (180 * (1) +
(0.005184/c)^(1/b))^(b-1) * 180 + (180 * (1) + (0.005184/c)^(1/b))^(b-1) * 180);
% % ---- 70 dyne/cm^2, 40 s (variable Exposure Time) ------------------------
eq37 = 0.0209221 - c * b * ((2 * 0.77 * ((71/2)^(a/b)) + 40 * (70^(a/b)) + (a/b) * (70-1) * (0.77 * 70^((a/b)-1) +
41.54 * 1) + (0.005131/c)^(1/b))^(b-1) * 41.54);
eq38 = 0.0312898 - c * b * ((2 * 0.77 * ((71/2)^(a/b)) + 40 * (70^(a/b)) + (a/b) * (70-1) * (0.77 * 70^((a/b)-1) +
41.54 * 1) + (0.005131/c)^(1/b))^(b-1) * 41.54 + (138.46 * (1) + (0.005131/c)^(1/b))^(b-1) * 138.46);
```

```
eq39 = 0.0361134 - c * b * ((2 * 0.77 * ((71/2)^(a/b)) + 40 * (70^(a/b)) + (a/b) * (70-1) * (0.77 * 70^((a/b)-1) +
41.54 * 1) + (0.005131/c)^(1/b))^(b-1) * 41.54 + (138.46 * (1) + (0.005131/c)^(1/b))^(b-1) * 138.46 + (180 * (1) +
(0.005131/c)^(1/b))^(b-1) * 180);
eq40 = 0.0354258 - c * b * ((2 * 0.77 * ((71/2)^(a/b)) + 40 * (70^(a/b)) + (a/b) * (70-1) * (0.77 * 70^((a/b)-1) +
41.54 * 1) + (0.005131/c)^(1/b))^(b-1) * 41.54 + (138.46 * (1) + (0.005131/c)^(1/b))^(b-1) * 138.46 + (180 * (1) +
(0.005131/c)^(1/b))^(b-1) * 180 + (180 * (1) + (0.005131/c)^(1/b))^(b-1) * 180);
eq41 = 0.0392182 - c * b * ((2 * 0.77 * ((71/2)^(a/b)) + 40 * (70^(a/b)) + (a/b) * (70-1) * (0.77 * 70^((a/b)-1) +
41.54 * 1) + (0.005131/c)^(1/b))^(b-1) * 41.54 + (138.46 * (1) + (0.005131/c)^(1/b))^(b-1) * 138.46 + (180 * (1) +
(0.005131/c)^(1/b))^(b-1) * 180 + (180 * (1) + (0.005131/c)^(1/b))^(b-1) * 180 + (180 * (1) +
(0.005131/c)^(1/b))^(b-1) * 180);
eq42 = 0.0468981 - c * b * ((2 * 0.77 * ((71/2)^(a/b)) + 40 * (70^(a/b)) + (a/b) * (70-1) * (0.77 * 70^((a/b)-1) +
41.54 * 1) + (0.005131/c)^(1/b))^(b-1) * 41.54 + (138.46 * (1) + (0.005131/c)^(1/b))^(b-1) * 138.46 + (180 * (1) +
(0.005131/c)^(1/b))^(b-1) * 180 + (180 * (1) + (0.005131/c)^(1/b))^(b-1) * 180 + (180 * (1) +
(0.005131/c)^(1/b))^(b-1) * 180 + (180 * (1) + (0.005131/c)^(1/b))^(b-1) * 180);
% % ---- 70 dyne/cm^2, 30 s (variable Exposure Time) ----------
eq43 = 0.0096355 - c * b * ((2 * 0.77 * ((71/2)^(a/b)) + 30 * (70^(a/b)) + (a/b) * (70-1) * (0.77 * 70^((a/b)-1) +
31.54 * 1) + (0.004289/c)^(1/b))^(b-1) * 31.54);
eq44 = 0.0117141 - c * b * ((2 * 0.77 * ((71/2)^(a/b)) + 30 * (70^(a/b)) + (a/b) * (70-1) * (0.77 * 70^((a/b)-1) +
31.54 * 1) + (0.004289/c)^(1/b))^(b-1) * 31.54 + (148.46 * (1) + (0.004289/c)^(1/b))^(b-1) * 148.46);
eq45 = 0.0139984 - c * b * ((2 * 0.77 * ((71/2)^(a/b)) + 30 * (70^(a/b)) + (a/b) * (70-1) * (0.77 * 70^((a/b)-1) +
31.54 * 1) + (0.004289/c)^(1/b))^(b-1) * 31.54 + (148.46 * (1) + (0.004289/c)^(1/b))^(b-1) * 148.46 + (180 * (1) +
(0.004289/c)^(1/b))^(b-1) * 180);
eq46 = 0.0123609 - c * b * ((2 * 0.77 * ((71/2)^(a/b)) + 30 * (70^(a/b)) + (a/b) * (70-1) * (0.77 * 70^((a/b)-1) +
31.54 * 1) + (0.004289/c)^(1/b))^(b-1) * 31.54 + (148.46 * (1) + (0.004289/c)^(1/b))^(b-1) * 148.46 + (180 * (1) +
(0.004289/c)^(1/b))^(b-1) * 180 + (180 * (1) + (0.004289/c)^(1/b))^(b-1) * 180);
eq47 = 0.0180173 - c * b * ((2 * 0.77 * ((71/2)^(a/b)) + 30 * (70^(a/b)) + (a/b) * (70-1) * (0.77 * 70^((a/b)-1) +
31.54 * 1) + (0.004289/c)^(1/b))^(b-1) * 31.54 + (148.46 * (1) + (0.004289/c)^(1/b))^(b-1) * 148.46 + (180 * (1) +
(0.004289/c)^(1/b))^(b-1) * 180 + (180 * (1) + (0.004289/c)^(1/b))^(b-1) * 180 + (180 * (1) +
(0.004289/c)^(1/b))^(b-1) * 180);
eq48 = 0.0160206 - c * b * ((2 * 0.77 * ((71/2)^(a/b)) + 30 * (70^(a/b)) + (a/b) * (70-1) * (0.77 * 70^((a/b)-1) +
31.54 * 1) + (0.004289/c)^(1/b))^(b-1) * 31.54 + (148.46 * (1) + (0.004289/c)^(1/b))^(b-1) * 148.46 + (180 * (1) +
(0.004289/c)^(1/b))^(b-1) * 180 + (180 * (1) + (0.004289/c)^(1/b))^(b-1) * 180 + (180 * (1) +
(0.004289/c)^(1/b))^(b-1) * 180 + (180 * (1) + (0.004289/c)^(1/b))^(b-1) * 180);
% % ---- 70 dyne/cm^2, 20 s (variable Exposure Time) ----------
eq49 = 0.0087302 - c * b * ((2 * 0.77 * ((71/2)^(a/b)) + 20 * (70^(a/b)) + (a/b) * (70-1) * (0.77 * 70^((a/b)-1) +
21.54 * 1) + (0.004525/c)^(1/b))^(b-1) * 21.54);
eq50 = 0.0083986 - c * b * ((2 * 0.77 * ((71/2)^(a/b)) + 20 * (70^(a/b)) + (a/b) * (70-1) * (0.77 * 70^((a/b)-1) +
21.54 * 1) + (0.004525/c)^(1/b))^(b-1) * 21.54 + (158.46 * (1) + (0.004525/c)^(1/b))^(b-1) * 158.46);
eq51 = 0.0106598 - c * b * ((2 * 0.77 * ((71/2)^(a/b)) + 20 * (70^(a/b)) + (a/b) * (70-1) * (0.77 * 70^((a/b)-1) +
21.54 * 1) + (0.004525/c)^(1/b))^(b-1) * 21.54 + (158.46 * (1) + (0.004525/c)^(1/b))^(b-1) * 158.46 + (180 * (1) +
(0.004525/c)^(1/b))^(b-1) * 180);
eq52 = 0.0101414 - c * b * ((2 * 0.77 * ((71/2)^(a/b)) + 20 * (70^(a/b)) + (a/b) * (70-1) * (0.77 * 70^((a/b)-1) +
21.54 * 1) + (0.004525/c)^(1/b))^(b-1) * 21.54 + (158.46 * (1) + (0.004525/c)^(1/b))^(b-1) * 158.46 + (180 * (1) +
(0.004525/c)^(1/b))^(b-1) * 180 + (180 * (1) + (0.004525/c)^(1/b))^(b-1) * 180);
eq53 = 0.0130556 - c * b * ((2 * 0.77 * ((71/2)^(a/b)) + 20 * (70^(a/b)) + (a/b) * (70-1) * (0.77 * 70^((a/b)-1) +
21.54 * 1) + (0.004525/c)^(1/b))^(b-1) * 21.54 + (158.46 * (1) + (0.004525/c)^(1/b))^(b-1) * 158.46 + (180 * (1) +
(0.004525/c)^(1/b))^(b-1) * 180 + (180 * (1) + (0.004525/c)^(1/b))^(b-1) * 180 + (180 * (1) +
(0.004525/c)^(1/b))^(b-1) * 180);
eq54 = 0.0107269 - c * b * ((2 * 0.77 * ((71/2)^(a/b)) + 20 * (70^(a/b)) + (a/b) * (70-1) * (0.77 * 70^((a/b)-1) +
21.54 * 1) + (0.004525/c)^(1/b))^(b-1) * 21.54 + (158.46 * (1) + (0.004525/c)^(1/b))^(b-1) * 158.46 + (180 * (1) +
(0.004525/c)^(1/b))^(b-1) * 180 + (180 * (1) + (0.004525/c)^(1/b))^(b-1) * 180 + (180 * (1) +
(0.004525/c)^(1/b))^(b-1) * 180 + (180 * (1) + (0.004525/c)^(1/b))^(b-1) * 180);
% % ---- 70 dyne/cm^2, 10 s (variable Exposure Time) ----------
eq55 = 0.0078392 - c * b * ((2 * 0.77 * ((71/2)^(a/b)) + 10 * (70^(a/b)) + (a/b) * (70-1) * (0.77 * 70^((a/b)-1) +
11.54 * 1) + (0.004214/c)^(1/b))^(b-1) * 11.54);
```

```
eq56 = 0.0061542 - c * b * ((2 * 0.77 * ((71/2)^(a/b)) + 10 * (70^(a/b)) + (a/b) * (70-1) * (0.77 * 70^((a/b)-1) +
11.54 * 1) + (0.004214/c)^(1/b))^(b-1) * 11.54 + (168.46 * (1) + (0.004214/c)^(1/b))^(b-1) * 168.46);
eq57 = 0.0067483 - c * b * ((2 * 0.77 * ((71/2)^(a/b)) + 10 * (70^(a/b)) + (a/b) * (70-1) * (0.77 * 70^((a/b)-1) +
11.54 * 1) + (0.004214/c)^(1/b))^(b-1) * 11.54 + (168.46 * (1) + (0.004214/c)^(1/b))^(b-1) * 168.46 + (180 * (1) +
(0.004214/c)^(1/b))^(b-1) * 180);
eq58 = 0.0063858 - c * b * ((2 * 0.77 * ((71/2)^(a/b)) + 10 * (70^(a/b)) + (a/b) * (70-1) * (0.77 * 70^((a/b)-1) +
11.54 * 1) + (0.004214/c)^(1/b))^(b-1) * 11.54 + (168.46 * (1) + (0.004214/c)^(1/b))^(b-1) * 168.46 + (180 * (1) +
(0.004214/c)^(1/b))^(b-1) * 180 + (180 * (1) + (0.004214/c)^(1/b))^(b-1) * 180);
eq59 = 0.0061095 - c * b * ((2 * 0.77 * ((71/2)^(a/b)) + 10 * (70^(a/b)) + (a/b) * (70-1) * (0.77 * 70^((a/b)-1) +
11.54 * 1) + (0.004214/c)^(1/b))^(b-1) * 11.54 + (168.46 * (1) + (0.004214/c)^(1/b))^(b-1) * 168.46 + (180 * (1) +
(0.004214/c)^(1/b))^(b-1) * 180 + (180 * (1) + (0.004214/c)^(1/b))^(b-1) * 180 + (180 * (1) +
(0.004214/c)^(1/b))^(b-1) * 180);
eq60 = 0.0072843 - c * b * ((2 * 0.77 * ((71/2)^(a/b)) + 10 * (70^(a/b)) + (a/b) * (70-1) * (0.77 * 70^((a/b)-1) +
11.54 * 1) + (0.004214/c)^(1/b))^(b-1) * 11.54 + (168.46 * (1) + (0.004214/c)^(1/b))^(b-1) * 168.46 + (180 * (1) +
(0.004214/c)^(1/b))^(b-1) * 180 + (180 * (1) + (0.004214/c)^(1/b))^(b-1) * 180 + (180 * (1) +
(0.004214/c)^(1/b))^(b-1) * 180 + (180 * (1) + (0.004214/c)^(1/b))^(b-1) * 180);
% % ---- 70 dyne/cm^2, 5 s (variable Exposure Time) ----------------------
eq61 = 0.0062505 - c * b * ((2 * 0.77 * ((71/2)^(a/b)) + 5 * (70^(a/b)) + (a/b) * (70-1) * (0.77 * 70^((a/b)-1) + 6.54
* 1) + (0.003708/c)^(1/b))^(b-1) * 6.54);
eq62 = 0.0053974 - c * b * ((2 * 0.77 * ((71/2)^(a/b)) + 5 * (70^(a/b)) + (a/b) * (70-1) * (0.77 * 70^((a/b)-1) + 6.54
* 1) + (0.003708/c)^(1/b))^(b-1) * 6.54 + (173.46 * (1) + (0.003708/c)^(1/b))^(b-1) * 173.46);
eq63 = 0.0055954 - c * b * ((2 * 0.77 * ((71/2)^(a/b)) + 5 * (70^(a/b)) + (a/b) * (70-1) * (0.77 * 70^((a/b)-1) + 6.54
* 1) + (0.003708/c)^(1/b))^(b-1) * 6.54 + (173.46 * (1) + (0.003708/c)^(1/b))^(b-1) * 173.46 + (180 * (1) +
(0.003708/c)^(1/b))^(b-1) * 180);
eq64 = 0.0062308 - c * b * ((2 * 0.77 * ((71/2)^(a/b)) + 5 * (70^(a/b)) + (a/b) * (70-1) * (0.77 * 70^((a/b)-1) + 6.54
* 1) + (0.003708/c)^(1/b))^(b-1) * 6.54 + (173.46 * (1) + (0.003708/c)^(1/b))^(b-1) * 173.46 + (180 * (1) +
(0.003708/c)^(1/b))^(b-1) * 180 + (180 * (1) + (0.003708/c)^(1/b))^(b-1) * 180);
eq65 = 0.0046747 - c * b * ((2 * 0.77 * ((71/2)^(a/b)) + 5 * (70^(a/b)) + (a/b) * (70-1) * (0.77 * 70^((a/b)-1) + 6.54
* 1) + (0.003708/c)^(1/b))^(b-1) * 6.54 + (173.46 * (1) + (0.003708/c)^(1/b))^(b-1) * 173.46 + (180 * (1) +
(0.003708/c)^(1/b))^(b-1) * 180 + (180 * (1) + (0.003708/c)^(1/b))^(b-1) * 180 + (180 * (1) +
(0.003708/c)^(1/b))^(b-1) * 180);
eq66 = 0.0048517 - c * b * ((2 * 0.77 * ((71/2)^(a/b)) + 5 * (70^(a/b)) + (a/b) * (70-1) * (0.77 * 70^((a/b)-1) + 6.54
* 1) + (0.003708/c)^(1/b))^(b-1) * 6.54 + (173.46 * (1) + (0.003708/c)^(1/b))^(b-1) * 173.46 + (180 * (1) +
(0.003708/c)^(1/b))^(b-1) * 180 + (180 * (1) + (0.003708/c)^(1/b))^(b-1) * 180 + (180 * (1) +
(0.003708/c)^(1/b))^(b-1) * 180 + (180 * (1) + (0.003708/c)^(1/b))^(b-1) * 180);
% % ---- 1 dyne/cm^2 control (variable Exposure Time) ----------------------
% eq73 = 0.0055100 - c * b * ((40 * 1 + (0.004716/c)^(1/b))^(b-1) * 40);
% eq74 = 0.0049060 - c * b * ((40 * 1 + (0.004716/c)^(1/b))^(b-1) * 40 + (140 * (1) + (0.004716/c)^(1/b))^(b-1) *
140);
% eq75 = 0.0042023 - c * b * ((40 * 1 + (0.004716/c)^(1/b))^(b-1) * 40 + (140 * (1) + (0.004716/c)^(1/b))^(b-1) *
140 + (180 * (1) + (0.004716/c)^(1/b))^(b-1) * 180);
% eq76 = 0.0038300 - c * b * ((40 * 1 + (0.004716/c)^(1/b))^(b-1) * 40 + (140 * (1) + (0.004716/c)^(1/b))^(b-1) *
140 + (180 * (1) + (0.004716/c)^(1/b))^(b-1) * 180 + (180 * (1) + (0.004716/c)^(1/b))^(b-1) * 180);
% eq77 = 0.0039658 - c * b * ((40 * 1 + (0.004716/c)^(1/b))^(b-1) * 40 + (140 * (1) + (0.004716/c)^(1/b))^(b-1) *
140 + (180 * (1) + (0.004716/c)^(1/b))^(b-1) * 180 + (180 * (1) + (0.004716/c)^(1/b))^(b-1) * 180 + (180 * (1) +
(0.004716/c)^(1/b))^(b-1) * 180);
% eq78 = 0.0034444 - c * b * ((40 * 1 + (0.004716/c)^(1/b))^(b-1) * 40 + (140 * (1) + (0.004716/c)^(1/b))^(b-1) *
140 + (180 * (1) + (0.004716/c)^(1/b))^(b-1) * 180 + (180 * (1) + (0.004716/c)^(1/b))^(b-1) * 180 + (180 * (1) +
(0.004716/c)^(1/b))^(b-1) * 180 + (180 * (1) + (0.004716/c)^(1/b))^(b-1) * 180);
% ---- System of Equations ---------------------------------------------
% This section assembles all the residual equations into a single vector "eq".
eq(1)  = eq1(1);  eq(2)  = eq2(1);  eq(3)  = eq3(1);  eq(4)  = eq4(1);  eq(5)  = eq5(1);  eq(6)  = eq6(1);
eq(7)  = eq7(1);  eq(8)  = eq8(1);  eq(9)  = eq9(1);  eq(10) = eq10(1); eq(11) = eq11(1); eq(12) = eq12(1);
eq(13) = eq13(1); eq(14) = eq14(1); eq(15) = eq15(1); eq(16) = eq16(1); eq(17) = eq17(1); eq(18) = eq18(1);
eq(19) = eq19(1); eq(20) = eq20(1); eq(21) = eq21(1); eq(22) = eq22(1); eq(23) = eq23(1); eq(24) = eq24(1);
eq(25) = eq25(1); eq(26) = eq26(1); eq(27) = eq27(1); eq(28) = eq28(1); eq(29) = eq29(1); eq(30) = eq30(1);
```

```
eq(31) = eq31(1); eq(32) = eq32(1); eq(33) = eq33(1); eq(34) = eq34(1); eq(35) = eq35(1); eq(36) = eq36(1);
eq(37) = eq37(1); eq(38) = eq38(1); eq(39) = eq39(1); eq(40) = eq40(1); eq(41) = eq41(1); eq(42) = eq42(1);
eq(43) = eq43(1); eq(44) = eq44(1); eq(45) = eq45(1); eq(46) = eq46(1); eq(47) = eq47(1); eq(48) = eq48(1);
eq(49) = eq49(1); eq(50) = eq50(1); eq(51) = eq51(1); eq(52) = eq52(1); eq(53) = eq53(1); eq(54) = eq54(1);
eq(55) = eq55(1); eq(56) = eq56(1); eq(57) = eq57(1); eq(58) = eq58(1); eq(59) = eq59(1); eq(60) = eq60(1);
eq(61) = eq61(1); eq(62) = eq62(1); eq(63) = eq63(1); eq(64) = eq64(1); eq(65) = eq65(1); eq(66) = eq66(1);
% ------------------------------------------------------------
```